USGS
science for a changing world

Prepared in cooperation with the U.S. Army Corps of Engineers

Development of Continuous Bathymetry and Two-Dimensional Hydraulic Models for the Willamette River, Oregon

Scientific Investigations Report 2022–5025

U.S. Department of the Interior
U.S. Geological Survey

Cover. The Willamette River facing upstream near Corvallis, Oregon, August 2016. Photo by James White (U.S. Geological Survey).

Development of Continuous Bathymetry and Two-Dimensional Hydraulic Models for the Willamette River, Oregon

By James S. White and J. Rose Wallick

Prepared in cooperation with the U.S. Army Corps of Engineers

Scientific Investigations Report 2022–5025

U.S. Geological Survey, Reston, Virginia: 2022

For more information on the USGS—the Federal source for science about the Earth, its natural and living resources, natural hazards, and the environment—visit https://www.usgs.gov or call 1–888–ASK–USGS.

For an overview of USGS information products, including maps, imagery, and publications, visit https://store.usgs.gov/.

Suggested citation:
White, J.S., and Wallick, J.R., 2022, Development of continuous bathymetry and two-dimensional hydraulic models for the Willamette River, Oregon: U.S. Geological Survey Scientific Investigations Report 2022–5025, 67 p., https://doi.org/10.3133/sir20225025.

ISSN 2328-0328 (online)

Acknowledgments

We wish to extend our thanks to the many people who contributed to the work reported here. Project oversight and direction were provided by Jacob Macdonald and Richard Piaskowski (U.S. Army Corps of Engineers [USACE]), with technical review provided by Jefferey Balantine and Paul Sclafani (USACE). This work was carried out as part of the Science for Willamette Instream Flow Team (SWIFT) process led by James Peterson (U.S. Geological Survey [USGS] Cooperative Fish and Wildlife Unit), with support from Jessica Pease and Tyrell Dewebber (Oregon State University). Brandon Overstreet and Gabriel Gordon (USGS) were instrumental in the collection, processing, and publication of Willamette River bathymetric data used in this study and they assisted with model development and analyses. Additional assistance was provided by USGS colleagues Stewart Rounds, Laurel Stewart, Mackenzie Keith, Adam Stonewall, Tess Harden, Alexandria Costello, Joseph Mangano, and Krista Jones. Mark Fonstand (University of Oregon) shared his 2015 Willamette River bathymetry datasets.

Contents

Figures

Tables

Conversion Factors

U.S. customary units to International System of Units

Multiply	By	To obtain
	Length	
foot (ft)	0.3048	meter (m)
mile (mi)	1.609	kilometer (km)
	Volume	
cubic foot (ft^3)	0.02832	cubic meter (m^3)
	Flow rate	
cubic foot per second (ft^3/s)	0.02832	cubic meter per second (m^3/s)

International System of Units to U.S. customary units

Multiply	By	To obtain
	Length	
meter (m)	3.281	foot (ft)
kilometer (km)	0.6214	mile (mi)
	Area	
square meter (m^2)	0.0002471	acre
square meter (m^2)	10.76	square foot (ft^2)
square kilometer (km^2)	247.1	acre
square kilometer (km^2)	0.3861	square mile (mi^2)
	Flow rate	
meter per second (m/s)	3.281	foot per second (ft/s)
millimeter per year (mm/yr)	0.03937	inch per year (in/yr)

Datums

Vertical coordinate information is referenced to the North American Vertical Datum of 1988 (NAVD 88).

Horizontal coordinate information is referenced to the North American Datum of 1983 (NAD 83).

Elevation, as used in this report, refers to distance above the vertical datum.

Abbreviations

Bi-Op	Biological Opinion
DEM	digital elevation model
GNSS	Global Navigation Satellite Systems
HEC-RAS	(U.S. Army Corps of Engineers) Hydrologic Engineering Center's River Analysis System
lidar	Light Detection and Ranging
ORGN	Oregon Realtime GNSS Network
RKM	River Kilometer
TIN	Triangular Irregular Network
USACE	U.S. Army Corps of Engineers
USGS	U.S. Geological Survey
WSE	water-surface elevation

Development of Continuous Bathymetry and Two-Dimensional Hydraulic Models for the Willamette River, Oregon

By James S. White and J. Rose Wallick

Abstract

The Willamette River is home to at least 69 species of fish, 33 of which are native, including Chinook salmon (*Oncorhynchus tshawytscha*) and steelhead (*Oncorhynchus mykiss*). These fish need suitable hydraulic conditions, such as water depth and velocity, to fulfill various stages of their life. Hydraulic conditions are driven by interactions between channel morphology and streamflow, which throughout the Willamette River are strongly influenced by the operation of flood-control dams in upstream tributaries. To assess how streamflow management at these dams affects downstream fish habitat, the U.S. Geological Survey has developed high-resolution bathymetric datasets to support the development of two-dimensional hydraulic models. The datasets were created by combining data collected by airborne topo-bathymetric Light Detection and Ranging with boat-based sonar to create a seamless modeling surface over which a computational mesh with a resolution of roughly 5 by 5 meters was overlaid using the U.S. Army Corps of Engineers Hydraulic Engineering Center's River Analysis System 5.0.7 hydraulic modeling software. Models were developed for about 200 river kilometers, separated into five modeling reaches, and hydraulic conditions were simulated at flows ranging from extremely low values to annual peak flows. Results of the simulations highlight distinct patterns of inundation extents, water depths, and velocities that vary longitudinally along the Willamette River. In the two farthest upstream model reaches, from Eugene to Corvallis, the river is slower, shallower, and inundates more area at similar seasonal flows than in reaches downstream from Corvallis, where the river generally is deeper and faster. These findings align with previous geomorphic analysis of the Willamette River showing the upper reaches of the river to be geomorphically more dynamic compared to the largely single-thread channel farther downstream. Results of simulations made with these hydraulic models can be used to drive fish-habitat models to further inform flow-management decisions.

Introduction

The Willamette River, which drains 28,800 square kilometers (km^2) of northwestern Oregon (fig. 1), provides aquatic habitats for more than 33 species of native fish, including anadromous salmon and steelhead (*Oncorhynchus spp.*), as well as other aquatic organisms (Williams, 2014). These fish each require specific habitat conditions at different stages of their lives, and these habitats are determined partly by hydraulic characteristics of the river channel. In regulated rivers like the Willamette River, where flow releases from upstream dams are managed partly to support Endangered Species Act-listed salmon and steelhead, detailed assessments of fish habitat are necessary to inform environmental flow programs and to provide a basis for assessing benefits of different management scenarios. Accurately characterizing fish habitat throughout long river reaches, however, can be challenging because hydraulic conditions vary laterally and longitudinally as a function of channel morphology and streamflow. To inform fish habitat assessments, hydraulic models are often used to simulate variations in water depth, velocity, and inundation extents for a range of streamflows. The output from hydraulic models can be coupled with habitat criteria and supplementary data to evaluate spatial and temporal patterns of habitat availability for various aquatic organisms.

Background

Streamflow in the Willamette River is largely regulated by a system of 13 high-head dams operated by the US Army Corps of Engineers (USACE) that were built in the mid-20th century to provide flood control, power production, storage for agricultural and municipal uses, flow augmentation for downstream navigation, and recreation. These dams and their impounded reservoirs are part of the USACE's Willamette Valley Project. In 2008, the National Marine Fisheries Service issued a Biological Opinion (hereinafter, Bi-Op) that determined the construction and continued operation of the dams have a deleterious effect on the recovery of spring Chinook salmon (*Oncorhynchus tshawytscha*) and winter steelhead

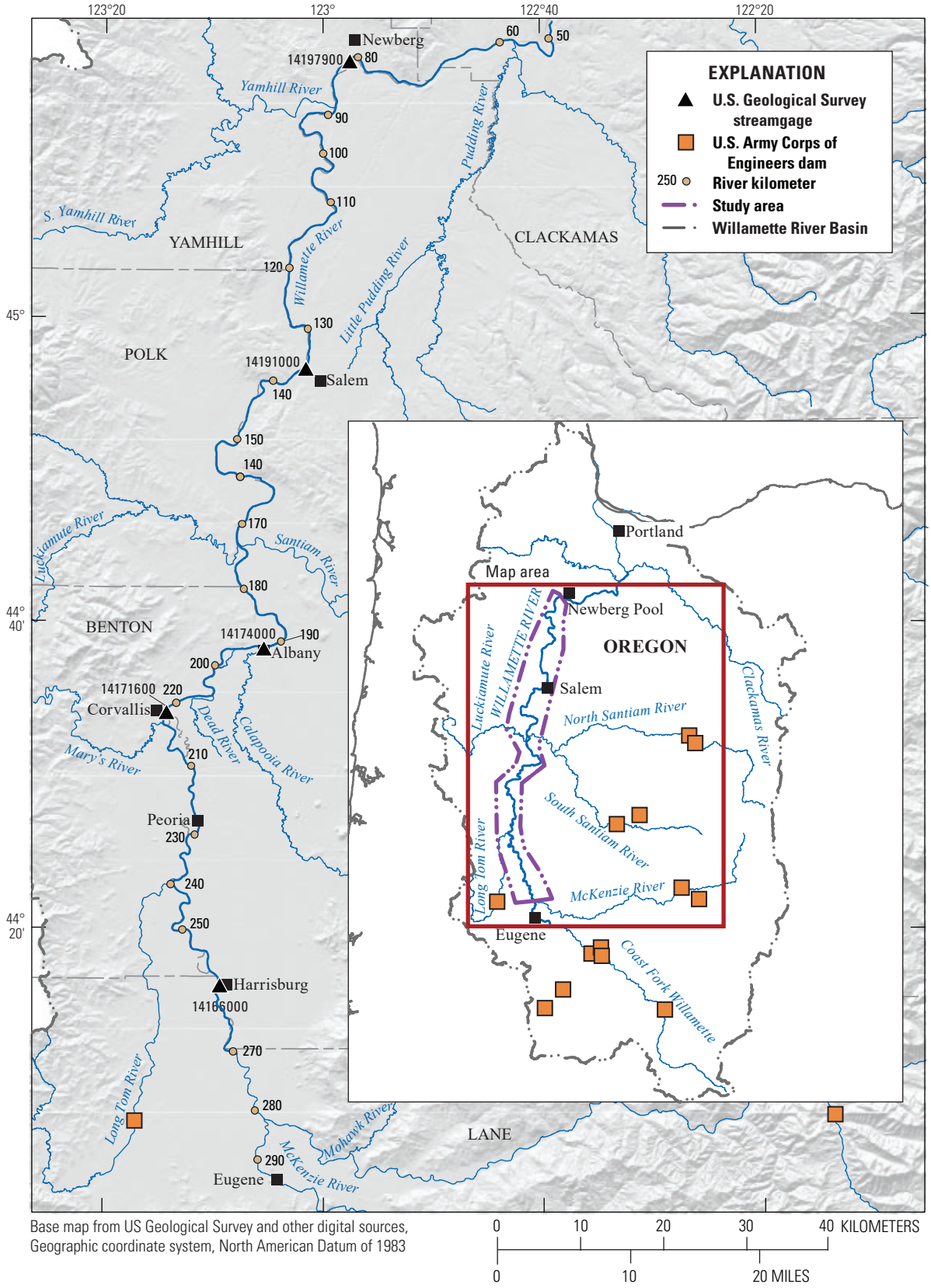

Figure 1. Willamette River study area, Oregon.

(*Oncorhynchus mykiss*), both listed as threatened under the Federal Endangered Species Act. The Bi-Op outlined mitigation actions for USACE to reduce the effects of dam operations on these species (National Marine Fisheries Service, 2008), among which was establishing minimum instream flows (referred to as flow objectives; National Marine Fisheries Service, 2008, table 2-8) for dam operations to maintain adequate streamflow downstream from dams to support spring Chinook salmon and winter steelhead at various life stages. The Bi-Op acknowledged, however, that the flow objectives were based on limited scientific understanding of the relation between streamflow and habitat availability and called for additional research to refine these flow objectives.

To address the knowledge gap identified in the Bi-Op, this study, done by the U.S. Geological Survey (USGS) in cooperation with the USACE, developed a high-resolution bathymetry dataset and detailed, two-dimensional hydraulic models to better understand how habitat varies with streamflow. The models span nearly 200 kilometers (km) of the Willamette River from its confluence with the McKenzie River, near the city of Eugene (River Kilometer [RKM] 282), to the Newberg Pool (RKM 82), near the city of Newberg. This study was completed as part of a broader research effort to assess the effects of dam operations on spring Chinook salmon and winter steelhead as part of the Science of the Willamette Instream Flow Team (DeWeber and Peterson, 2020).

The two-dimensional hydraulic models of the Willamette River developed in this study can simulate high-resolution datasets of inundation extents, water depths, and water velocities for a wide range of streamflows. The output from these models will enable the development of spatially explicit datasets of juvenile rearing habitat for spring Chinook salmon and winter steelhead as well as to quantify the availability of habitat at different streamflows to inform flow-management decisions by the USACE at upstream dams. The hydraulic models developed in this study can simulate a wide range of streamflows that occur in a typical year. The study focuses on the following objectives, to:

- Develop a spatially continuous bathymetric surface of the Willamette River and overbank areas to provide a foundation for hydraulic model development;
- Develop a suite of contiguous, reach-scale, high-resolution two-dimensional hydraulic models encompassing the study area; and
- Simulate a range of streamflows that occur on the Willamette River in a typical year, from low flows of summer months to higher flows experienced in most winters.

Purpose and Scope

This report documents the methods used to develop river-channel bathymetry and hydraulic models for the Willamette River and includes descriptions of model calibration and limitations of the bathymetric and hydraulic models. The report also summarizes hydraulic conditions simulated by the models and their potential applications. Although the channel bathymetry and hydraulic models developed in this study were created for the purpose of modeling habitat conditions for juvenile salmon and steelhead, the bathymetry and hydraulic models can inform a wide range of other floodplain management issues.

Hydrology and Morphology of the Willamette River Study Area

The Willamette River drains 28,800 km^2 of northwestern Oregon before joining the Columbia River near Portland, Oregon (fig. 1). The main stem of the Willamette River begins at the confluence of the Middle Fork Willamette and Coast Fork Willamette Rivers near Eugene and flows northward for 300 km, joined by major tributaries from the Cascade Range, including the McKenzie, Santiam, and Clackamas Rivers, which drain 3,450, 4,660, and 2,450 km^2, respectively. The river and its associated valley are bounded by the Coast Range to the west and the Cascade Range to the east.

The Willamette Valley has a Mediterranean climate (Beck and others, 2018), with cool, wet winters and warm, dry summers. The valley floor receives 1,000 millimeters per year of precipitation, primarily as rainfall during the winter (Oregon State University, 2013). Peak flows typically occur in winter months and are regulated by 13 USACE dams located in tributary basins (fig. 1). During the flood-control season, from October through April, peak flows are captured in storage reservoirs to minimize flood risk to downstream communities and maintain flows beneath the bankfull thresholds established at points downstream from each dam (table 2–4 in National Marine Fisheries Service, 2008). From April 1 to October 31, flows in the Willamette River are largely managed to meet or exceed Bi-OP Flow Objectives. In most years, streamflows in April through May exceed the Flow Objectives because of contributions from unregulated tributaries, but by June, unregulated inflows decrease, and streamflows primarily indicate releases of stored water from USACE dams to satisfy the Bi-OP Flow Objectives.

The Willamette River is a large, gravel-bed stream bordered by a wide floodplain that supports a blend of agricultural, forest, and other land uses. Within the study area, the river is fully alluvial, flowing predominantly on a bed composed of gravel to cobble substrate and occupying a sinuous, single-thread channel with occasional side-channels. Gravel bars of various sizes intermittently flank the river and support varying levels of vegetation cover, including areas of bare (unvegetated) ground, patches of 2–3 meters (m) high

willow and cottonwood shrubs, and more stable bar areas with dense stands of young (less than 50-year-old) forest. Modern floodplains and Pleistocene terraces also flank the river, rising gradually to relatively higher elevations above the main channel as the river flows northward from Eugene to Willamette Falls (Wallick and others, 2007; 2013). Locally, the river impinges on bank stabilization structures (revetments) and bedrock outcrops.

The overall morphology of the Willamette River varies substantially along its length, indicating geologic controls, historical transformations, and present-day patterns of lateral stability. Four geomorphically distinct valley segments influence channel hydraulics and fish habitats. These segments include the upper and middle Willamette Rivers, which are within the study area, and the Newberg Pool and lower Willamette River, which are downstream from the study area. Descriptions of these four valley segments are summarized from Wallick and others (2013):

- The upper Willamette River extends roughly 88 km from the confluence of the Coast Fork Willamette and Middle Fork Willamette Rivers (RKM 301) to near Corvallis (at approximately RKM 213). This valley segment is relatively steep (gradient of 0.001), with more abundant off-channel features and gravel bars than in downstream segments. In those downstream segments, the Willamette River occupies a predominantly single-thread channel with occasional multithreaded sections and numerous off-channel features (for example, alcoves and seasonally connected side channels). Floodplains along the upper Willamette River typically rise 1–2 m above the low-flow channel.
- The middle Willamette River extends 131 km from near Corvallis (RKM 213) to the mouth of the Yamhill River near Newberg (RKM 82). Within this valley segment, the Willamette River was historically, and continues to be, a laterally stable, single-thread, sinuous channel that evolved by gradual meander migration and floodplain aggradation. As a result of geologically imposed lateral stability, the middle Willamette River has far fewer off-channel features and gravel bars than the upper Willamette River. Here, floodplains rise 2–5 m above the low-flow channel, indicating historical and ongoing overbank sedimentation.
- The Newberg Pool (immediately downstream from the study area) is a 37-km-long, deep, slow-moving section of the Willamette River created by backwater conditions, imposed by 15-m high Willamette Falls (RKM 43), that extend upstream to about the Yamhill River confluence near Newberg (RKM 80).
- The lower Willamette River (downstream from study area) is tidally influenced, extending 43 km from Willamette Falls to the mouth of the Willamette River with the Columbia River at Portland. The geomorphology and bathymetry of this reach is described in Simenstad and others (2011).

Locations and Reporting Units

The units of measurement used in this report are consistent with those used by floodplain managers of the Willamette River Basin and include a blend of International System (SI) of Units and U.S. customary units; conversion factors are listed in report front matter. Streamflow is reported in cubic feet per second (ft^3/s) to align with the standard language used by dam operators, the USGS, and in streamflow requirements established in the Bi-OP (National Marine Fisheries Service, 2008). Measurements of length, area, and stream velocity are reported in meters (m), square meters (m^2) and meters per second (m/s), respectively. Distances along the Willamette River are stated in terms of river-kilometers (RKM), measured along the centerline of the low-flow wetted channel, as digitized from aerial photos. The RKM values begin at the mouth of the Willamette River in Portland, Oregon (RKM = 0), and increase in magnitude upstream. Unless otherwise specified, values of river gradient are determined from the 2017 Willamette River bathymetry of White and others (2019).

Study Approach

Evaluating the hydraulic characteristics of streams at scales relevant to juvenile salmonids requires high-resolution, two-dimensional hydraulic models. The datasets needed to develop these models include (1) a detailed terrain model that accurately represents channel bathymetry and floodplain topography, (2) land-cover data to characterize variation in channel roughness, and (3) streamflow data to provide boundary conditions for each modeled scenario.

Collection of Bathymetric Data and Creation of Digital Elevation Models

Continuous high-resolution datasets that depict channel bathymetry and floodplain topography provide the necessary foundation for hydraulic model development. To meet these objectives, topographic-bathymetric Light Detection and Ranging (lidar) and boat-based sonar data were combined to develop high-resolution, spatially continuous digital elevation models (DEMs) of the study area, which were then incorporated in the model terrain.

Collection of Lidar Data in Shallow Areas of the Main Channel and Floodplain

From May to June 2017, topographic-bathymetric lidar data were collected throughout the study reach by Quantum Spatial Inc. (2018). Topographic-bathymetric lidar uses shorter wavelength pulses, typically in the green wavelength, compared to traditional near-infrared lidar. Whereas near infrared light is rapidly attenuated in water, the shorter green wavelength can penetrate water and reflect off underwater surfaces, such as the riverbed. However, the depth to which topographic-bathymetric lidar (henceforth lidar) can detect underwater surfaces is limited to approximately one to two times the Secchi depth (Quantum Spatial Inc., 2018). Areas deeper than this, from which no data are returned, are referred to as "void areas." Bed detections on the Willamette River typically extended to depths of 2.0–3.0 m, leaving large void areas (fig. 2). To create a spatially continuous topo-bathymetric surface, these voids were filled with sonar data collected from 2015 to 2018. Small parts of floodplain were not captured in the 2017 lidar. In these areas, topographic lidar data collected in 2008 were used to fill in the gaps in coverage (Watershed Sciences, 2009).

Collection of Sonar Data in Deep Areas of the Main Channel

Sonar data collected in several different surveys of the Willamette River channels spanning the years 2015–18 were used to characterize bed elevations of the main channel and off-channel areas where lidar datasets did not capture bathymetry. The USGS and the University of Oregon collected intermittent bathymetry data using sonar along the upper Willamette River (Eugene to Corvallis) in 2015 and 2016 as part of unrelated studies. Most of these data were collected in the center of the channel and thus only partly address the issue of missing data in the void areas described in the preceding sections. To better characterize the void areas, additional sonar data were collected in these areas in 2017 and 2018.

Sonar data were collected via boat-mounted single-beam sonar, connected to high-precision Global Navigation Satellite System (GNSS) receivers (Trimble R8 and R10), which received corrections from the Oregon Realtime GNSS Network and provided horizontal and vertical precision generally to 0.05 m or less (White and others, 2019). The sonar (Seafloor Systems SonarMite) was connected to GNSS receivers via Bluetooth and was programmed to collect water-depth data every second, concurrently with GNSS positional data. The sonar used a 4-degree beam width at a 200 kilohertz frequency and has manufacturer-provided accuracies of 0.1 percent of depth from 0.3 to 75 m. Bed elevation was then calculated by subtracting water depth from instrument elevation. Surveys were opened and closed daily on known or created benchmarks to ensure the reliability of Oregon Realtime GNSS Network and the GNSS receiver, while bar-checks were done at the beginning of each survey to ensure sonar accuracy. Data were collected in the projected coordinate system North American Datum of 1983 Universal Transverse Mercator Zone 10, using vertical geoid model 12B and the North American Vertical Datum of 1988. Multiple quality-assurance metadata were recorded by the receiver, including vertical and horizontal dilution of precision, and horizontal and vertical accuracies (White and others, 2019).

After collection, sonar data underwent two rounds of quality assurance to check their reliability and to ensure the sonar data aligned with lidar data. Where lidar and sonar datasets overlapped, bed-elevation values from sonar were compared to lidar values to ensure datum alignment and that the two datasets could be combined to create a single DEM for hydraulic modeling purposes. This comparison was possible in shallow areas where lidar was able to identify the bed surface and where water depths were sufficient to permit boat access and the collection of sonar data within equipment specifications. In total, 113,293 water-depth points were compared throughout the study reach. Summary comparison statistics are provided in table 1, and figure 3 shows the magnitude and distribution of discrepancies between the sonar and lidar data longitudinally along the river. Combining sonar and lidar data appear sufficiently accurate for DEM and modeling purposes, with median differences of -0.04 m and a standard deviation of 0.58 m. Data collected in 2017 and 2018 are generally more accurate (median error = -0.03 m) than data collected in 2015 and 2016 and have significantly less variation between collection platforms (standard deviation = 0.21 m). Clear spatial trends in the magnitude and variation of error are evident, whereby the more geomorphically dynamic channel of the upper Willamette River has less agreement between the sonar and lidar data than do the lower reaches. A visual comparison of 2008 and 2017 lidar, as well as historical aerial photos from 2014 and 2017, indicate that these differences are likely owing to channel migration between surveys. In areas where clear change occurred, data collected prior to 2017 were removed to create the DEM.

Combining Sonar and Lidar Data in the Digital Elevation Model

To develop the model terrain necessary for detailed hydraulic and habitat modeling of the Willamette River, the sonar and lidar datasets were combined to create a single, spatially continuous DEM encompassing the main channel, off-channel features, and overbank areas. The lidar and sonar datasets used to create the DEM had different underlying spatial resolutions; the lidar DEM was published at 1-m^2 resolution (Quantum Spatial Inc., 2018), whereas spatial resolution of the sonar data was variable, but generally coarser than 0.5 points/m^2. However, to accommodate the lower-resolution sonar and facilitate more efficient modeling, the combined DEM was developed at 3 × 3 m resolution.

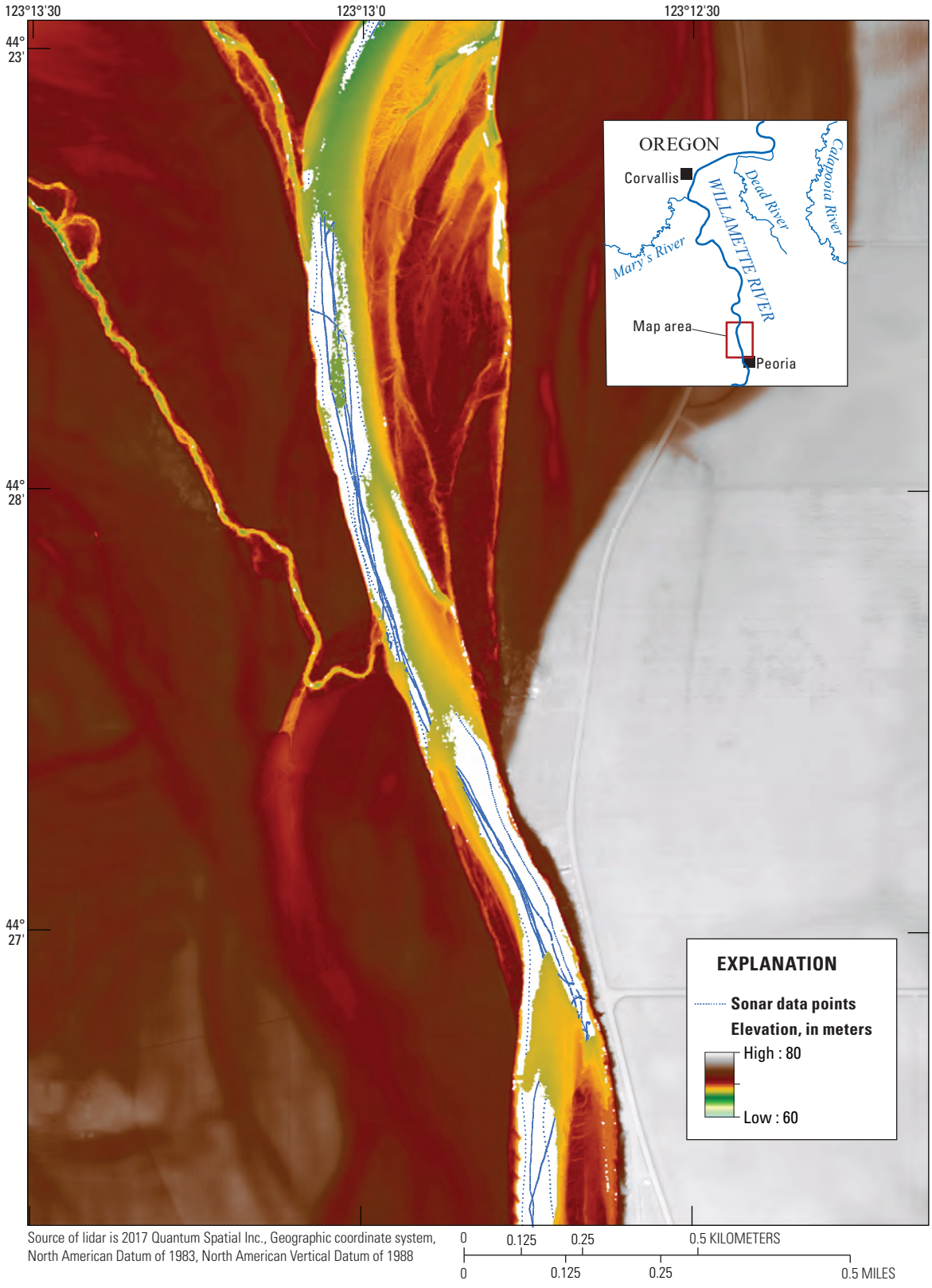

Figure 2. Example reach of topo-bathymetric Light Detection and Ranging (lidar) data, with void areas in white, overlain by sonar data, for the Willamette River, Oregon.

Table 1. Summary goodness-of-fit statistics for lidar and single-beam sonar data for the Willamette River, Oregon.

Performance metric	Value		Unit
	2015–18 data	2017–18 data	
Mean absolute error	-0.22	0.02	Meter
Percent Bias	-26.0	-0.04	Percent
Root mean square error	0.62	0.21	Meter
Standard deviation	0.58	0.21	Meter
Median	-0.04	-0.03	Meter

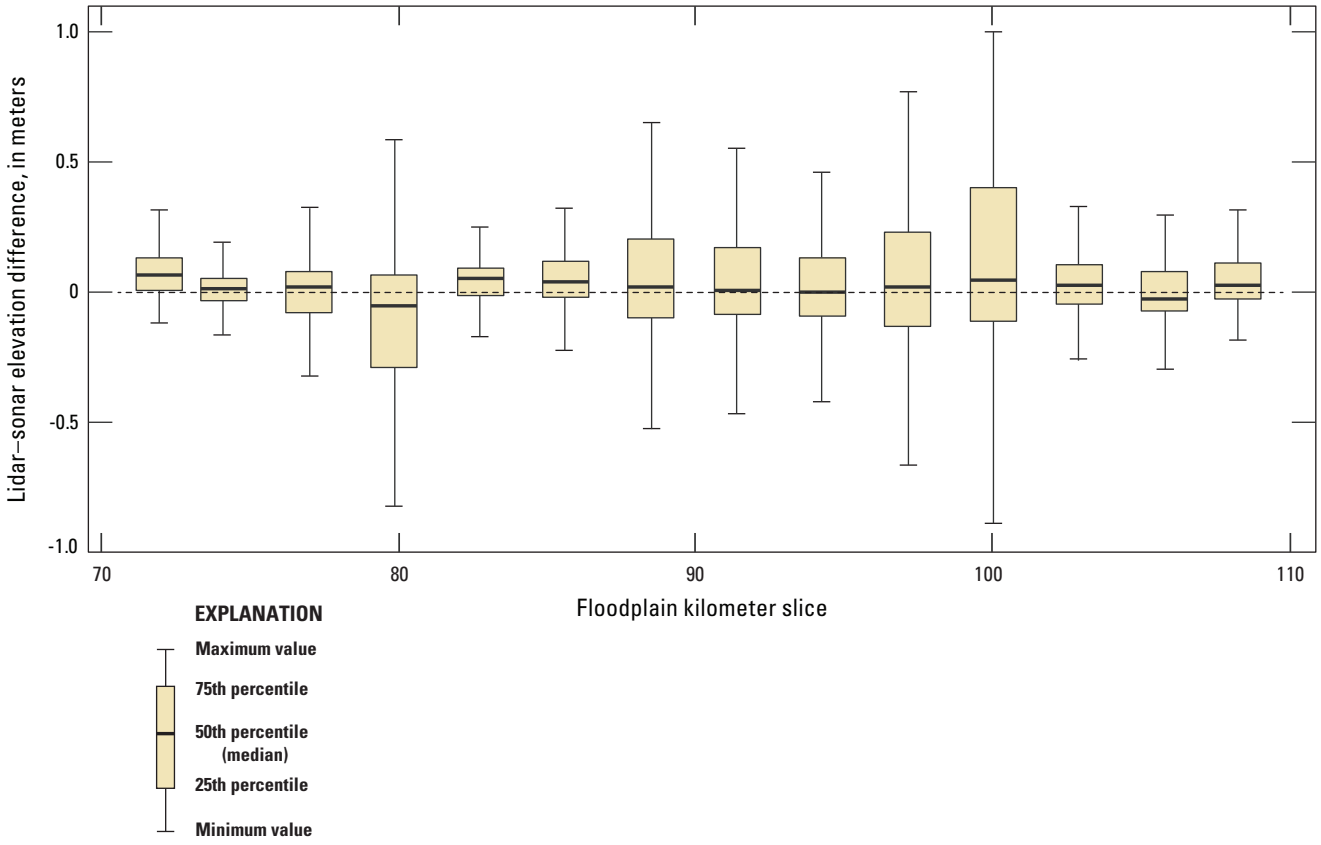

Figure 3. Comparison of elevation difference between 2017 topo-bathymetric lidar and sonar data collected along the Willamette River upstream from Newberg, Oregon.

Several data processing steps were required to prepare the lidar and sonar data so that they could be merged into a single terrain model dataset. First, the lidar DEM was converted to a point cloud dataset with 1-m^2 horizontal resolution. A Triangular Irregular Network (TIN) was then generated using the lidar point cloud data and 90 percent of sonar point cloud data. The remaining 10 percent of sonar data not used in the TIN development were withheld and used for validation purposes. Where lidar and sonar point cloud datasets overlapped, the lidar data were used to develop the terrain model dataset, although some sonar data were used to fill in void areas in the lidar data. The TIN was closely reviewed and where necessary, spurious interpolations were removed or breaklines were added. These spurious interpolations occurred occasionally along channel-banks and the thalweg, where abrupt changes in bed elevation produced interpolated surfaces that did not represent actual bed topography (fig. 4). Finally, the TIN was converted to a raster with 3-m^2 grid resolution using a nearest neighbor approach.

Once a raster was generated from the lidar and sonar data, the sonar data retained for validation were compared to corresponding values on the DEM. Results of this comparison for a reach of the Willamette River between the city of Corvallis and the Santiam River are available in table 2 and figure 5, where validation results suggest DEM accuracy within 0.02 m and a standard deviation of 0.26 m, with a negative bias of 8.3 percent.

Characterization of Bathymetry in Off-Channel Features

The Willamette River has numerous off-channel features such as alcoves and side channels that may be inundated at various streamflow levels. Many of these features are large (20–100 m wide) and some extend for several kilometers, with highly variable channel bathymetry, including deep pools and shallow areas. Where water depths in the off-channel feature exceeded the streambed detection limits of lidar, sonar data were collected in features that were hydraulically connected to the main channel at the time of the sonar survey. However, several of the off-channel features containing void areas were inaccessible by boat because of dense aquatic vegetation or too shallow water at their entrance. In these instances, breaklines were added to lidar point clouds, connecting the bed elevations between the last (and typically deepest) bed detections on either end of the channel segment lacking bathymetric data. This approach forces a linear interpolation of bed elevations between the areas of the main channel and off-channel features for which bathymetric data are available, thus ensuring that depths in the void areas are at least as deep as the lidar detection limit points selected at each end of the breakline (as shown in fig. 6). While the interpolated elevations applied to void areas have greater vertical uncertainty than other areas with actual survey measurements or lidar detections, this approach creates a more realistic and accurate model terrain for off-channel areas than would otherwise be possible if the data gaps were not filled with interpolated data.

Development of the Hydraulic Models

Hydraulic modeling in this study was done in the USACE Hydraulic Engineering Center's River Analysis System (HEC-RAS) platform (version 5.0.7; U.S. Army Corps of Engineers, 2016), which uses a finite volume scheme in conservation of mass. The models were run using full conservation of mass, energy, and momentum equations, with timesteps typically from 2 to 5 seconds, with a goal of limiting the number of occurrences in which the Courant parameter exceeds 1. The models were run using a quasi-steady-state approach, whereby the unsteady flow solver was used to simulate hydraulics but streamflow was held steady, typically for at least 30 model hours, to mimic steady-state conditions, before ramping to the next highest streamflow of interest. Model outputs were visually assessed to ensure inundation, depth, and velocity were in equilibrium before increasing the simulated flow.

Reaches and Boundary Conditions

The 200-km Willamette River channel was divided into five contiguous reaches, ranging in length from 28 to 58 km, to facilitate the efficient development, calibration, and subsequent simulations of the hydraulic models (fig. 7). Reaches were delineated with the objectives of (1) encompassing river segments with broadly similar channel morphology, (2) simplifying hydrologic boundary conditions to indicate the locations of major tributaries, and (3) ensuring that suitable hydraulic boundary conditions were provided for each reach.

Delineation of the separate model reaches was an iterative process. First, reaches spanning approximately 40 km each were identified to characterize areas of the river corridor with similar morphologic conditions, on the basis of characteristics described in Wallick and others (2013). These geomorphically based reaches were adjusted so that the upstream and downstream boundaries of each modeled reach were located at or near USGS streamgages. The extents of the reaches were finalized by further adjustments to minimize hydraulic complexity at the upstream and downstream boundaries of each model. To the extent possible, reach boundaries were placed in areas where the river was relatively straight and confined to a single, uniform channel. Boundaries also were placed where flow remained in a single channel at all modeled flows; this was not possible, however, at the downstream boundaries of two of the modeled reaches.

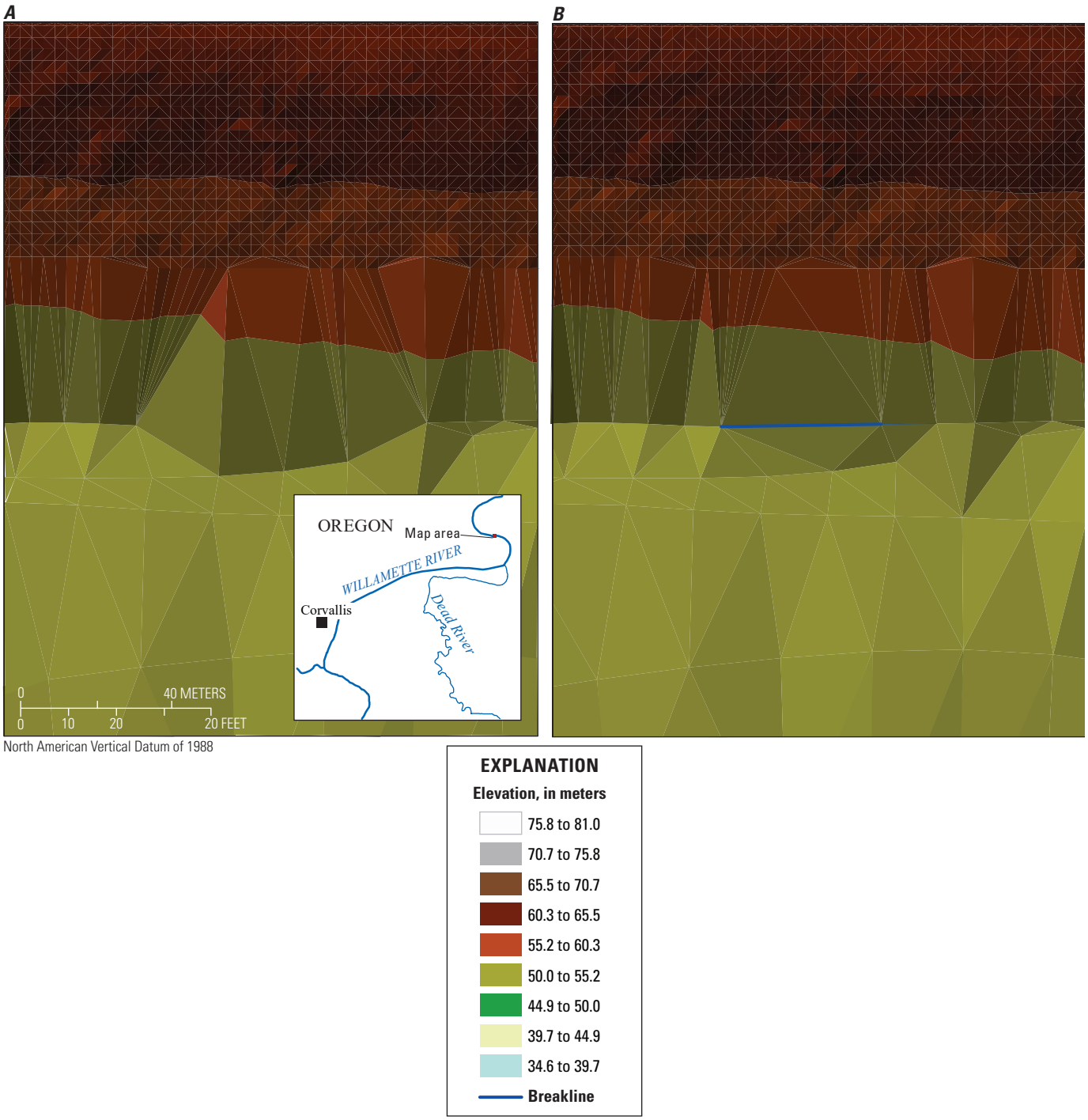

Figure 4. Example using breaklines along bank to correct spurious interpolation. *A*, shows elevation from Triangular Irregular Network dataset before using breaklines and *B*, shows edited Triangular Irregular Network with breakline.

Table 2. Performance metrics of channel interpolation of the Willamette River between Corvallis and Santiam River confluence ("Albany reach"), Oregon.

Performance metric	Value	Unit
Mean absolute error	0.04	Meter
Percent bias	-8.3	Percent
Root mean square error	0.26	Meter
Standard deviation	0.26	Meter
Median	-0.02	Meter

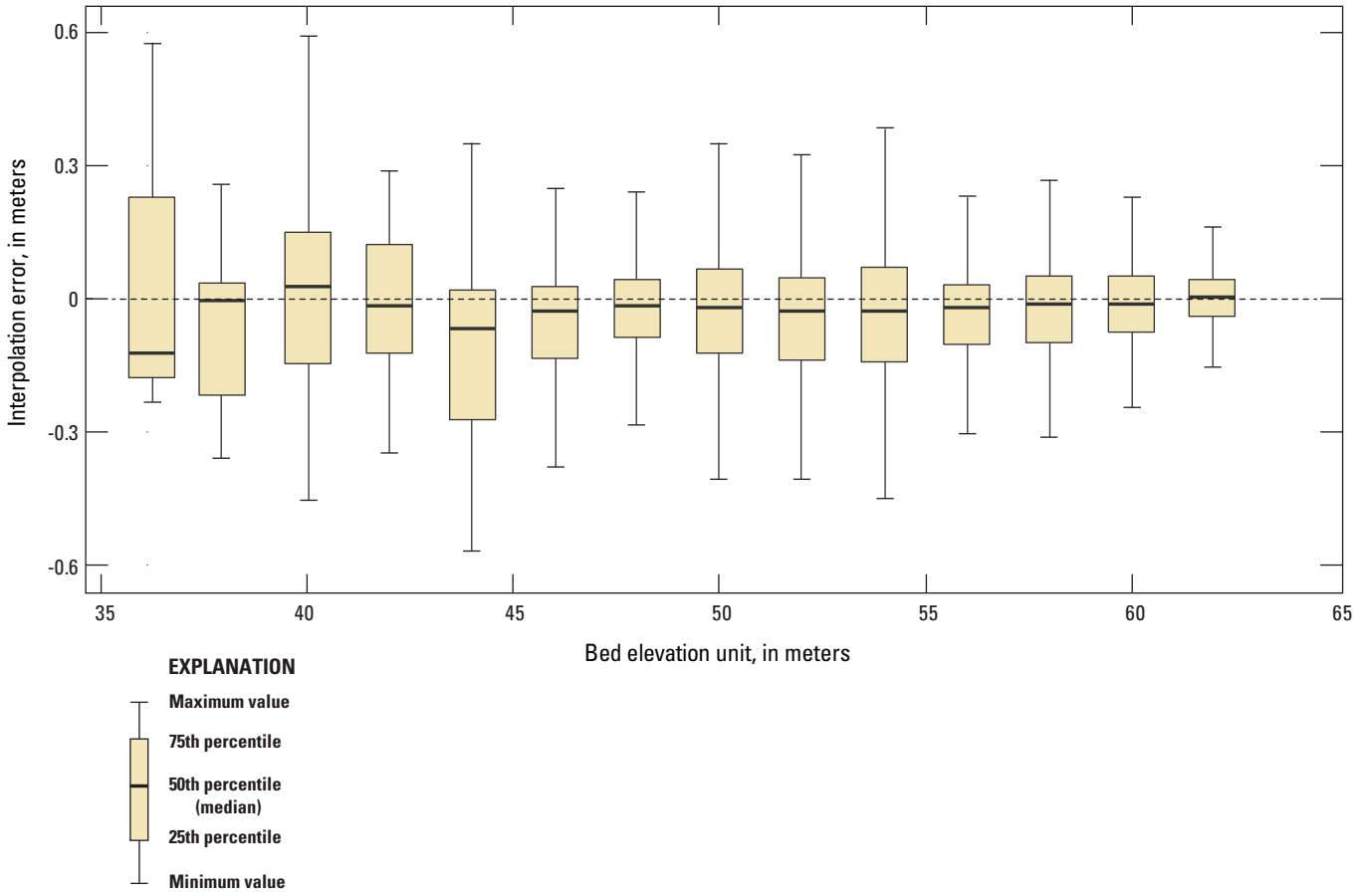

Figure 5. Channel interpolation error from withheld validation points and the interpolated Digital Elevation Model, between the City of Corvallis and the Santiam River confluence.

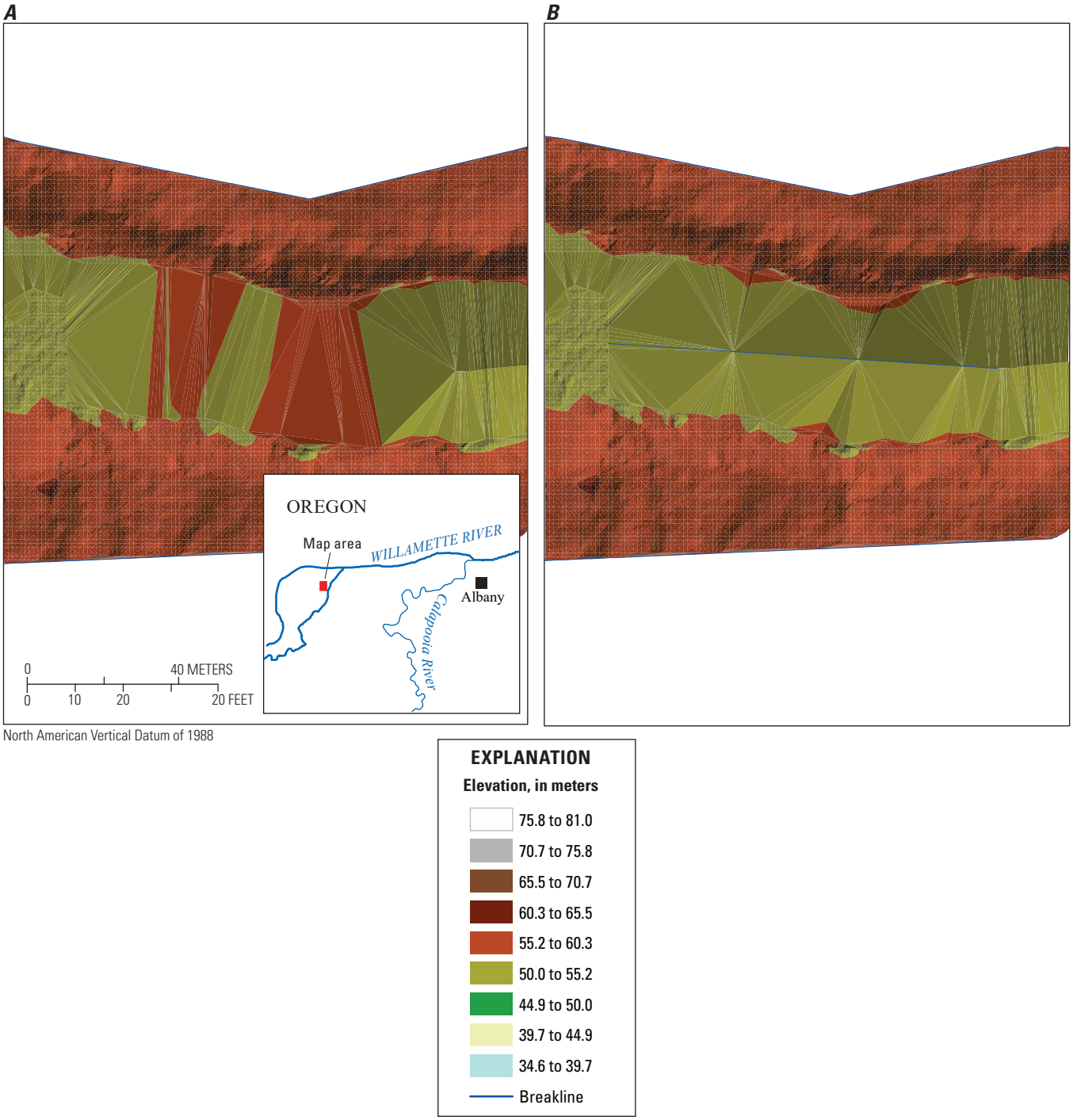

Figure 6. Example of using breaklines in a void area of an off-channel feature to create a more accurate model surface. *A*, displays side channel elevations prior to breaklines and *B*, displays side channel elevations with a breakline added.

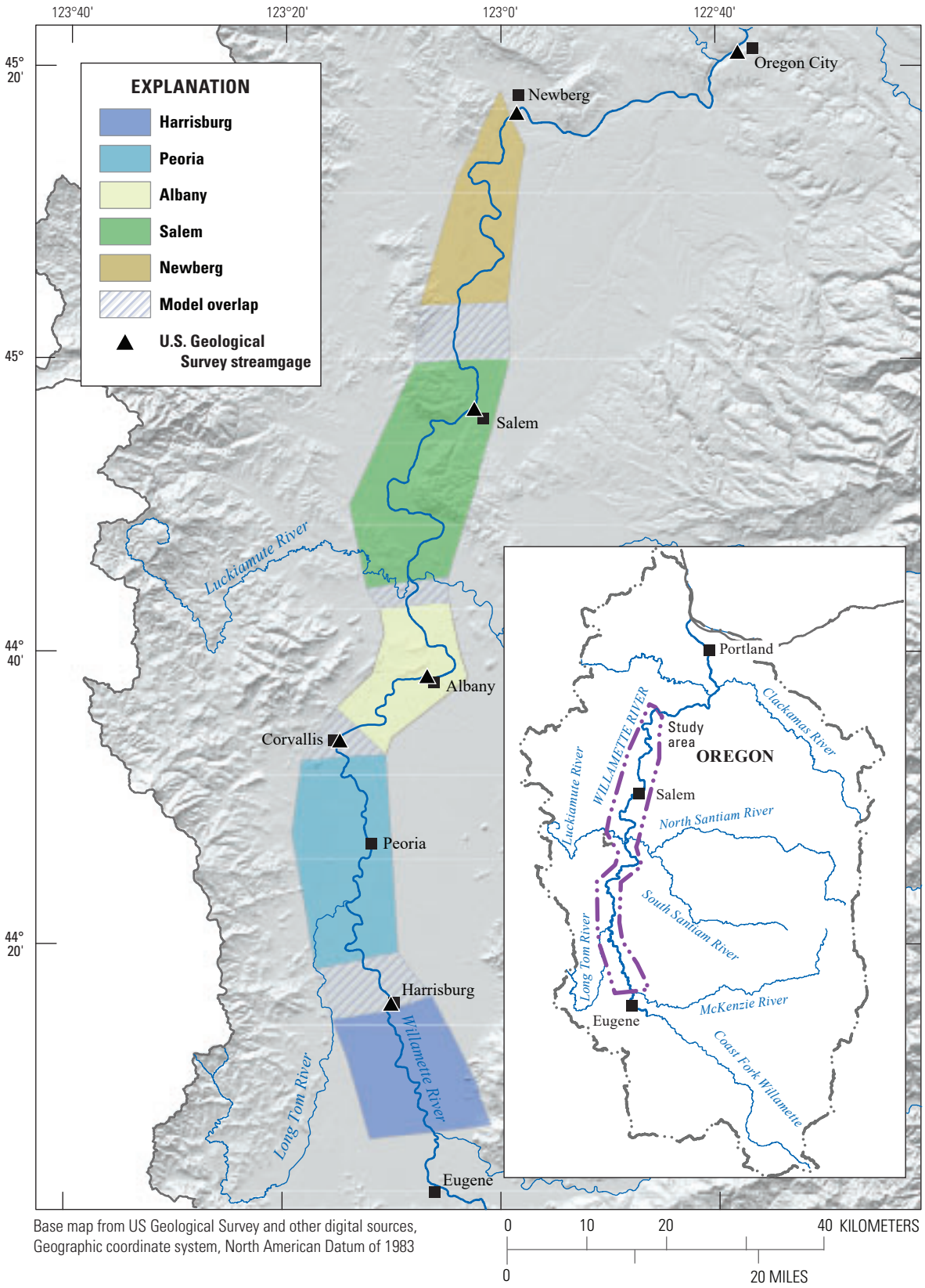

Figure 7. The five modeled reaches of the Willamette River, Oregon.

The boundary conditions applied to each of the hydraulic models were developed to satisfy the overall study goal of characterizing hydraulic conditions at a wide range of streamflows, not to simulate specific streamflow hydrographs or hydrologic events. This approach produced model outputs that can be compared with Willamette River Bi-OP Flow Objectives, which specify the total flow in the main channel of the Willamette River at select USGS streamgages for various periods from April 1 to September 30 of each year. Hence, the hydrologic boundary conditions for this study were defined using a single streamflow boundary condition applied to the upstream end of each model reach, except for the reach extending from upstream from the Santiam River confluence to Salem, where a second boundary condition is added to represent inflows from the Santiam River. Inputs from all other tributaries entering the Willamette River within the study area were not specifically included because (1) flows from major tributaries —the McKenzie, Middle Fork Willamette, and Coast Fork Willamette Rivers—enter the Willamette River upstream from the study area, and are therefore represented by the applied boundary conditions, and (2) unregulated tributaries entering the Willamette River within the study area are much smaller than regulated tributaries and generally contribute less than 2 percent of the total Willamette River flow within this study reach during late spring and summer, which are the focus of this study. During winter, unregulated tributary contributions from the Coast Range tributaries, the Calapooia River, and other sources can substantially influence flow in the main channel of the Willamette River, but these contributions vary considerably depending on antecedent conditions, storm characteristics, and season, considerations that extend beyond the scope of this study.

The range of streamflows simulated for this study were selected to indicate the range of typical conditions that have occurred on the Willamette River in the decades since construction of the 13 USACE flood-control dams. Streamflow percentiles were computed using mean daily flow data from USGS streamgages at Harrisburg, Corvallis, Albany, Salem, and Newberg for the period 1970–2019 (table 3). Using the flow percentiles as reference conditions, the range of simulated streamflows for each reach was selected to span flows ranging from historically low flows to the 95th percentile flow, which represents roughly the annual peak flow. These hydrologic boundary conditions were developed in consultation with fish biologists and flow managers from USACE, National Oceanic and Atmospheric Administration, Oregon Department of Fish and Wildlife, and Oregon State University to ensure that the range of flows simulated in the hydraulic models would be sufficient for characterizing habitat conditions across a wide range of likely flows and would also support salmon and steelhead life-cycle models developed by Oregon State University (Peterson and others, 2021).

Downstream boundary conditions for each of the modeled reaches were established by specifying normal depth conditions. The parameters required for this boundary condition are water-surface slope, which was derived from the 2008 and 2017 lidar datasets as the quotient of the change in water-surface elevation measured at points approximately 250 m upstream and downstream from the boundary, and the length of channel between these points. A summary of flow-boundary conditions is shown in table 4.

Computational Mesh

HEC-RAS uses an irregular mesh scheme and sub-grid bathymetry, which can leverage bathymetry data with higher resolution than computational cells via elevation-volume lookup tables, for more efficient processing while retaining resolution (U.S. Army Corps of Engineers, 2016). Irregular meshes allow for cells of various shapes and sizes, which enables faster processing and better representation of channel features. The computational meshes developed for each of the five model reaches in this study were developed using a similar approach. First, the underlying model terrain for each reach was extracted from the 3-m^2 topo-bathymetric DEM (see section, “Combining Sonar and Lidar Data in the Digital Elevation Model”) and an initial computational mesh was generated in HEC-RAS using a uniform cell size of 10 × 10 m. A polygon outlining the main channel and large off-channel features was then overlain on the initial mesh and used to create a finer resolution mesh (5 × 5 m cell size) within the channel features to convey most of the modeled streamflows. Breaklines were added as necessary to prevent simulated streamflows from erroneously crossing topographic boundaries, a common product of sub-grid bathymetry, whereby water can pass through features smaller than those delineated in the computational mesh. Breaklines were most commonly applied at gravel extraction ponds (former gravel pits), levies, and along floodplain channels. Meshes were refined in iterative model simulations to identify areas warranting additional refinement.

Structures such as bridges and culverts that affect channel hydraulics are not included in the models. For large structures like bridges in the main channel, the primary consequence of their omission at modeled flows is likely to be local variations in depth and velocity at and near bridge pilings. Side channels may contain culverts and bridges not captured in the bathymetry data nor included in the model. The effect of these factors is likely to be largest at higher flows, when more water is flowing outside the main channel.

Table 3. Summary of flow percentiles at U.S. Geological Survey streamgages (U.S. Geological Survey, 2021) used to inform selection of upstream boundary conditions in modeled reaches, on the Willamette River, Oregon, 1970–2019 (see table 4).

Streamgage number	Streamage location	Streamflow percentile (percent)				
		0.1	1.0	10	50	95
14166000	Harrisburg	2,874	3,540	4,520	7,780	32,600
14171600	Corvallis	3,597	3,778	4,772	8,960	34,990
14174000	Albany	3,103	3,890	4,890	9,070	42,300
14191000	Salem	4,925	5,650	6,870	15,000	71,805
14197900	Newberg	4,876	5,440	7,110	16,900	76,080

Table 4. Summary of boundary conditions used for modeled reaches of the Willamette River, Oregon.

[**Abbreviations:** RKM, River Kilometer; km, kilometers; ft^3/s, cubic feet per second; m/m, meter per meter]

Reach name	Model length (km)	Upstream reach boundary		Downstream reach boundary		Upstream boundary conditions		Downstream boundary condition
		Reach start	RKM	Reach end	RKM	Lowest modeled streamflow (ft^3/s)	Highest modeled streamflow (ft^3/s)	Normal-depth slope (m/m)
Harrisburg	28.5	McKenzie River confluence	282	Harrisburg	254	3,000	42,000	0.005
Peoria	51	Harrisburg	261	Corvallis	210	3,000	40,000	0.002
Albany	41	Corvallis	214	Santiam River	174	3,500	40,000	0.0008
Salem	58.5	Santiam River	182	Salem	120	5,000	80,000	0.001
Newberg	43.5	Salem	127	Newberg	82	5,000	80,000	0.0004

Model Calibration

Hydraulic Roughness and Model Calibration

Hydraulic roughness, an important parameter in hydraulic models, represents frictional resistance by the substrate and vegetation on flow and is commonly used as the primary variable to calibrate models. In this study, roughness was the only parameter used for calibration. HEC-RAS uses Manning's n coefficients (hereinafter referred to as "roughness coefficients") to represent hydraulic roughness. Continuous maps of roughness coefficients were generated by creating a dataset of vegetation canopy-height, which was produced by subtracting the bare earth DEM from the highest-hits DEM (Quantum Spatial Inc., 2018). Vegetation heights were grouped into six categories and each was assigned a roughness value (fig 8) based on common terrain-roughness references (for example, Barnes, 1967, and Chow, 1959).

This initial range of roughness coefficients was applied to each model reach and was refined within reasonable ranges using iterative model simulations until each reach-specific model produced water-surface elevations (WSEs) that best matched measured elevations (see section, "Datasets Used in Model Calibration and Validation"). The spatially continuous measurements of WSEs from sonar surveys (White and others, 2019) and the 2017 lidar dataset (Quantum Spatial Inc., 2018) were the primary datasets used to calibrate roughness coefficients in main channel areas. Roughness coefficients for overbank areas (where vegetation height generally ranged from 4 to 10 m) were calibrated by comparing simulated WSEs with measurements of WSEs from USGS streamgages the only known source of high-accuracy WSE data for streamflow levels at which overbank areas are inundated.

Final roughness values in all five modeled reaches were similar. Within the main channel, where roughness is controlled primarily by the cobble substrate, roughness coefficients for each of the model reaches varied from 0.023 to 0.026. Overbank areas, which encompass a much broader variety of vegetation types and canopy heights than the main channel, from agricultural fields to mature forest, had a much broader range of roughness coefficients, ranging from 0.026 to 0.15 (table 5; fig 8).

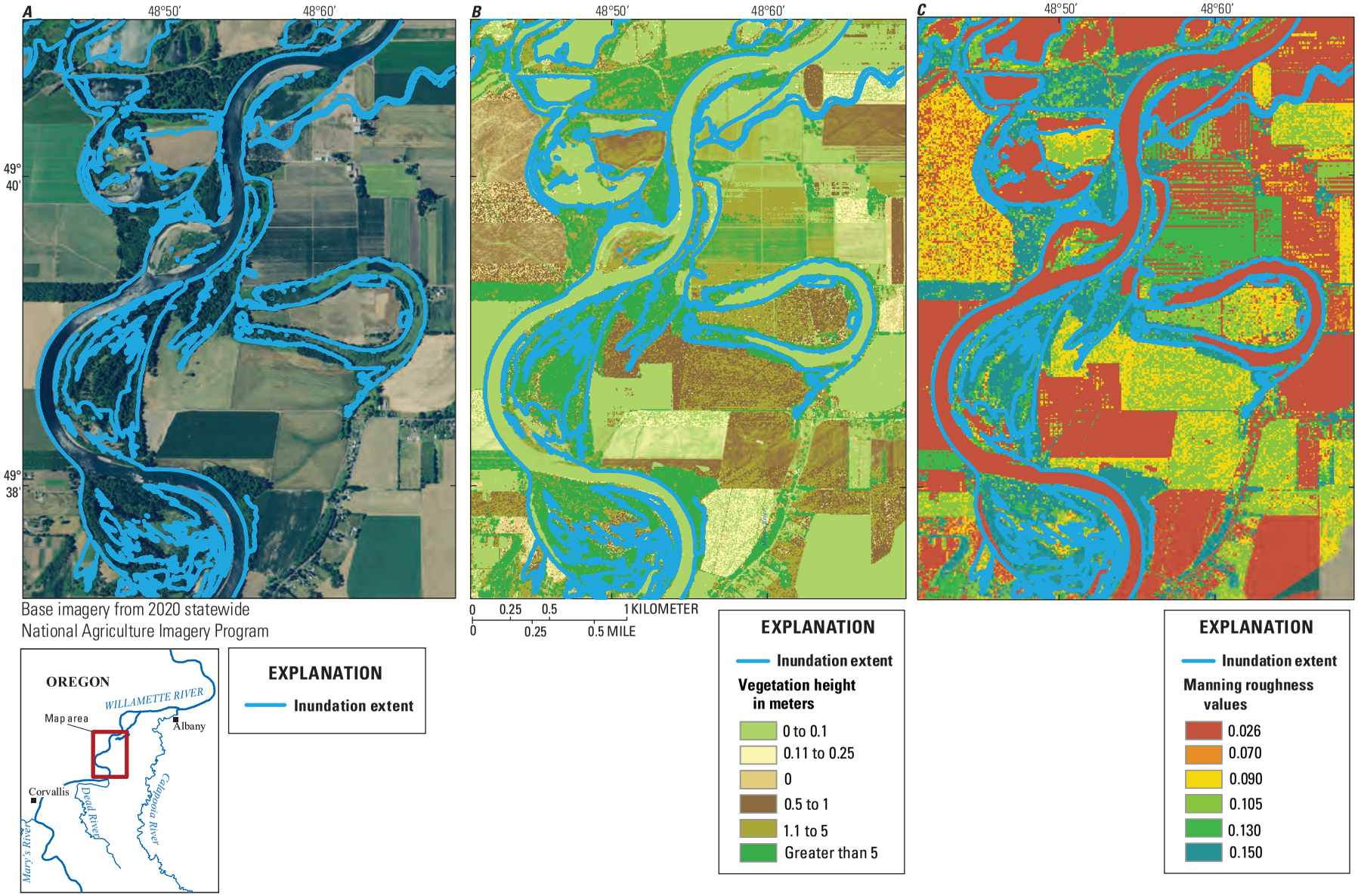

Figure 8. Example of hydraulic roughness development along the reach of the Willamette River between Corvallis and Albany, Oregon. *A*, shows modeled inundated extent *B*, represents binned canopy height, and *C*, shows final Manning's roughness coefficients used in the model.

Table 5. Summary of Manning's roughness coefficients used in each of the hydraulic model reaches on the Willamette River, Oregon.

[**Symbol:** >, greater than]

Model reach	Reach name	Categories of vegetation canopy height						
		Main channel	Vegetation height (meters)					
			0–0.1	0.11–0.25	0.26–0.5	0.51–1	1.1–5.0	> 5.0
McKenzie River confluence to Harrisburg	Harrisburg	0.026	0.026	0.065	0.085	0.105	0.13	0.17
Harrisburg to Corvallis	Peoria	0.026	0.026	0.07	0.09	0.105	0.13	0.15
Corvallis to Santiam River	Albany	0.026	0.026	0.07	0.09	0.105	0.13	0.15
Santiam River to Salem	Salem	0.025	0.025	0.08	0.11	0.125	0.17	0.2
Salem to Newberg	Newberg	0.026	0.026	0.065	0.085	0.09	0.11	0.13

Datasets Used in Model Calibration and Validation

To evaluate model performance, simulated and measured WSE values were compared at the same location and flow. Three types of WSE measurements were compared against modeled WSEs and used in the calibration process:

1.. Continuous measurements of water stage from USGS streamgages (U.S. Geological Survey, 2021) at Harrisburg (14166000), Corvallis (14171600), Albany (14174000), and Salem (14191000), which were converted to continuous measurements of WSE by adding measured stage to the streamgage datum. Data from the streamgage at Newberg (14197900) were not used, as this station is subject to backwater effects from the Newberg pool, and thus stage is not a reliable indicator of streamflow at the site.

2.. Spatially continuous measurements of WSE from longitudinal profiles of the water surface collected by sonar during bathymetric surveys for this study (White and others, 2019).

3.. Measurements of WSE made during acquisition of the 2017 topographic-bathymetric lidar dataset and published in lidar point clouds (Quantum Spatial Inc., 2018). Ten percent of lidar points classified as "water" within the Willamette River channel were extracted from the lidar point cloud dataset and compared with modeled WSE.

The three calibration datasets differ in their magnitudes of measurement uncertainty and utility to the calibration and validation of a model. The stage versus discharge rating curves from USGS streamgages generally had the lowest uncertainty, with WSE accuracies to within 0.1 m. The rating curves provide a basis for calibrating models and comparing modeled and measured WSE across all the streamflow values simulated in this study. Each rating curve represents a single location in a river network (a USGS streamgage); however, streamgages are generally located at sites where streamflow is confined to a single channel with minimal geomorphic complexity. Thus, the rating curves may not be representative of reach-scale hydraulic conditions. WSE from bathymetric surveys have estimated accuracies of roughly 0.2 m and points were generally collected longitudinally every 3–5 m along 10–20-km-long sections of the channel, thereby creating spatially expansive datasets for evaluating variation in WSE on long reaches of the Willamette River. Each dataset of surveyed WSE represents a single streamflow value, however, and within each of the modeled reaches, longitudinal profiles were collected for only a few streamflow levels. Finally, elevations of the Willamette River water surface from the 2017 lidar dataset have estimated accuracies of approximately 0.1 m (Quantum Spatial Inc., 2018), and are spatially continuous along the entire length of the river within the study area, but these data are available for only a single streamflow level (coinciding with conditions during lidar acquisition).

For each of the five modeled reaches, a series of validation simulations were run at streamflows similar to those during field data collection. However, each of the field data collection events took place over a period of several days and thus actual flow conditions varied during data acquisition, so that the resulting maps of WSE elevations indicate a range of streamflows. In some cases, variation in flow during a survey was modest (less than 200 ft^3/s) and resulting WSE data were deemed suitable for model calibration and validation. In instances in which more substantial changes in streamflow occurred during the field data collection period (typically more than 2,000 ft^3/s per day), the resulting WSE data were not used in model calibration or validation.

During the calibration and validation process, modeled WSE were exported to GeoTiffs (rasters) and overlaid by field survey and lidar derived datasets of WSE. The WSE data from each measurement point were then compared to the underlying value from the model output raster.

Simulated velocities were compared to measured values at USGS gaging stations to evaluate reliability of model results. Measured velocity data were obtained from acoustic Doppler current profiler measurements taken as part of regular USGS streamgage operations. Measurements used in model calibration and validation were limited to those made in 2017 or 2018, to minimize any potential channel changes since lidar data collection in 2017. A low- and high-flow measurement from each streamgage in the reach was simulated and matched

to the nearest modeled streamflow (table 6). To enable georeferencing, the measurements for which data were used were also limited to those that used Global Positioning System for bottom tracking. Once specific streamflow measurements were identified as meeting that requirement, all associated transect data from each measurement were processed with the Velocity Mapping Toolbox (Parsons and others, 2013) to generate georeferenced mean streamwise-velocity values every 1 m across the channel. Modeled velocity values were then extracted at each of these points and compared to measured values for accuracy.

Model Limitations

The hydraulic models developed in this study broadly characterize spatial patterns in Willamette River hydraulic conditions over a range of flows. The models are not intended to replicate specific observed or forecasted hydrologic events, and therefore represent a simplified characterization of conditions at a specified flow. For example, off-channel features, such as side channels, alcoves, or ponds, may have greater inundated extents at a particular flow than that represented in the model because of earlier conditions that may have established hydraulic connectivity with the adjacent main channel of the Willamette River, or because of precipitation or tributary inflows that are not represented in the model. Conversely, if summer streamflow increases rapidly, such as those which occurred in 2016 when the USACE released additional water from upstream dams to maintain cooler stream temperatures during a heatwave, off-channel features may not have the same inundation patterns as those depicted in the equivalent modeled streamflow because of the time it takes for the long reaches of the Willamette River to become inundated and equilibrated to a static flow condition.

Local river management actions also affect river hydraulics. For example, flashboards that are installed seasonally at Willamette Falls create a nearly 1-m backwater effect upstream through the Newberg Pool that extends for an unknown distance into the farthest downstream model reach. Finally, because the Santiam River was the only tributary explicitly included in the model, local hydraulic variation at and near other tributary confluences are not represented in the model results.

Hydraulic conditions in side-channels, alcoves, and various off-channel features of the Willamette River are complex, particularly in the more morphologically dynamic upper Willamette River. Some of these features (especially those in floodplain areas and adjacent to agricultural lands) have bridges, culverts and other anthropogenic barriers to inundation that affect hydraulic conditions in varying, but potentially large degrees, especially at higher streamflows. It is unknown to what accuracy these types of features were captured and represented with the lidar data and resulting model terrain. Additionally, bridges, culverts, and other structures were not explicitly included in the hydraulic models. While the hydraulic model results of this study provide broad characterization of inundation, water depths, and velocities at various flow conditions, these conditions are likely most accurate in the primary channels, where lidar and survey data can accurately capture bathymetric features. Additionally, the models developed in this study indicate the topographic, bathymetric, and hydraulic roughness conditions in underlying datasets collected from 2016 to 2017, and channel changes that occur in subsequent years may alter the hydraulic conditions represented by these models. Any application and site-specific analysis using the models of this study should confirm model performance using measurements of current, local hydraulic conditions.

The bathymetric data used in these models are primarily those collected in 2017, with additional, though less spatially dense, data from 2015–2018. Together, the combination of these data indicate river conditions at the time of collection. However, the Willamette River, like all rivers, is dynamic and will continue to change over time. While general trends in the distribution of depth, velocity, and inundated area are likely to persist, local changes may result in considerably different hydraulic conditions. These changes will increase over time and will be exacerbated by high flow events. Furthermore, conditions that drive hydraulic roughness, particularly vegetation, will change as vegetation matures or dies, thereby creating hydraulic conditions different from those simulated in this study. Because of such changes, any site-scale application of this model should involve verification of hydraulic conditions at the time of interest.

Table 6. Summary of flow measurements at U.S. Geological Survey streamgages on the Willamette River, Oregon (U.S. Geological Survey, 2021).

[Flow values used for velocity validation in hydraulic models. **Abbreviations:** mm-dd-yyyy, month-day-year; ft^3/s, cubic feet per second]

Flow value	Harrisburg		Corvallis		Albany		Salem	
	Streamgage 14166000		Streamgage 14171600		Streamgage 14174000		Streamgage 14191000	
	Measurement date (mm-dd-yyyy)	Flow (ft^3/s)	Measurement date (mm-dd-yyyy)	Flow (ft^3/s)	Measurement date (mm-dd-yyyy)	Flow (ft^3/s)	Measurement date (mm-dd-yyyy)	Flow (ft^3/s)
Low	09-17-2018	3,790	07-09-2018	5,030	08-15-2018	4,800	10-29-2018	8,190
High	04-09-2018	19,100	01-24-2018	21,700	04-12-2018	20,100	01-26-2018	60,800

Results and Discussion

Model Validation

The five hydraulic models developed for this study typically replicated measured water-surface elevations (WSEs) to within 0.2 m of observed conditions (fig. 9). Comparison of modeled WSE with spatially continuous measurements from sonar and lidar data do not show systemic bias in any modeled reach; however, nearly all individual validation datasets have a small degree of bias compared to measured data. With the spatially continuous data, no model reach shows a correlation between bias and streamflow, whereby models perform incrementally better or worse with increasing streamflows. Generally, neither sonar- nor lidar-sourced datasets show a consistent bias across model reaches, suggesting each method of comparison is reliable.

Comparison of simulated water-surface elevations and elevations measured at USGS gaging stations indicate that models perform reasonably well across the spectrum of simulated flows (fig. 10). At three of the four sites where model results were compared with data from the gaging stations, however, a correlation between magnitude of flow and residual model error is apparent. Model results from the Harrisburg and Corvallis streamgages (USGS 14166000 and 14171600, respectively; U.S. Geological Survey, 2021) show that the magnitude of error increases with modeled flows greater than 15,000 and 20,000 ft³/s, respectively. At the Harrisburg streamgage, the model overestimates WSEs at flows greater than 15,000 ft³/s, whereas at the Corvallis streamgage, the model underestimates WSE for flows greater than 20,000 ft³/s. Modeled WSEs at the Albany streamgage (USGS 1417400) show that the magnitude of residual error gradually increases with flow, reaching a maximum of 0.25 m at 40,000 ft³/s. Albany is the only streamgage at which the model results reveal consistent bias, where modeled WSEs are consistently higher than measured WSEs (as indicated by a negative residual) at all modeled flows. Modeled WSEs at the Salem streamgage (USGS 1419100) show an excellent match with measured WSEs, whereby the magnitude of model residuals are less than 0.1 m. Overall, these results represent the best balance that could be achieved by leveraging the available validation and calibration data to minimize errors across a spectrum of flows throughout the 200-km modeled reach of the Willamette River. Although it was possible to achieve smaller errors at specific gaged locations by using different roughness values, these changes resulted in greater errors in the spatially continuous validation dataset. Modeler judgement was used to determine the best balance and distribution of error between the various validation data sources.

Discrepancies between modeled and measured values of WSEs have several possible sources and determining the precise sources of error throughout the large study area is challenging. A likely source of error common to all five modeled reaches, however, is the simplified hydrologic boundary conditions applied to each reach. The boundary conditions for most reaches are modeled using a single inflow transect and model results reflect a suite of static streamflows. During

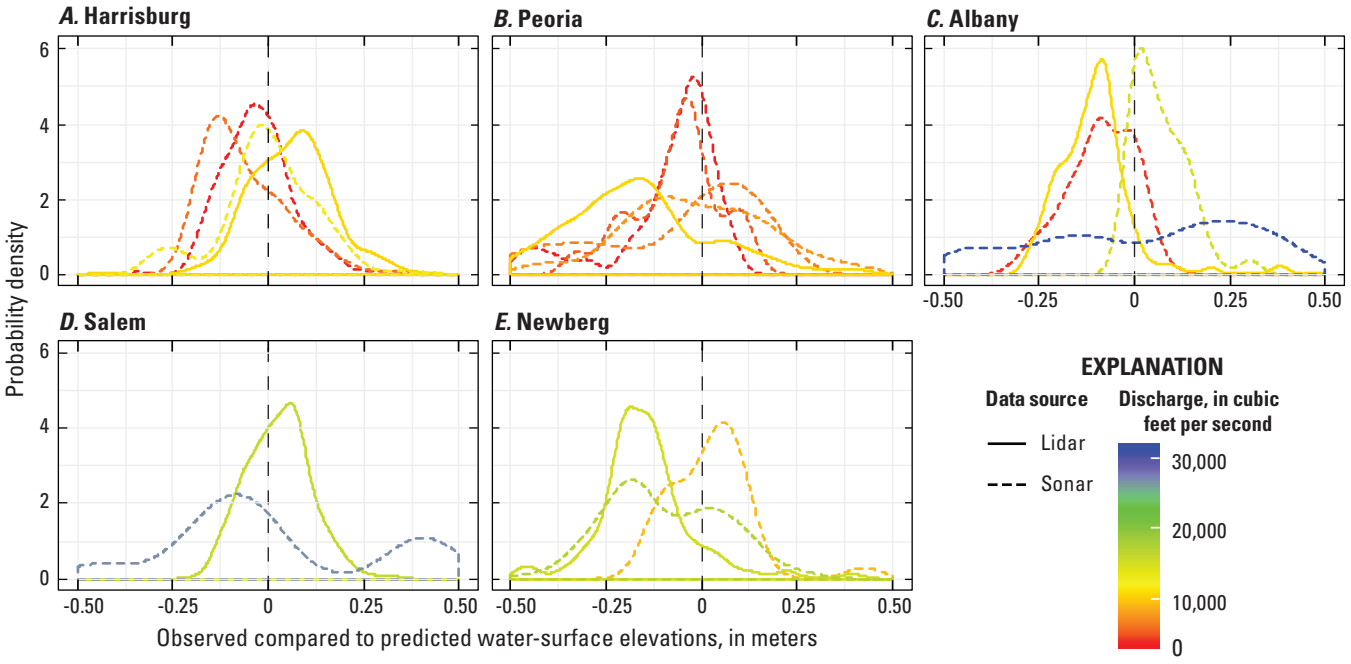

Figure 9. Relative distribution of model error (from probability density functions) for each of the five modeled reaches of the Willamette River, Oregon. Distribution of model error is determined by subtracting modeled water-surface elevations produced by the hydraulic models from measurements of water-surface elevation from sonar and lidar data.

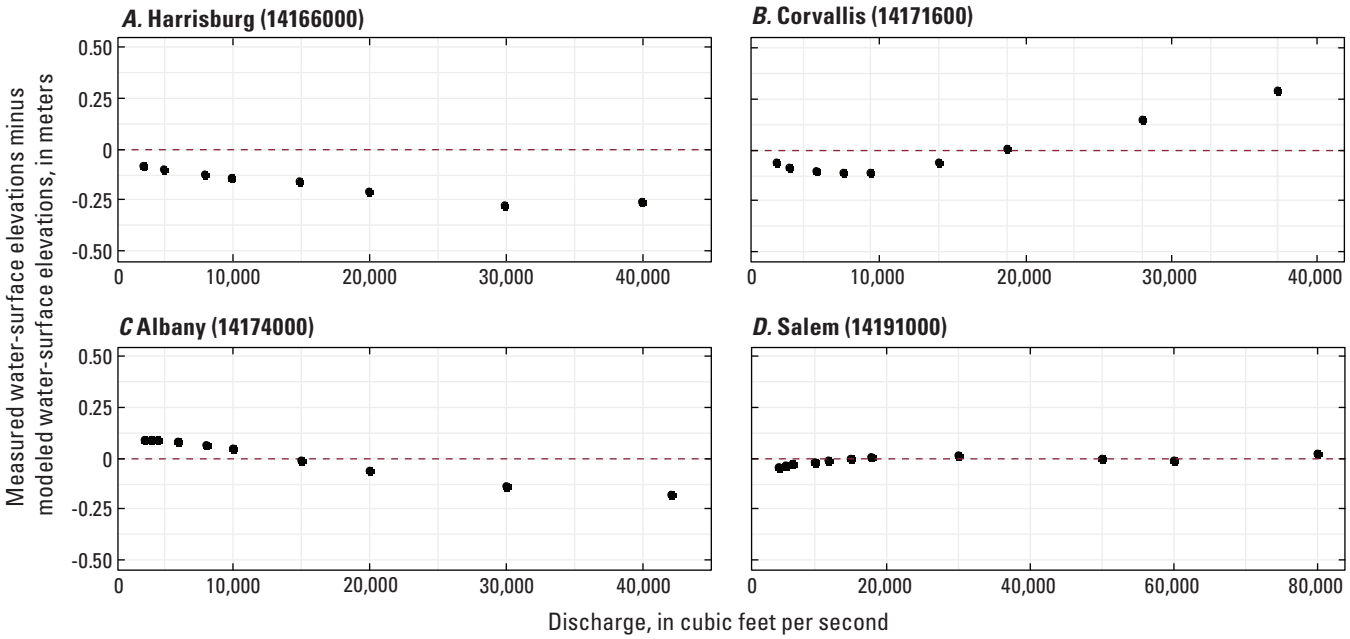

Figure 10. Difference between measured and modeled water surface elevations at U.S. Geological Survey streamgages (U.S. Geological Survey, 2021) for the range of flows simulated in this study, on the Willamette River, Oregon.

model validation trials, streamflow conditions that occurred during sonar and lidar surveys were simulated in model runs to produce outputs that would be comparable to the WSE during those surveys. For each reach, the calibration simulations were created by implementing hydrologic boundary conditions that matched average daily streamflow during the period of WSE data collection as determined from measurements at nearby USGS streamgages. For some of the measured WSE datasets, changes in daily streamflow were moderate (greater than about 1,000 ft^3/s). In such cases, the simulated WSE may not be representative of the measured WSE, because the measured WSE may reflect flows that are slightly greater than, or less than, the simulated flow. Another potential source of error within the validation data is a consequence of the pitch and roll of the boat during sonar surveys that is unaccounted for in WSE data, which uses a single value of instrument draft. The potential error created by pitch and roll of the boat is likely greater in downstream reaches, where larger boats were used at higher speeds, and may explain the greater range of error in the validation data in reaches of the Willamette River between Corvallis and Newberg. Finally, roughness in this model is primarily parametrized by vegetation height, whereas actual roughness is controlled by many factors, including vegetation type and density, and bank and substrate composition. The resulting simplification of roughness may result in areas of erroneous model results.

Comparisons of measured and modeled velocities show that modeled velocity captures the trends and magnitudes of measured velocity reasonably well (fig. 11). Cross-sectional patterns of velocity are well captured where channel velocity is lowest along the banks before quickly accelerating across the channel. Results at low flow tend to underestimate velocities in the middle of the channel, on the order of approximately 0.1 m/s. Measured data generally show more variability than modeled results, which in turn show more smoothed velocities. This variability is likely an indication of the underlying bathymetry in these reaches, where the lidar was not able to detect the bed surface and thus the surface was interpolated between sonar points. Simulation results from Corvallis, Salem, and Albany suggest the modeled channel is slightly narrower than the measured channel. This narrowing is also attributable to the underlying bathymetry in these reaches where lidar was not able to detect the inflection point, or toe, of the banks, and thus the channel bed was interpolated to the nearest sonar point. In contrast, lidar was generally able to detect these areas in the upper reaches, where the modeled velocity aligns with measured values across the full cross section of the channel at both low and high flows.

General Patterns of Simulated Inundation Extent, Water Depths, and Velocities

To illustrate variation in inundation extents, water depths, and velocities that were simulated by the hydraulic models of this study, maps showing 2- to 5-km segments from each of the five modeled reaches were generated (app. 1). Maps were also generated to show simulated patterns of inundation for local areas within two morphologically distinct reaches (Harrisburg and Newberg reaches) and to highlight examples of local variation in inundated areas and wetted perimeters at various streamflow levels (figs. 12–13). Near RKM 95, within

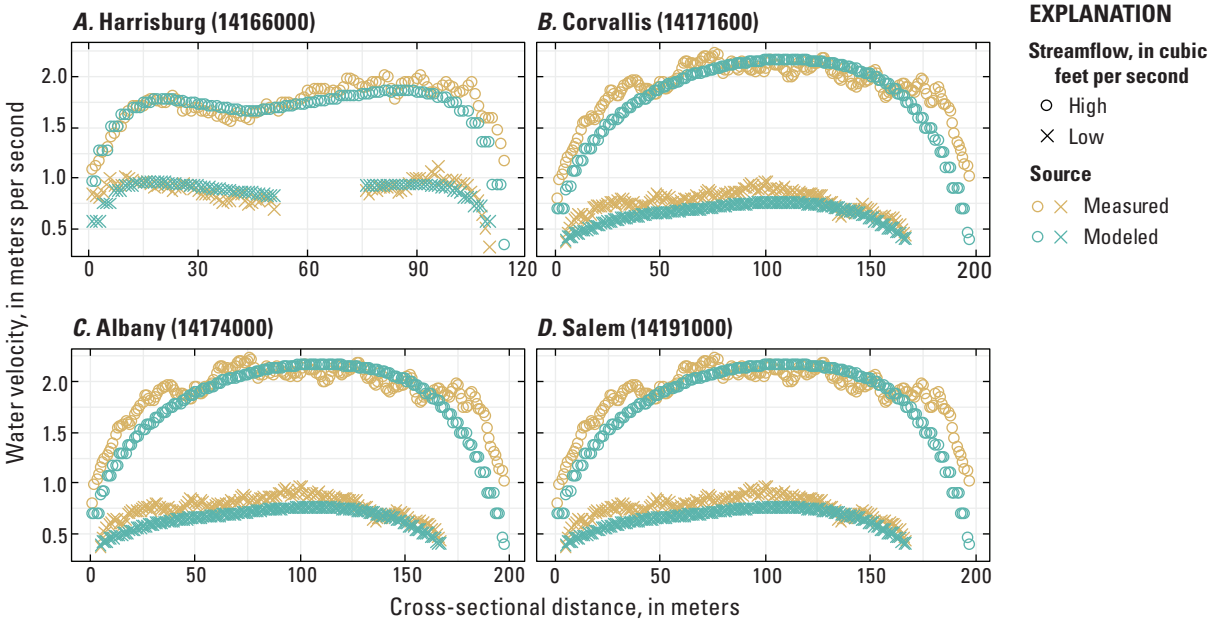

Figure 11. Measured compared to modeled water velocities at U.S. Geological Survey streamgages (U.S. Geological Survey, 2021) for a range of simulated flows on the Willamette River, Oregon.

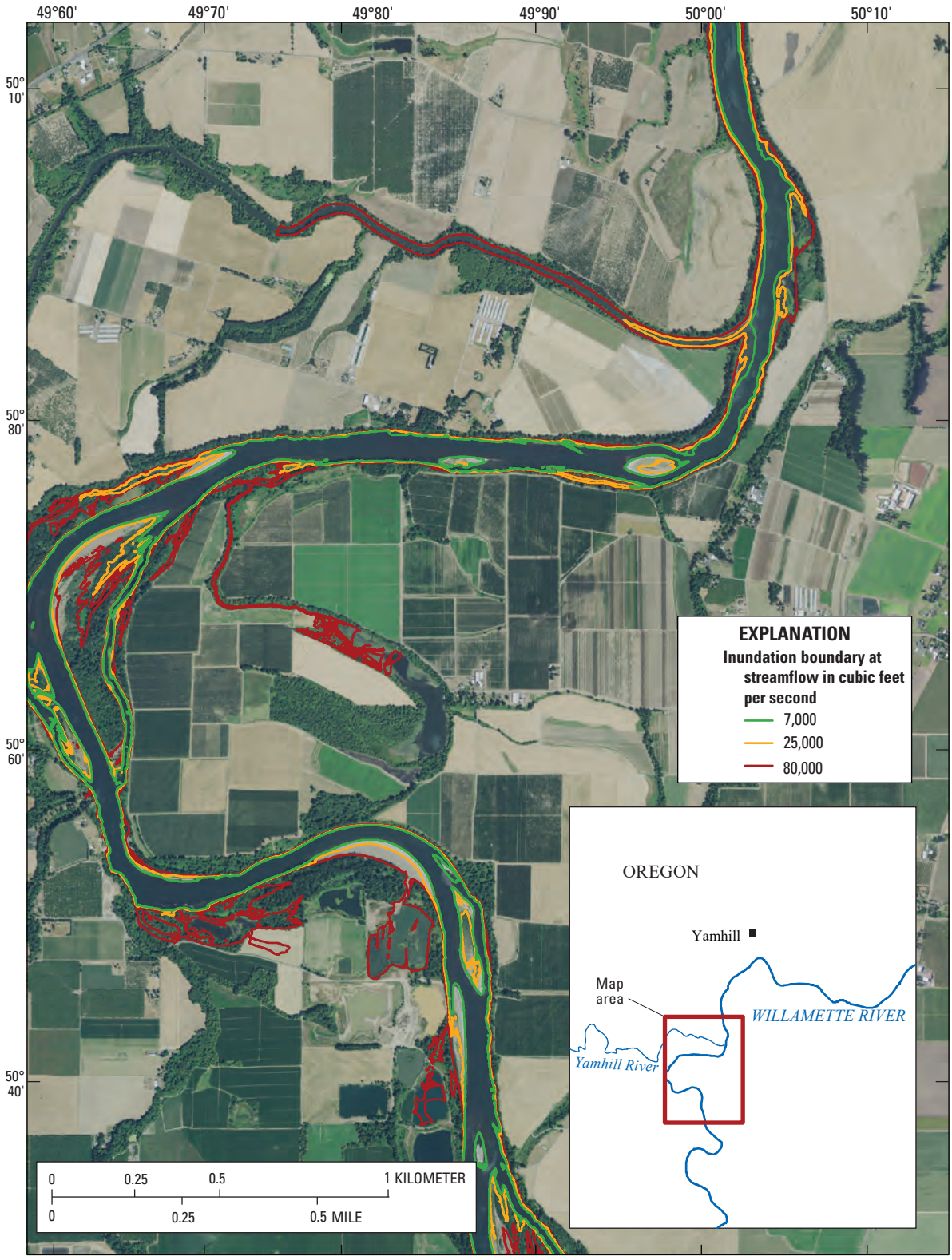

Base imagery from 2020 statewide National Agriculture Imagery Program

Figure 12. Examples of variation in simulated inundation extent with streamflow along River Kilometers 87–99 of the Newberg model reach, on the Willamette River, Oregon. The Newberg model reach is the most downstream modeled reach in this study.

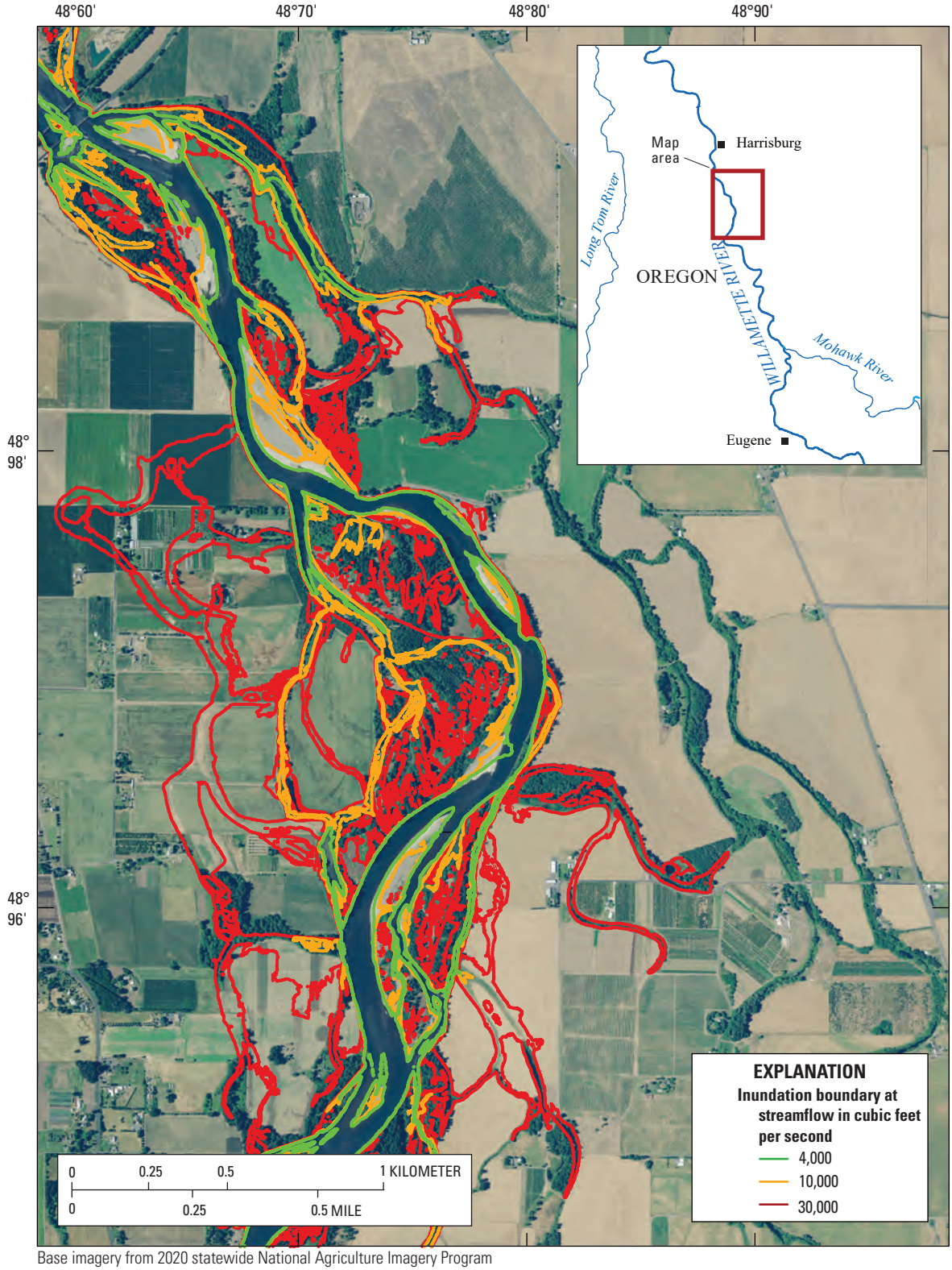

Figure 13. Example of variation in simulated inundation extent with streamflow along River Kilometers 262–270 of the Harrisburg model reach, on the Willamette River, Oregon. The Harrisburg model reach is the farthest upstream modeled reach in this study.

the Newberg reach (fig. 12), few changes occur in inundation extent between flows of 7,000 and 25,000 ft³/s. Even when flow increases to 80,000 ft³/s, changes in inundation extent are modest throughout much of the channel, although some off-channel features become wetted. In contrast, simulated inundation along RKM 262–270 of the Harrisburg reach (fig. 13) show systematic increases in inundation extent between flows and highlights the complex inundation patterns that occur along the upper Willamette River, where gravel bars and off-channel features are more numerous. Simulated inundation patterns in the Harrisburg reach also highlight how overbank areas of the upper Willamette River are more readily inundated by increasing streamflow owing to lower bank height than overbank areas along the downstream reaches (such as at RKM 95 in the Newberg reach), which require comparatively larger flows to become inundated.

Using channel cross sections to assess how WSE and inundated area respond to changes in streamflow provides a useful way to compare reaches at the site scale. Figure 14 shows a cross section and associated water-surface elevation at various flows at RKM 267 of the Harrisburg reach, whereas figure 15 shows a cross section in the most downstream (Newberg) modeling reach (RKM 124). These sections were selected for illustration because they are broadly representative of conditions within their respective modeling reaches. In the upstream reach (fig. 14), there are a considerable number of low-lying gravel and vegetated bars and side channels to inundate, even at low flows. At the highest simulated flows, only the highest elevations of gravel bars remain dry, while more side channels are filled, all features within the primary banks are inundated, and flows begin to spill into the present-day floodplain. The response to increasing flows in the downstream reach, where the channel is much more confined, provides a stark contrast; here, the bars and floodplains take considerably greater flow to become inundated. This change of channel form illustrates why inundated area and perimeter in downstream reaches are much less sensitive to increasing streamflow compared to upstream reaches, as flows are largely confined to the primary channel, with limited ability to reach floodplains and off-channel features. The channel form change also helps illustrate why depth and velocity increase at a faster rate in these more downstream reaches, as flows are largely confined to the primary channel, and water becomes deeper and faster with additional streamflow.

Reach-Aggregated Trends in Simulated Water Velocity and Depth with Changes in Streamflow

In all modeled reaches, increases in simulated streamflow resulted in increases in the magnitude and range of simulated water velocity and depth (figs. 16–17). To compare reach-aggregated patterns in water velocity and depth, and how these parameters vary with streamflow, model results for each simulated flow and for each computational cell were exported into reach-specific datasets. Simulated velocities at low flows (less than the 10th percentile) within each reach show bimodality, with highest densities at low velocities (typically less than 0.5 m/s) but with a minor mode typically near 1 m/s. As modeled streamflow increases, the low-velocity major mode becomes more pronounced and increases slightly, while the minor mode migrates to higher velocities. The minor mode likely consists of the channel thalweg and its immediate surroundings. In the two most upstream modeled reaches, Harrisburg and Peoria, the area of low velocity increases sharply with added streamflow, while downstream reaches tend to show increased low velocity area only at the highest flows. This condition is a product of the extent of the wetted area of these reaches being more sensitive to added streamflow, thus additional flow results in large areas of relatively low-velocity areas. Across all model reaches, higher streamflow always resulted in higher mean and peak velocities.

The distribution of depths along each reach at increasing streamflow are generally similar to velocity results; all flows and reaches show bi-modality, whereby the major mode centers at less than 0.5 m depth, indicating a major part of the inundated area is situated in shallow areas that are typically nearshore. A lesser, although still substantial part of the inundated area (represented by the minor mode within each of the reach plots of fig. 16), lies within deeper areas of the channel, typically representing the thalweg. Whereas the thalweg areas of the stream channel represented by the minor mode show increasing water depths with increasing streamflow across all modeled reaches, the shallow areas of the channel constituting the major mode expand with increasing streamflow, indicating shallow inundation of bars, islands, and floodplains.

Reach-scale trends in channel hydraulic characteristics can also be identified when looking at the 10th-, 50th-, and 90th-percentile depth and velocity values at each streamflow (fig. 18). Together, these factors indicate general trends in the low, median, and high values for depth and velocity for each modeled streamflow. Results of the simulations show that peak water depths, those in the 90th percentile, increase with additional flow, and these peak depths generally increase with distance downstream. However, areas with moderate and shallow depths, those in the 50th and 10th percentiles, respectively, begin to decrease in the middle of the modeled range of streamflows. This decrease of depth is a result of the increased inundation of shallow areas associated with high streamflows, as indicated in figure 17.

Trends in simulated velocities are similar to those in depth, whereby the highest velocities increase with distance downstream and with increases in streamflow; the 50th- and 10th-percentile velocities, however, generally peak at moderate flows before decreasing sharply (fig. 19). This decrease is a result of the increase in extent of shallow, low-velocity areas as water overtops the primary channel and inundates adjacent bars and off-channel features. In four of the five modeled reaches, as streamflow increases, the 50th-percentile velocity approaches the 10th-percentile velocity, further highlighting the expansive areas of low velocity as water inundates overbank areas outside the main channel. The 50th- and 10th-percentile velocities decrease more rapidly than their depth counterparts, indicating that channel friction imparted by vegetation, rather than shallow depths, plays a dominant role in slowing the water.

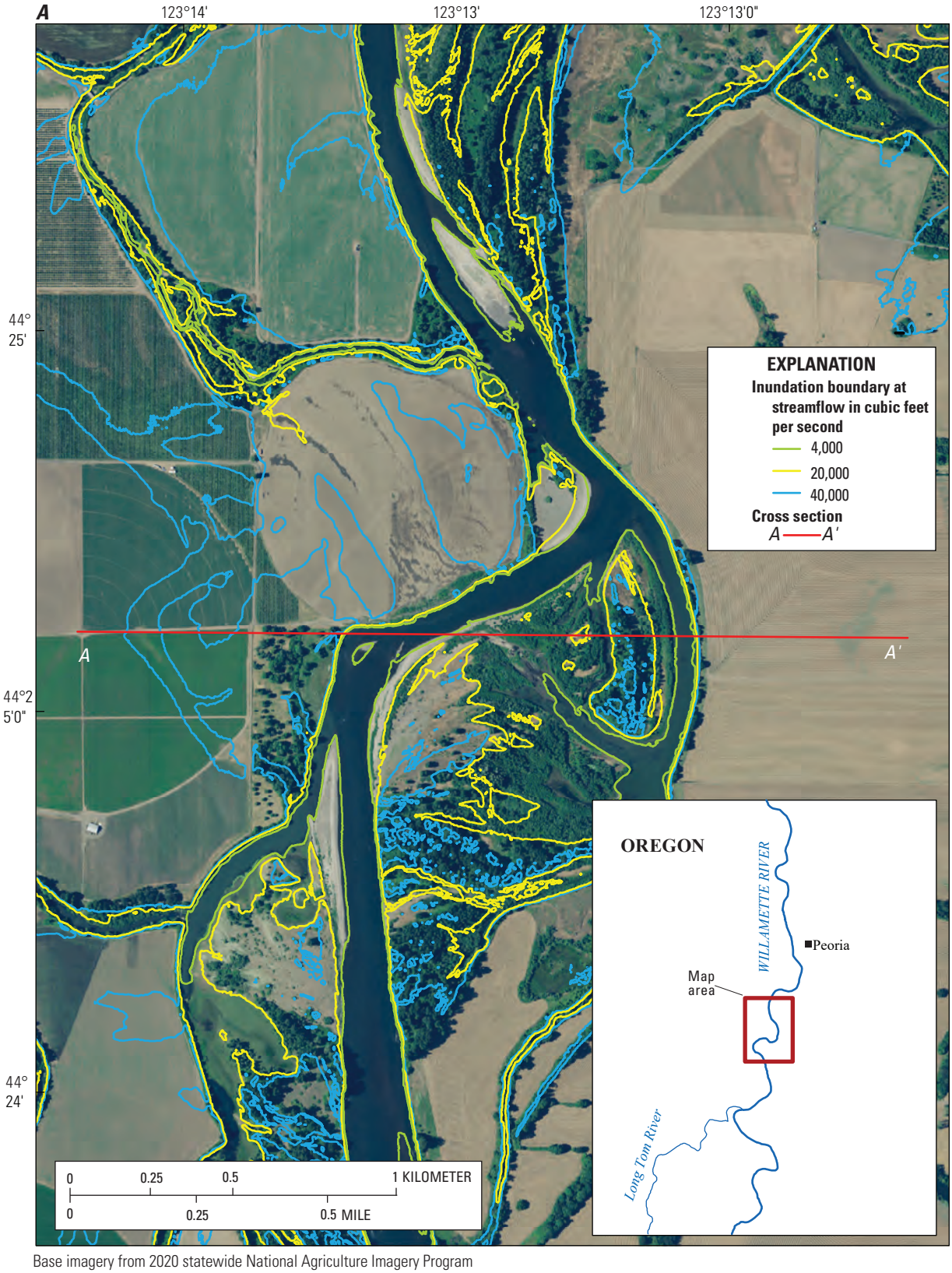

Base imagery from 2020 statewide National Agriculture Imagery Program

Figure 14. *A*, simulated extent of inundation and *B*, cross section showing corresponding water-surface elevations at various flows near River Kilometer 267, Willamette River, Oregon.

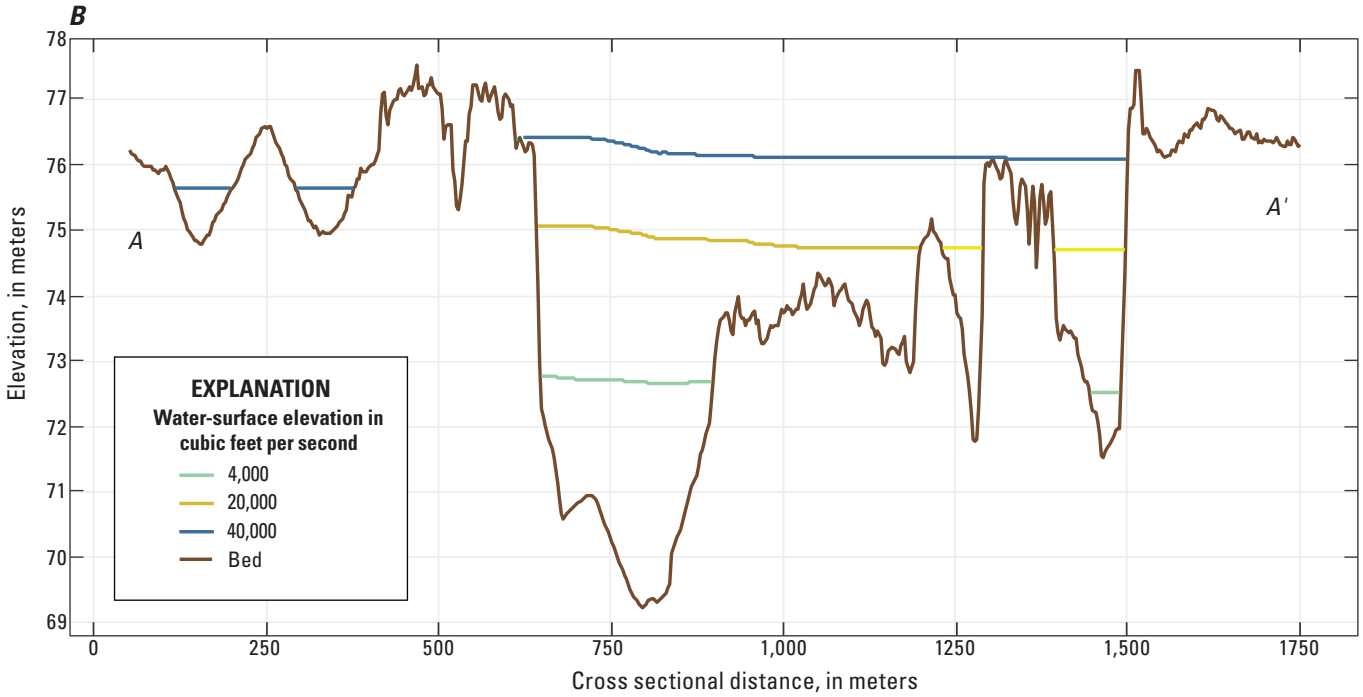

Figure 14.—Continued

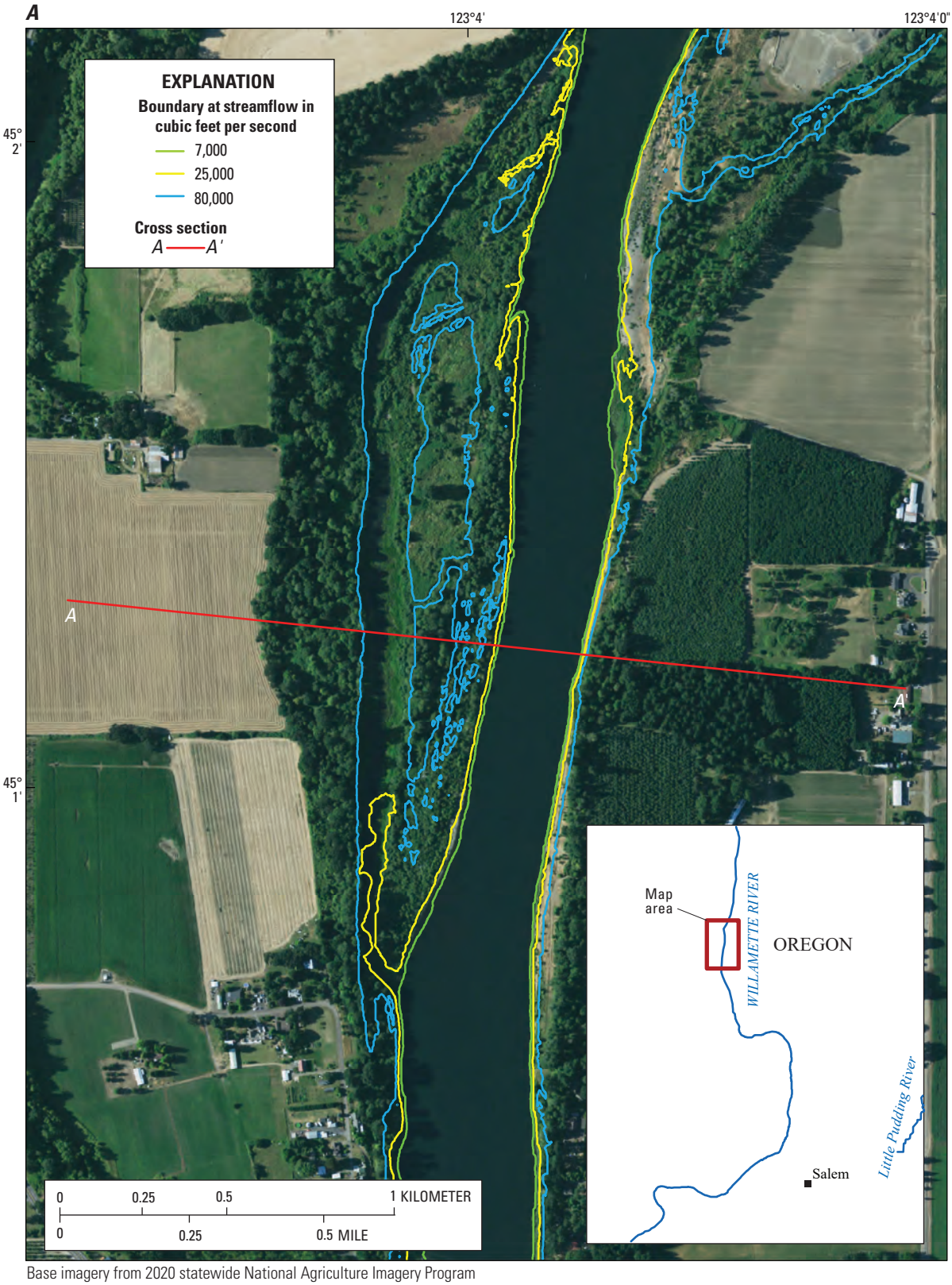

Base imagery from 2020 statewide National Agriculture Imagery Program

Figure 15. *A*, simulated extent of inundation and *B*, cross section showing corresponding water-surface elevations at various flows near River Kilometer 124, Willamette River, Oregon.

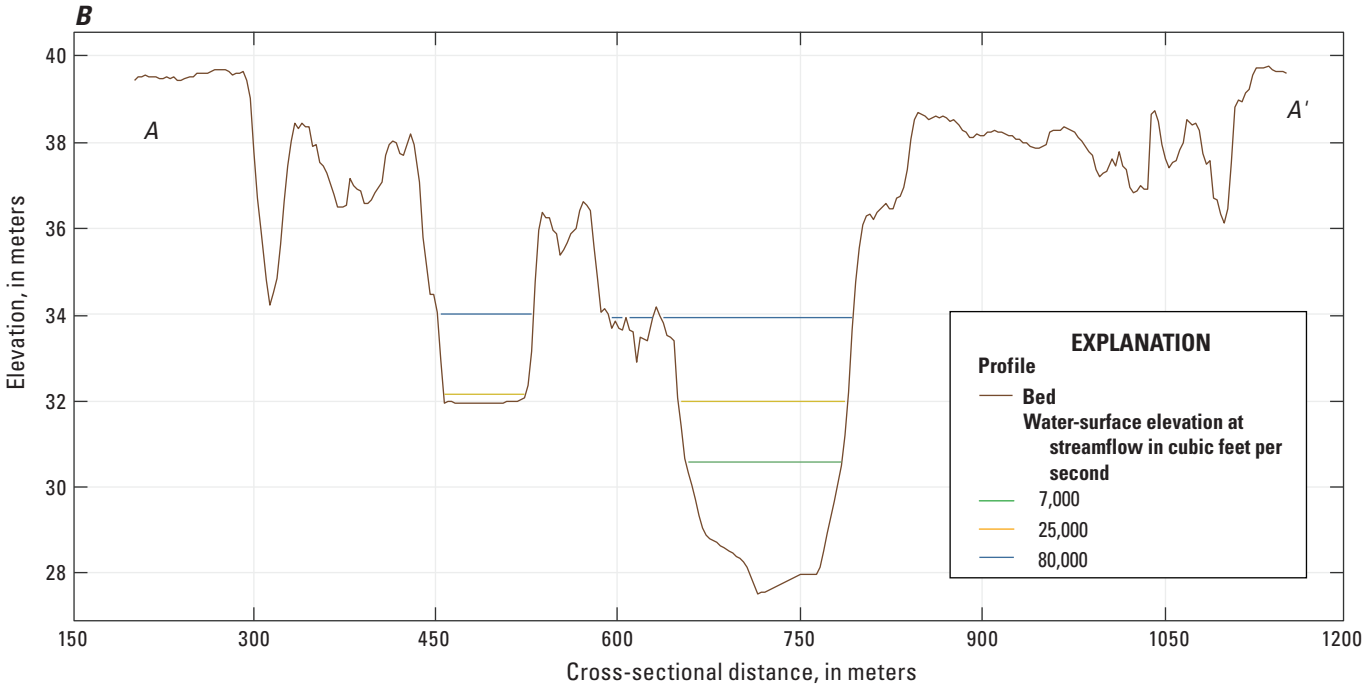

Figure 15.—Continued

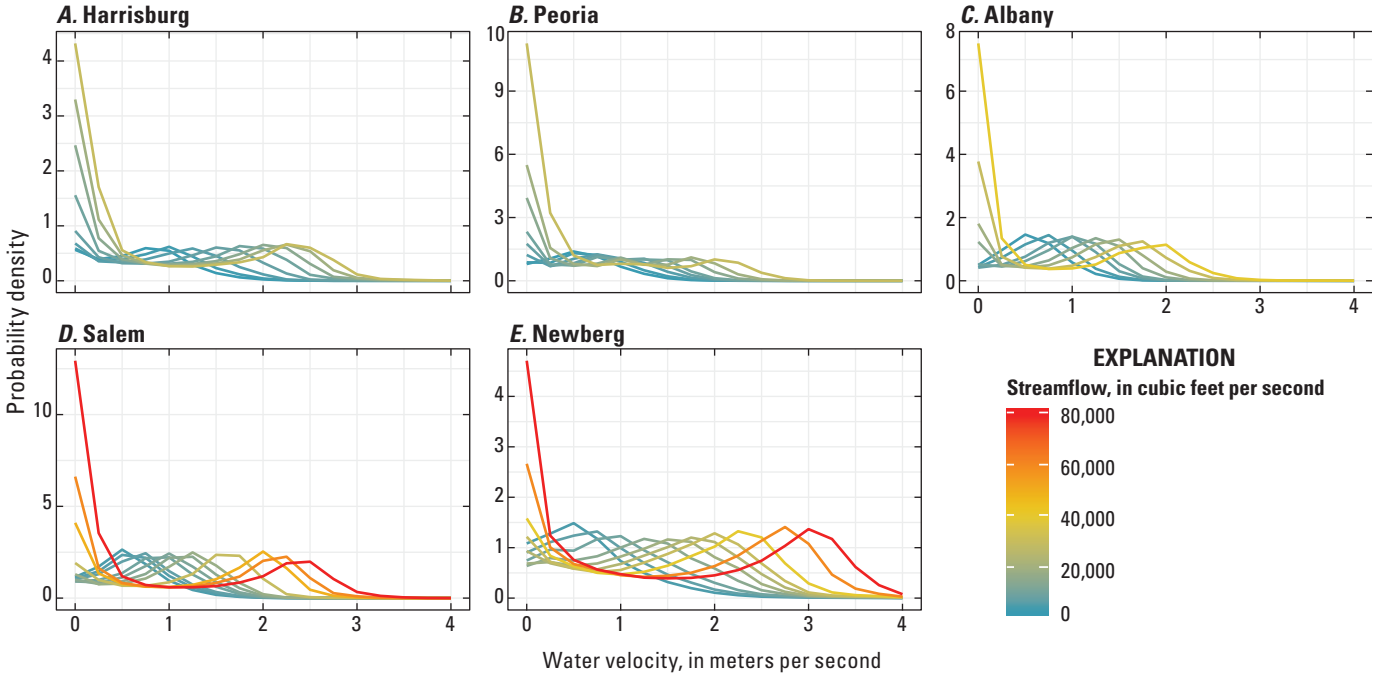

Figure 16. Relative distribution of water velocities (from probability density functions) along each modeled reach at each simulated streamflow, on the Willamette River, Oregon.

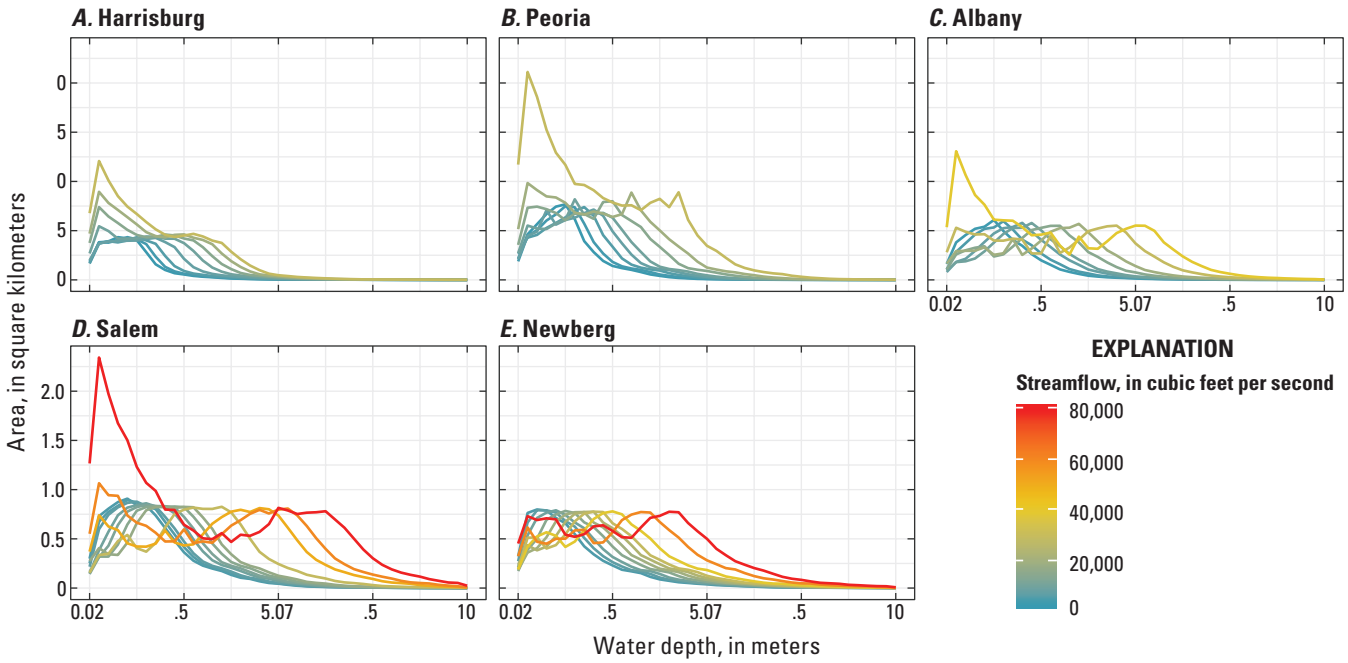

Figure 17. Distribution of water depth along each modeled reach at each simulated streamflow, on the Willamette River, Oregon.

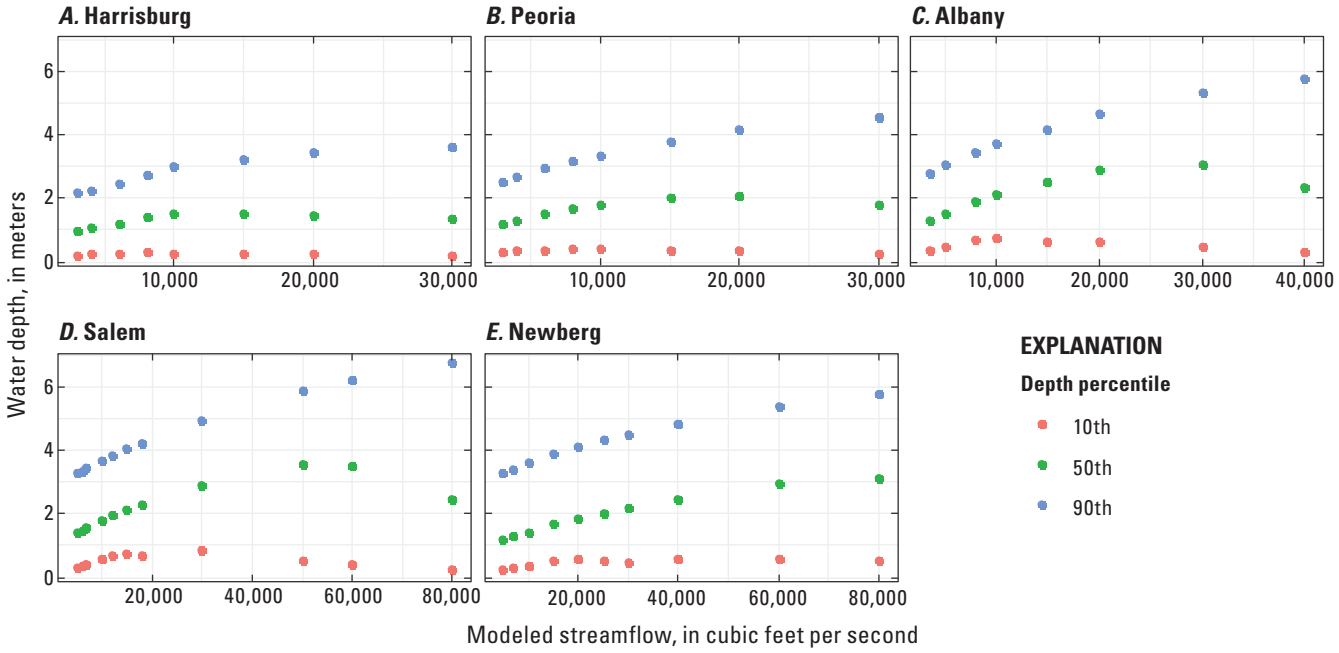

Figure 18. Variation in simulated water depths with streamflow, for model output from the 10th-, 50th-, and 90th-percentile velocity values within each modeled reach at specified streamflows, in the Willamette River, Oregon.

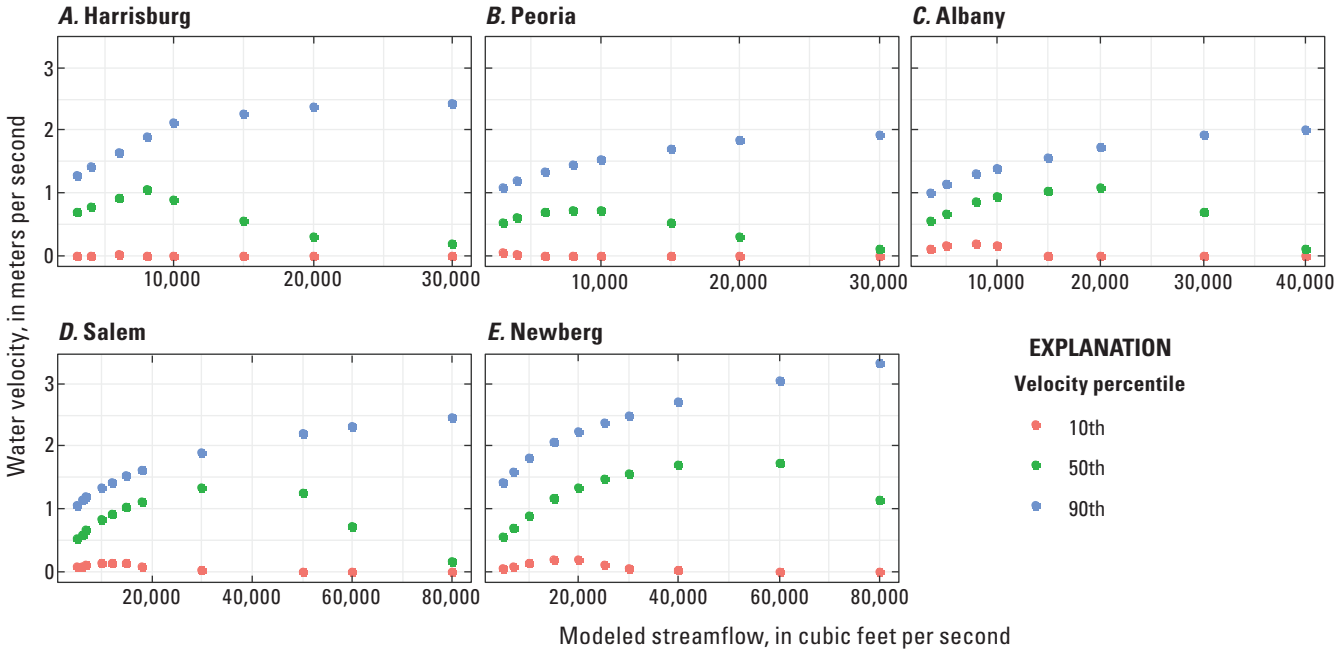

Figure 19. 10th-, 50th-, and 90th-percentile water velocity values within each model reach at specified streamflows, in the Willamette River, Oregon.

Reach-Aggregated Trends in Simulated Inundated Area and Wetted Perimeter with Changes in Streamflow

The total inundated area within each of the modeled reaches varied considerably with streamflow, reach length, and channel morphology. Because the lengths of the modeled reaches differed (table 4), the inundated area produced by each reach-specific model simulation was normalized by corresponding reach length to facilitate more direct comparisons between reaches (figs. 20–21). Comparisons of normalized inundated area reveal that for the Harrisburg and Peoria model reaches, inundated area increases linearly with streamflow. These reaches show the highest sensitivity of inundated area to increasing streamflow, whereby area is roughly doubled with each 10,000 ft^3/s increase in streamflow. From Corvallis to the confluence with the Santiam River (the Albany reach), the Willamette River has lower values of normalized inundated area at all but the lowest modeled streamflows, and inundated area is less sensitive to increasing discharge than upstream reaches. Downstream from the Santiam River confluence (along the Salem and Newberg Reaches), normalized inundated area at flows less than 10,000 ft^3/s is greater than in upstream reaches, but inundated area for these reaches is considerably less sensitive to added streamflow than the upper Willamette River reaches. As a result, an increase in streamflow of nearly 50,000 ft^3/s (from 10,000 to 60,000 ft^3/s) is required to double the normalized inundated areas in the Salem and Newberg reaches.

Differences in normalized inundated area (and by proxy, wetted width) between each of the five Willamette River models indicate longitudinal differences in channel geometry as well as hydrology (increasing volume of streamflow as tributaries enter the Willamette River). To better understand how inundated area varies across the range of typical streamflows and diverse channel morphologies of the five model reaches, model results were compared using the daily streamflow percentiles at each respective model reach (fig. 21; table 3). Results of this analysis show that from low to moderate flows (streamflow percentiles from 0.1 to 70 percent), the normalized inundated area is largest for downstream reaches (Salem and Newberg) and is nearly 50 percent greater than for the Harrisburg, Peoria, and Albany reaches (fig 21). As streamflows increase above the 70th percentile, normalized inundated area is largest on the upper Willamette River reaches (Harrisburg and Peoria; fig 21).

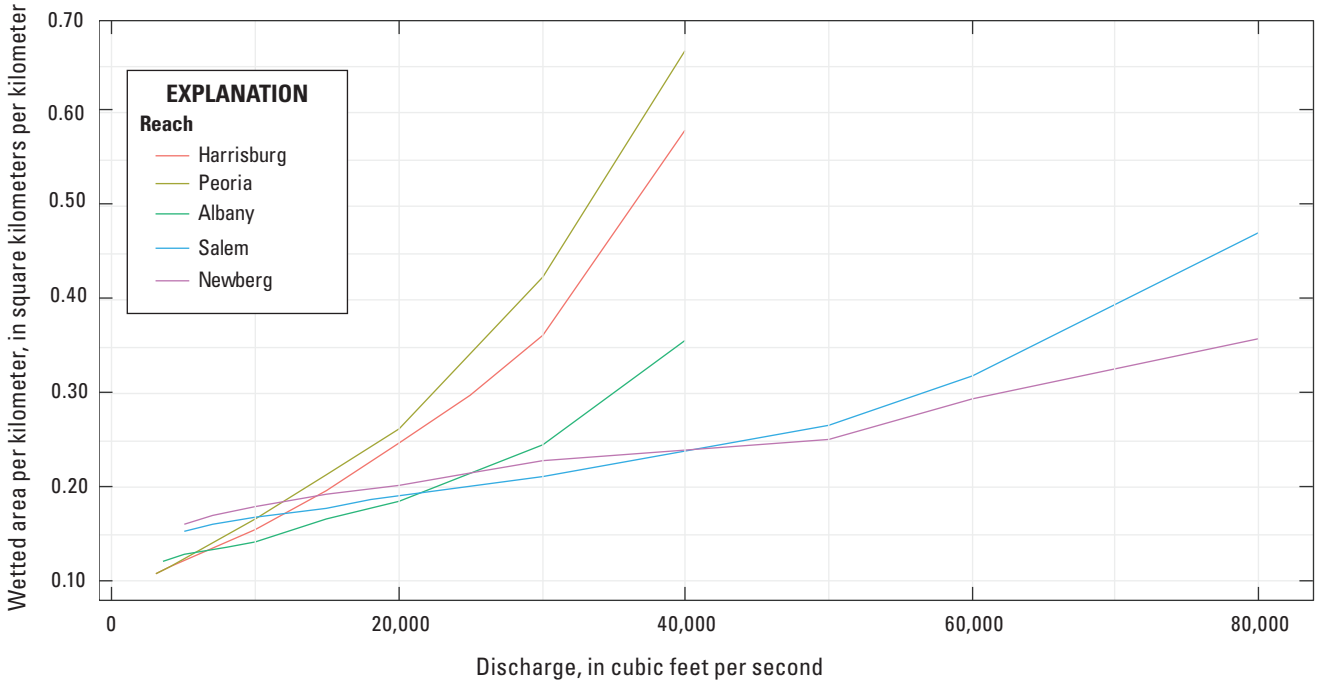

Figure 20. Normalized wetted perimeter at various streamflows for each reach, Willamette River, Oregon. Wetted perimeter for each simulated streamflow and modeled reach is normalized by the corresponding reach length (table 4).

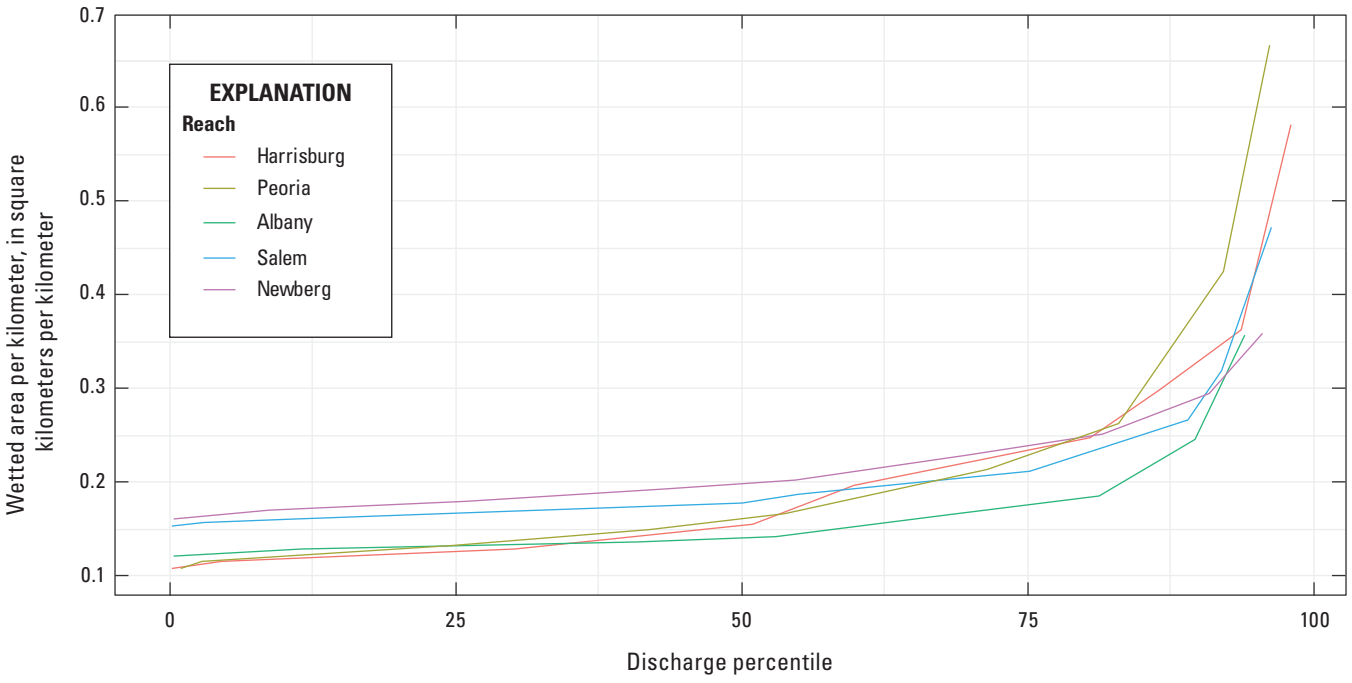

Figure 21. Comparison of simulated inundated area with streamflow, Willamette River, Oregon. Modeled inundated area for each of the model reaches is normalized by reach length of corresponding hydraulic models and streamflow is normalized by percentile of daily flow.

Similar analyses were made on the relation of wetted perimeter to simulated streamflow in each modeled reach. When the wetted perimeter at each simulated flow was normalized by total reach length, the trends in the perimeter largely followed those of the inundated area. The farthest upstream reaches have considerably greater wetted perimeter per kilometer of river than the downstream reaches at nearly all flows (fig 22, table 7). The largest wetted perimeter values at all modeled reaches occur at the highest streamflow; within downstream reaches (Salem, Newberg), however, maximum normalized wetted perimeter is roughly half that of the upper reaches (Harrisburg, Peoria). A comparison of wetted perimeter at normalized streamflows (fig 23) further highlights differences in hydraulic characteristics among the upstream and downstream reaches of this study. The Harrisburg and Peoria reaches respond similarly to increased streamflow, with considerable linear gains in wetted perimeters. In contrast, normalized wetted perimeter in the farthest downstream reach, Newberg, is greater than that in the Peoria reach at the lowest modeled flows, but is rapidly surpassed by other reaches as flow increases. At the highest modeled streamflows, the Newberg Reach has least amount of normalized wetted perimeter. Wetted perimeters along the Albany and Salem model reaches respond almost identically to increasing streamflows, and consistently indicate nearly one-half of the wetted perimeter as the upper reaches (Harrisburg, Peoria).

Synthesis of Findings

Taken together, the findings of this study indicate the underlying diversity of channel forms in the Willamette River and exemplify previous work that explored the geomorphology of the river (Wallick and others, 2013). The upper Willamette River is a morphologically complex stream with multiple channels, whereas in its lower reaches the river becomes increasingly entrenched by high-elevation floodplains with few side channels or gravel bars. Key findings of the study indicate that:

- Along the upper Willamette River between Eugene and Corvallis, relatively low bank heights and complex channel and floodplain morphologies allow rising streamflows to easily inundate channel-flanking bars, off-channel features, and the floodplains. Because the forested bars and floodplains along the upper Willamette River are large, numerous, and commonly bisected by swales and channel-like features, the flow of water into overbank areas and adjacent off-channel features produces complex inundation patterns at the low, moderate, and high flows simulated in this study (fig. 14). As a result of these complex inundation patterns, inundated area and perimeter rapidly increase with rising streamflow; water depths and velocities in overbank areas are lower compared to those within the thalweg; and a greater proportion of the inundated area has lower velocities and depths compared to those in downstream reaches for flows of similar magnitude (figs. 16–17).

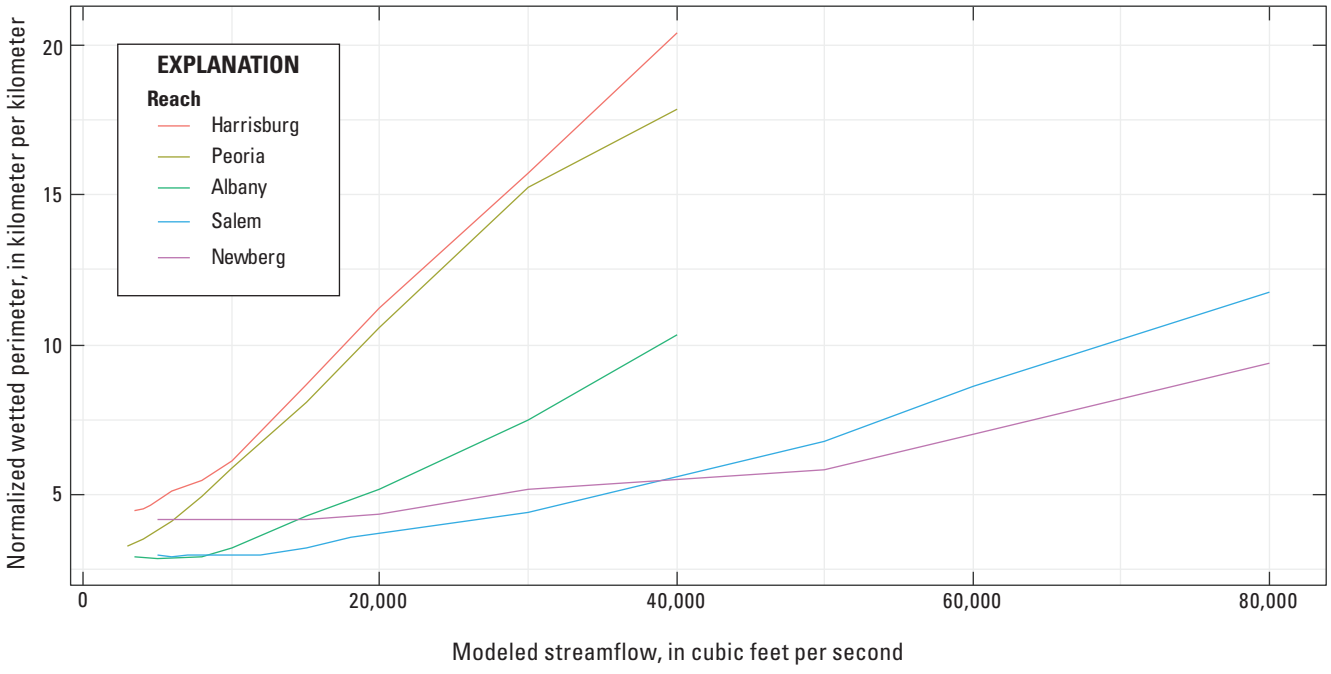

Figure 22. Variation in reach-aggregated wetted perimeter with streamflow. Wetted perimeter simulated by hydraulic models is normalized by reach length, Willamette River, Oregon.

Table 7. Summary of inundated area and wetted perimeter values for each reach simulated streamflow value and corresponding flow percentile, Willamette River, Oregon.

[**Abbreviations:** ft^3/s, cubic feet per second; km, kilometer; km/km, kilometer per kilometer; km^2, square kilometers]

Model reach name	Reach length (km)	Simulated streamflow		Simulated inundated area		Simulated wetted perimeter	
		Streamflow (ft^3/s)	Streamflow percentile (percent)	Inundated area (km^2)	Normalized inundated area (km^2)	Inundated perimeter (km)	Normalized perimeter (km/km)
Harrisburg	28.5	4,000	5	3.30	0.12	129.50	4.54
		10,000	51	4.43	0.16	174.54	6.12
		30,000	87	10.33	0.36	448.19	15.73
Peoria	51	4,000	3	5.95	0.12	178.89	3.51
		10,000	54	8.54	0.17	301.17	5.91
		30,000	92	21.71	0.43	778.37	15.26
Albany	41	5,000	3	5.26	0.13	116.71	2.85
		10,000	53	5.83	0.14	132.79	3.24
		30,000	90	10.10	0.25	306.95	7.49
Salem	58.5	6,000	3	9.25	0.16	171.87	2.94
		15,000	50	10.43	0.18	188.21	3.22
		60,000	89	18.72	0.32	503.58	8.61
Newberg	43.5	5,000	1	7.02	0.16	180.92	4.16
		15,000	55	8.36	0.19	181.76	4.18
		60,000	91	12.84	0.30	304.16	6.99

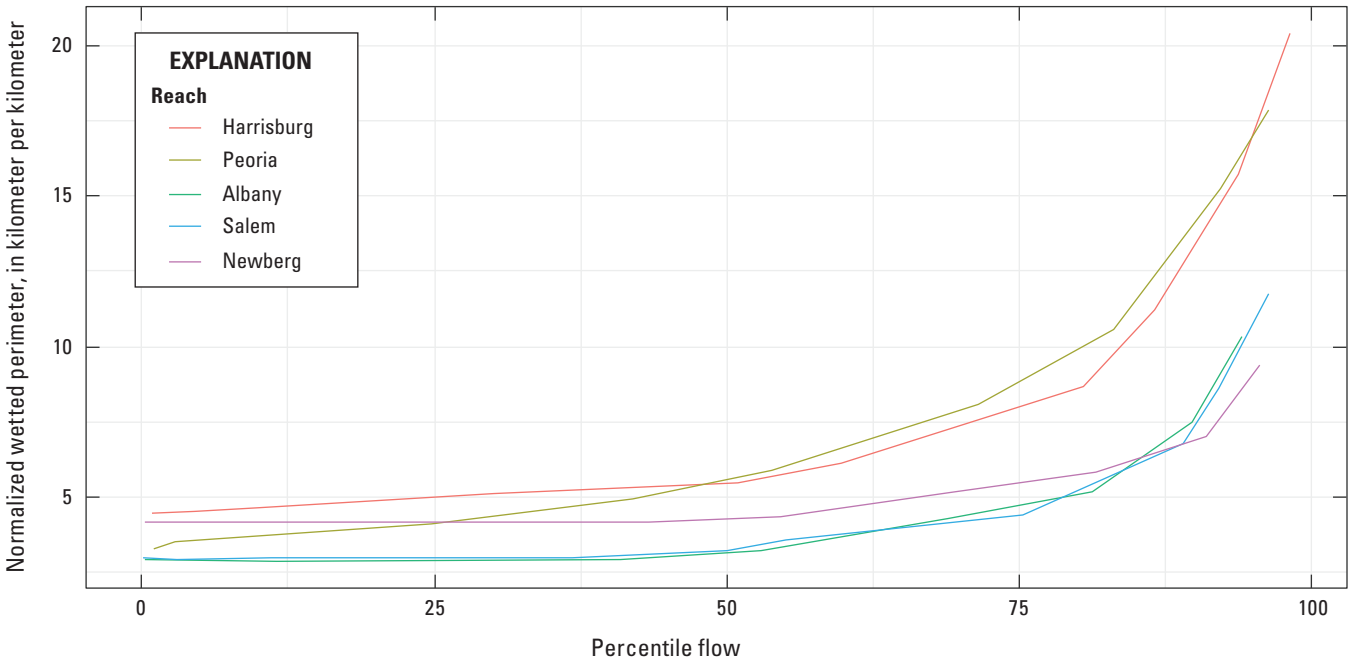

Figure 23. Variation in reach-aggregated wetted perimeter normalized by percentile streamflows. Wetted perimeter simulated by hydraulic models is normalized by reach length, Willamette River, Oregon.

- Along the middle Willamette River, the reach between Corvallis and Newberg Pool, the main channel of the river is increasingly confined (in a downstream direction) to a single channel, occurrences of gravel bars and off-channel features diminish, the gradient decreases, and bank height rises. These morphological transformations, coupled with increases in the width of the low-flow channel and increasing volume as tributaries enter the main-stem Willamette River, produce hydraulic conditions distinct from those in the upper Willamette River. At lowest flows, these middle reaches have wider wetted widths (fig. 15), but as flows increase, wetted width remains relatively stable while channel depths increase until flows become high enough to inundate overbank areas. Unlike the upper Willamette River, the middle reaches have fewer gravel bars, side channels, and low-lying floodplain areas, which provide fewer opportunities for complex inundation patterns to occur at moderate flows. As a result, increasing flows in the Albany, Salem, and Newberg reaches cause water depths and velocities to steadily increase while wetted width and perimeter remain largely static until overtopping occurs. Altogether, the Willamette River between Corvallis and Newberg has higher water depths and velocities for moderate to high flows compared with the upper Willamette River reaches (figs. 16–17).

Conclusion

Detailed bathymetry and hydraulic models of a river provide a method to characterize water depth, velocity, and inundated area at specified flows. Comparisons of the results of simulations made with hydraulic models of the Willamette River in Oregon developed in this study to observed conditions show that models can replicate observed conditions reasonably well across a wide range of flows.

The Willamette River has a diversity of hydraulic characteristics throughout the 200-kilometer study reach, and distributions of depth and velocity across a wide range of flows vary with variations in local geomorphology and hydrology. Reaches of the river upstream from Corvallis typically have lower mean velocities than downstream reaches, while also generally having more shallow areas, despite having the highest gradient of the study area. Downstream reaches are more confined and tend to be deeper and faster.

Response to increases in streamflow varies longitudinally along the river. In the upstream reaches, total inundated area and wetted perimeter respond primarily to increases in flow, and depths and velocities are less sensitive to the greater flow. Downstream from Corvallis, however, where the channel is more confined with fewer gravel bars, off-channel areas are not available to inundate as flows increase. As a result, inundated area and perimeter are less sensitive to increased flow, resulting in a deeper main channel and greater velocities. It is not until at relatively high flows (greater than 85th-percentile flows) that off-channel features begin to become inundated, resulting in shallower and low-velocity areas.

The distribution of depth, velocity, and inundated area and how they respond to changes in streamflow are key variables in understanding the effects of flow management on aquatic habitats. These findings are important building blocks for understanding the distribution of aquatic habitats, how they vary with streamflow, and how sensitive those habitats may be to changes in streamflow and dam operations.

References Cited

Barnes, H.H., Jr., 1967, Roughness characteristics of natural channels: U.S. Geological Survey Water-Supply Paper 1849, 213 p.

Beck, H.E., Zimmermann, N.E., McVicar, T.R., Vergopolan, N., Berg, A., and Wood, E.F., 2018, Present and future Köppen-Geiger climate classification maps at 1-km resolution: Scientific Data, v. 5, no. 180214, accessed August 24, 2020, at https://doi.org/10.1038/sdata.2018.214.

Chow, V.T., 1959, Open channel hydraulics: New York, McGraw Hill, 680 p.

DeWeber, J.T., and Peterson, J.T., 2020, Comparing environmental flow implementation options with structured decision making—Case study from the Willamette River, Oregon: Journal of the American Water Resources Association, v. 56, no. 4, p. 599–614, accessed November, 2020, at https://doi.org/10.1111/1752-1688.12845.

National Marine Fisheries Service, 2008, Willamette Basin Biological Opinion—Endangered Species Act Section 7(a)(2) consultation: National Oceanic and Atmospheric Administration Fisheries Log Number F/NWR/2000/02117 [variously paged], accessed March 22, 2018, at https://media.fisheries.noaa.gov/2021-11/willamette-2008-biological-opinion.pdf.

Oregon State University, 2013, Prism climate group: Corvallis, Oregon State University web site, accessed August 19, 2013, at http://www.prism.oregonstate.edu/.

Parsons, D.R., Jackson, P.R., Czuba, J. A., Engel, F.L., Rhoads, B.L., Oberg, K. A., Best, J.L., Mueller, D.S., Johnson, K. K., and Riley, J.D, 2013, Velocity Mapping Toolbox (VMT): a processing and visualization suite for moving-vessel ADCP measurements. Earth Surface Processes and Landforms, Earth Surface Processes and Landforms, v. 38, p. 1244–1260, accessed June, 2020, at https://doi.org/10.1002/esp.3367.

Peterson, J. T., Pease, J. E., Whitman, L., White, J.S, Stratton-Garvin, L., Rounds, S., & Wallick R., 2021, Integrated tools for identifying optimal flow regimes and evaluating alternative minimum flows for recovering at-risk salmonids in a highly managed system. River Research and Applications, v. 38, no. 2, p. 293–308, accessed December 15, 2021, at https://doi.org/10.1002/rra.3903.

Quantum Spatial Inc., 2018, Willamette River, Oregon topo-bathymetric lidar: Technical Data Report, Contract # W91278-16-D-0112/0001, 39 p.

Simenstad, C.A., Burke, J.L., O'Connor, J.E., Cannon, C., Heatwole, D.W., Ramirez, M.F., Waite, I.R., Counihan, T.D., and Jones, K.L., 2011, Columbia River estuary ecosystem classification—Concept and application: U.S. Geological Survey Open-File Report 2011–1228, 54 p. [Also available at https://pubs.usgs.gov/of/2011/1228.]

U.S. Army Corps of Engineers, 2016, HEC-RAS river analysis system—Hydraulic reference manual (version 5.0): Davis, California, U.S. Army Corps of Engineers, accessed April 10, 2020, at https://www.hec.usace.army.mil/software/hec-ras/documentation/HEC-RAS%205.0%20Reference%20Manual.pdf.

U.S. Geological Survey, 2021, National Water Information System: U.S. Geological Survey web interface, accessed May, 2021, at http://dx.doi.org/10.5066/F7P55KJN.

Wallick, J.R., Grant, G.E., Lancaster, S.T., Bolte, J.P., and Denlinger, R.P., 2007, Patterns and controls on historical channel change in the Willamette River, Oregon, *in* Gupta, A.V., ed., Large rivers—Geomorphology and management: Chichester, United Kingdom, John Wiley and Sons, p. 491–516.

Wallick, J.R., Jones, K.L., O'Connor, J.E., Keith, M.K., Hulse, D., and Gregory, S.V., 2013, Geomorphic and vegetation processes of the Willamette River floodplain, Oregon—Current understanding and unanswered questions: U.S. Geological Survey Open-File Report 2013–1246., 70 p., accessed June, 2019, at https://doi.org/10.3133/ofr20131246.

Watershed Sciences, 2009, Lidar remote sensing data collection—Department of Geology and Mineral Industries, Willamette Valley Phase 1, Oregon: Portland, Oregon, Watershed Sciences, Technical Report, 40 p., accessed June, 2019, at https://www.oregongeology.org/pubs/ldq/reports/Willamette_Valley_Lidar_Report_2009.pdf.

White, J.S., Gordon, G.W., and Overstreet, B.T., 2019, Single-beam echosounder bathymetry of the Willamette River, Oregon, 2015–2018: U.S. Geological Survey data release, accessed November, 2019, at https://doi.org/10.5066/P92TTY4R.

Williams, J.E., 2014, Habitat relationships of native and non-native fishes of the Willamette River, Oregon: Corvallis, Oregon State University, Master's thesis, accessed June, 2019, https://ir.library.oregonstate.edu/xmlui/handle/1957/49883.

Glossary

Bare earth DEM. Digital elevation model (DEM) built from lidar point cloud that represents the topographic surface of the ground with vegetation digitally removed.

Bi-OP. Specific reference to the 2008 Biological Opinion on the U.S. Army Corps of Engineers (USACE) Willamette River Basin Flood Control Project (National Marine Fisheries Service, 2008).

Bi-OP Flow Objectives. The Bi-OP identified minimum flows (termed "Flow Objectives"; table 2–8, in National Marine Fisheries Service, 2008) for USACE dams to maintain adequate flows in downstream river corridors to support spring Chinook salmon and winter steelhead at various life stages. The Willamette River Flow Objectives referenced in this report are those for the U.S. Geological Survey streamgages on the Willamette River at Albany (14174000) and Salem (14191000) (U.S. Geological Survey, 2021), where Flow Objectives are established for different time frames extending from April 1 to October 31.

Breakline (HEC). A user-generated line at which a separation between computational mesh cells in the USACE Hydrologic Engineering Center River Analysis System (HEC-RAS) model program is forced as a means of defining feature boundaries.

Breakline (TIN). A user-generated line to which local cells are interpolated as a means to define linear topographic features that may not occur in a Triangular Irregular Network (TIN) interpolation without user intervention because of node spacing or areas with data gaps.

Highest hit DEM. A digital elevation model built from a lidar point cloud that represents the surface of features with the most return points and thus typically featuring the vegetative canopy.

Main channel. Refers to the primary channel of the Willamette River that conveys most of the streamflow.

Normal depth. The depth of flow when the slope of the water surface and channel bottom are the same and the water depth remains constant. In the USACE HEC-RAS program (U.S. Army Corps of Engineers, 2016), a frictional slope (the loss of head along the length of the stream) is needed from the user to use normal depth as a downstream boundary condition.

Off-channel features. Generalized term for diverse array of side-channels, alcoves, sloughs, and other water bodies that were formed by historical or recent fluvial processes of the Willamette River but do not convey a substantial part of the river's streamflow. Some of these features are located near the main channel and are inundated in low-flow summer months whereas other off-channel features are topographically higher than the main channel and are only inundated during larger-magnitude streamflows in winter months. See Wallick and others (2013) for descriptions of off-channel features.

Overbank areas. Generalized term for channel-flanking features that are not inundated during summer low flows but may be inundated as streamflows increase in autumn, winter, and early spring. Overbank features include unvegetated gravel bars, vegetated gravel bars with shrub to young forest, and floodplains that support a diverse array of vegetation types from agriculture to mature forests. See Wallick and others (2013) for descriptions of these features.

Secchi depth. The depth at which a white and black disk (Secchi disk), which is slowly lowered down the water column, is no longer visible.

Sub-grid bathymetry. A method that HEC-RAS uses to interpolate depths and velocities at the resolution of the underlying topography rather than at the resolution of the computation mesh.

Appendix 1. Maps Showing Examples of Model Simulations

Hydraulic models in this study spanned the Willamette River from the McKenzie River confluence to the city of Newberg. These models were developed to evaluate fish habitat and how it varies with different streamflows. The primary output of these models are depth and velocity. A summary of findings has been included in the primary text of this report, but additional figures of depth and velocity results at select streamflows on all model reaches have been included here for additional context.

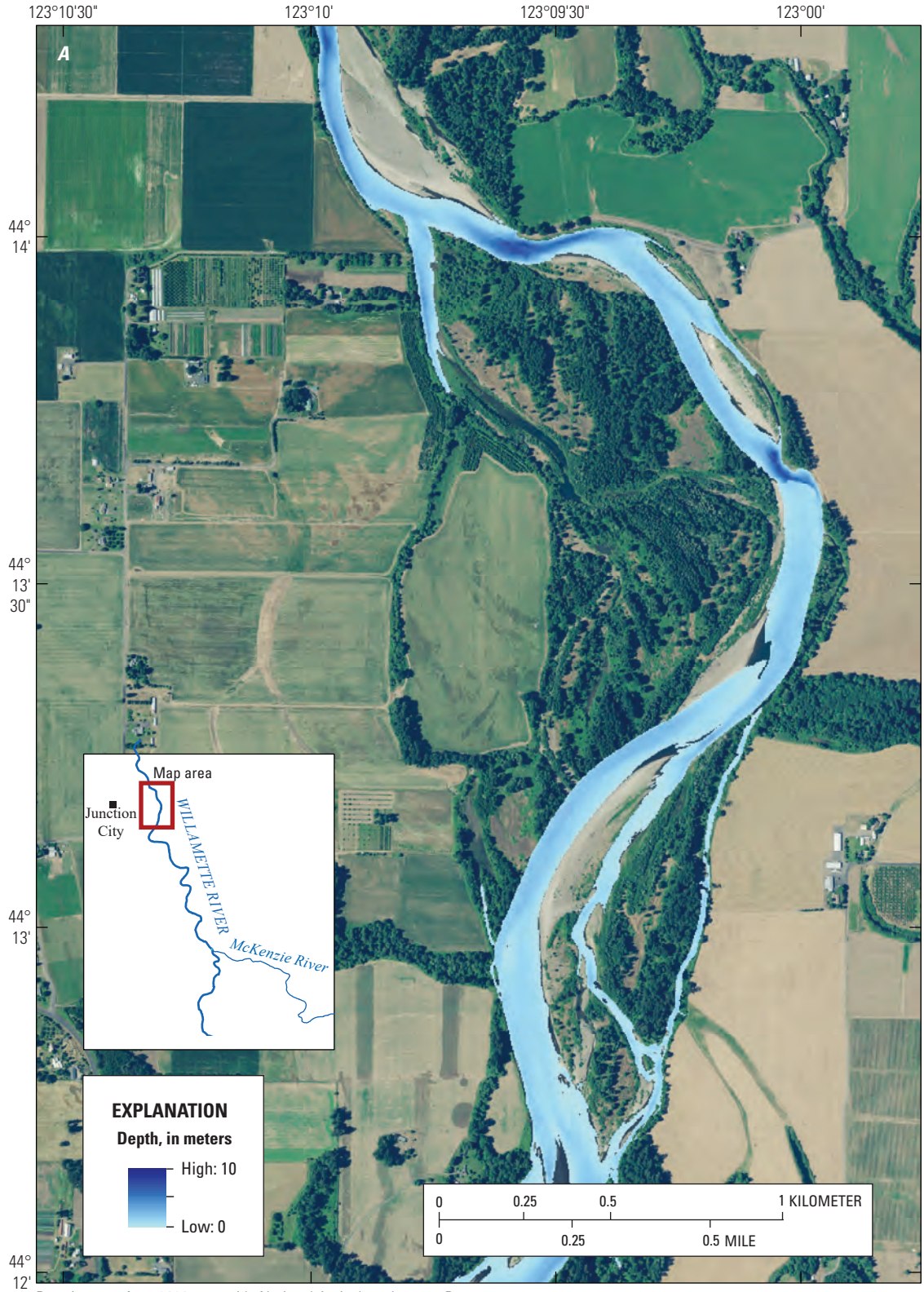

Figure 1.1. Example of water depth (*A*–*C*) and velocities (*D*–*F*) across three streamflow levels in the Harrisburg model reach of the Willamette River, Oregon, near River Kilometer 266.

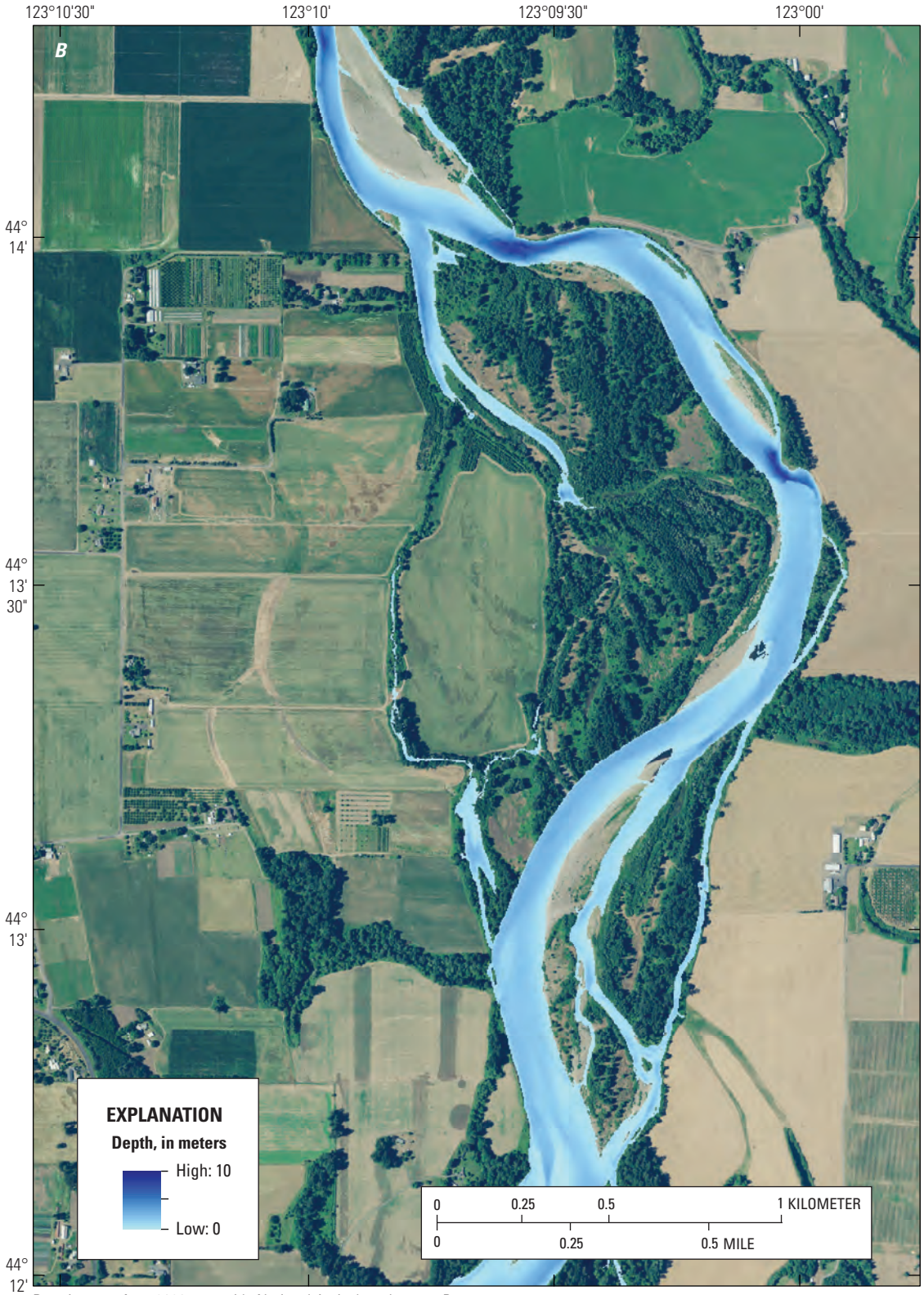

Base imagery from 2020 statewide National Agriculture Imagery Program, North American Vertical Datum of 1988

Figure 1.1.—Continued

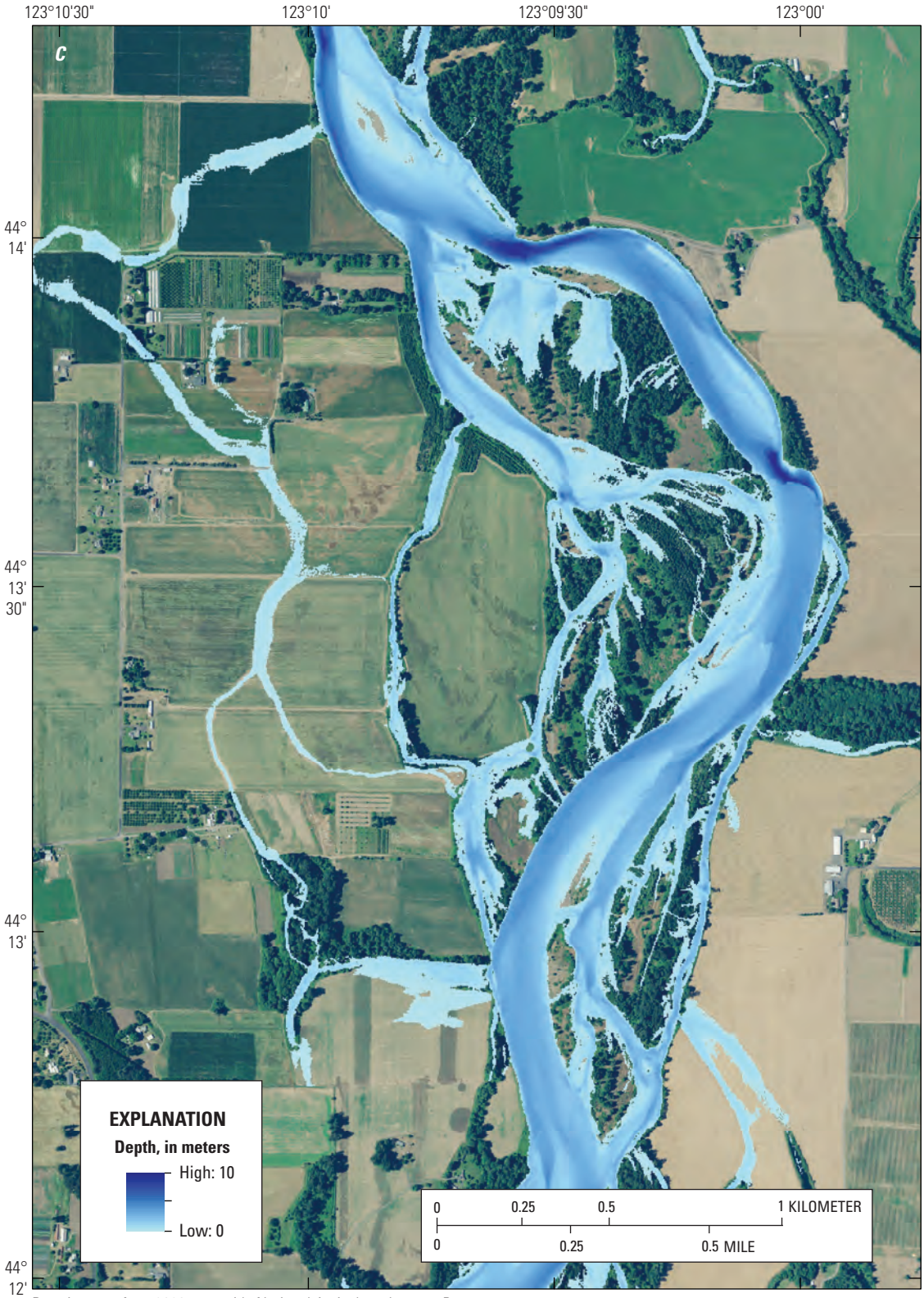

Base imagery from 2020 statewide National Agriculture Imagery Program, North American Vertical Datum of 1988

Figure 1.1.—Continued

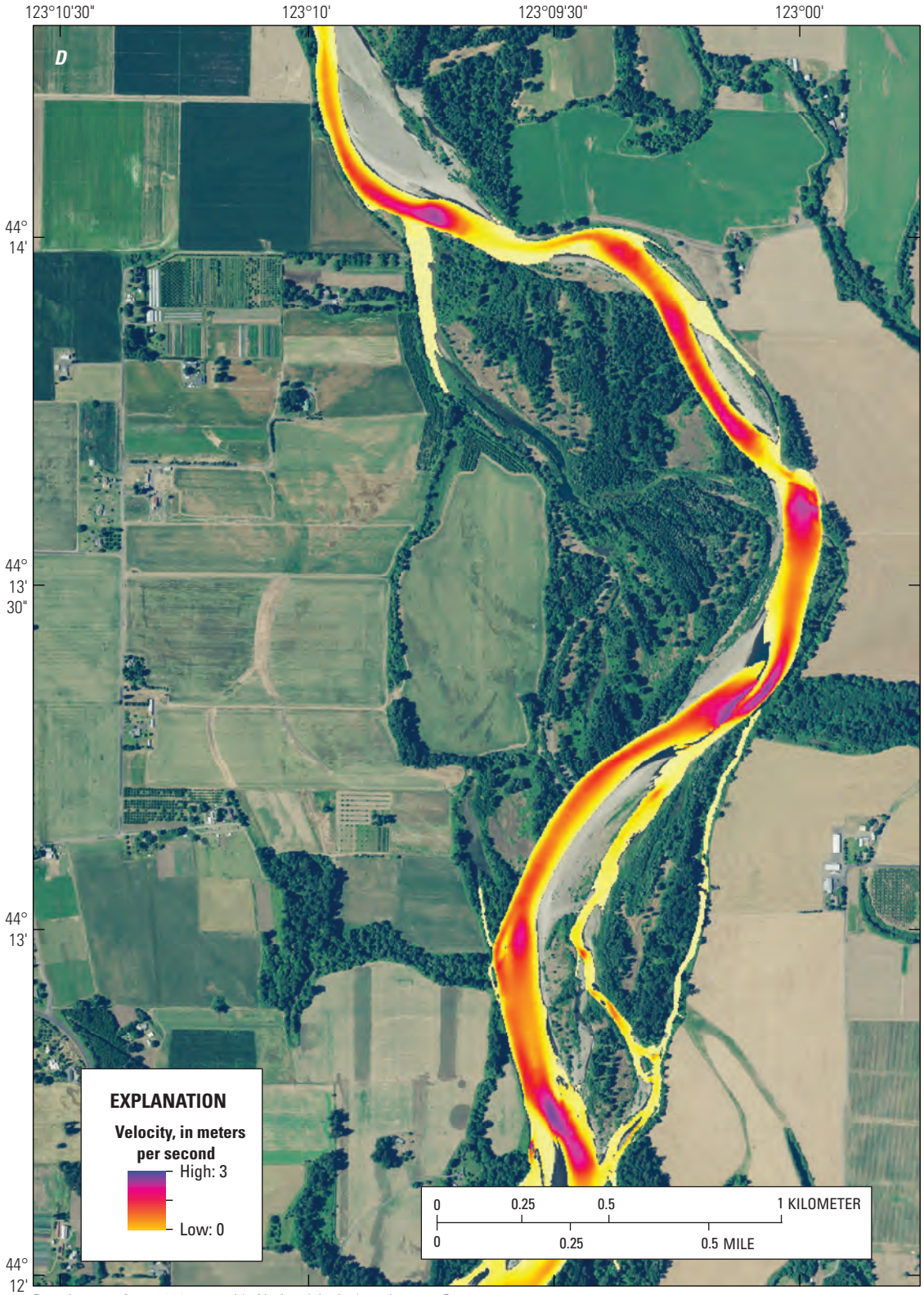

Base imagery from 2020 statewide National Agriculture Imagery Program, North American Vertical Datum of 1988

Figure 1.1.—Continued

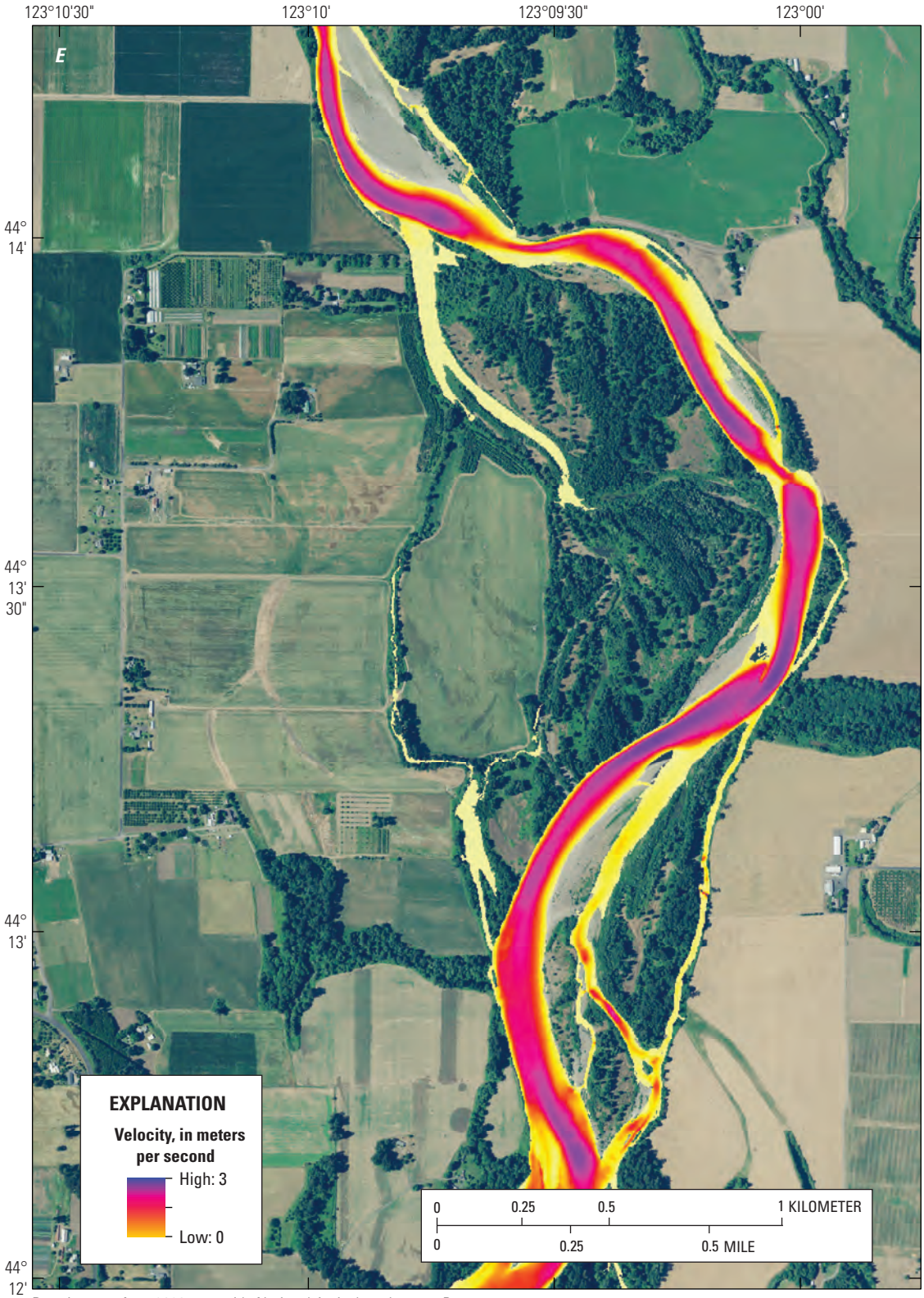

Base imagery from 2020 statewide National Agriculture Imagery Program, North American Vertical Datum of 1988

Figure 1.1.—Continued

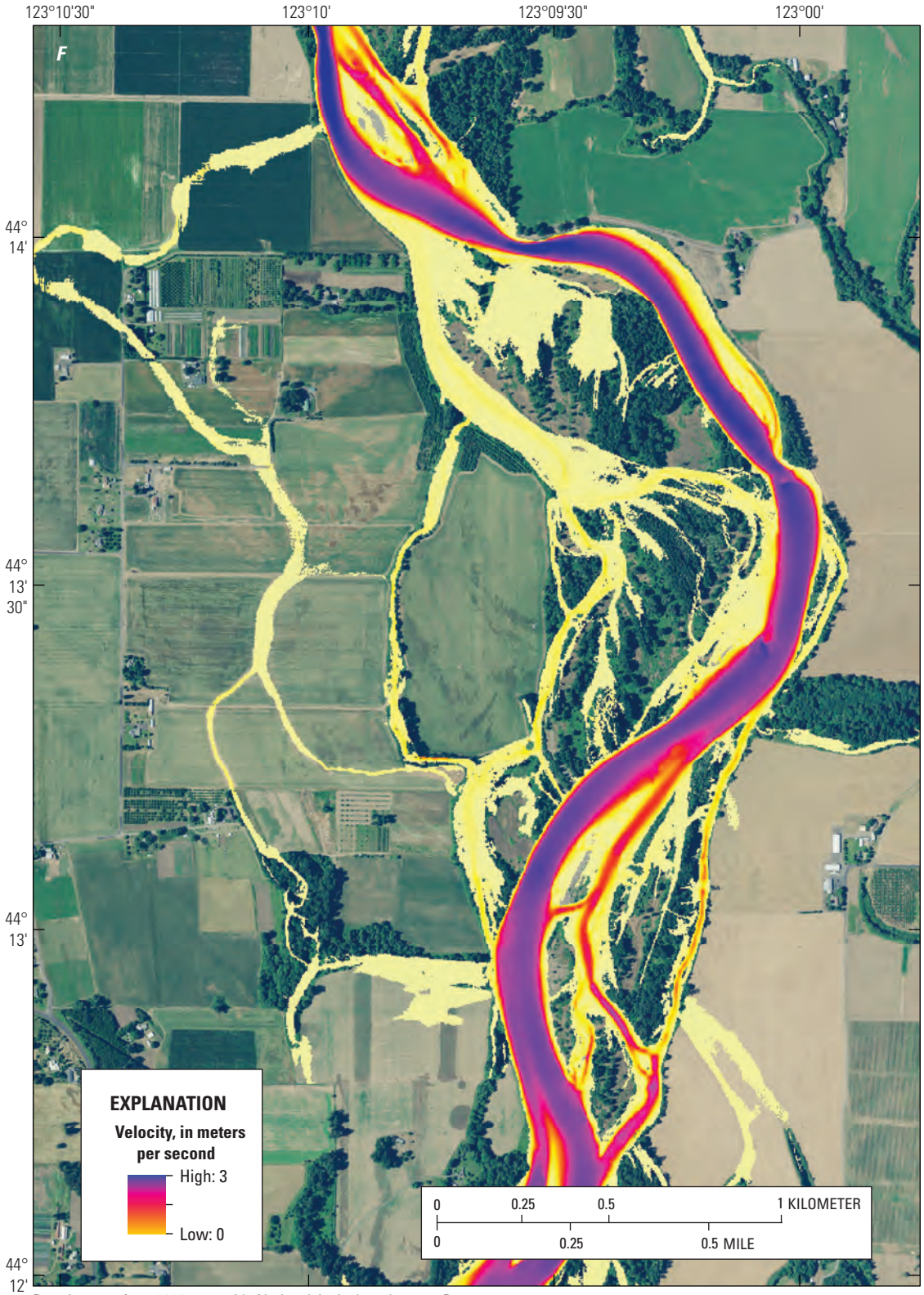

Base imagery from 2020 statewide National Agriculture Imagery Program, North American Vertical Datum of 1988

Figure 1.1.—Continued

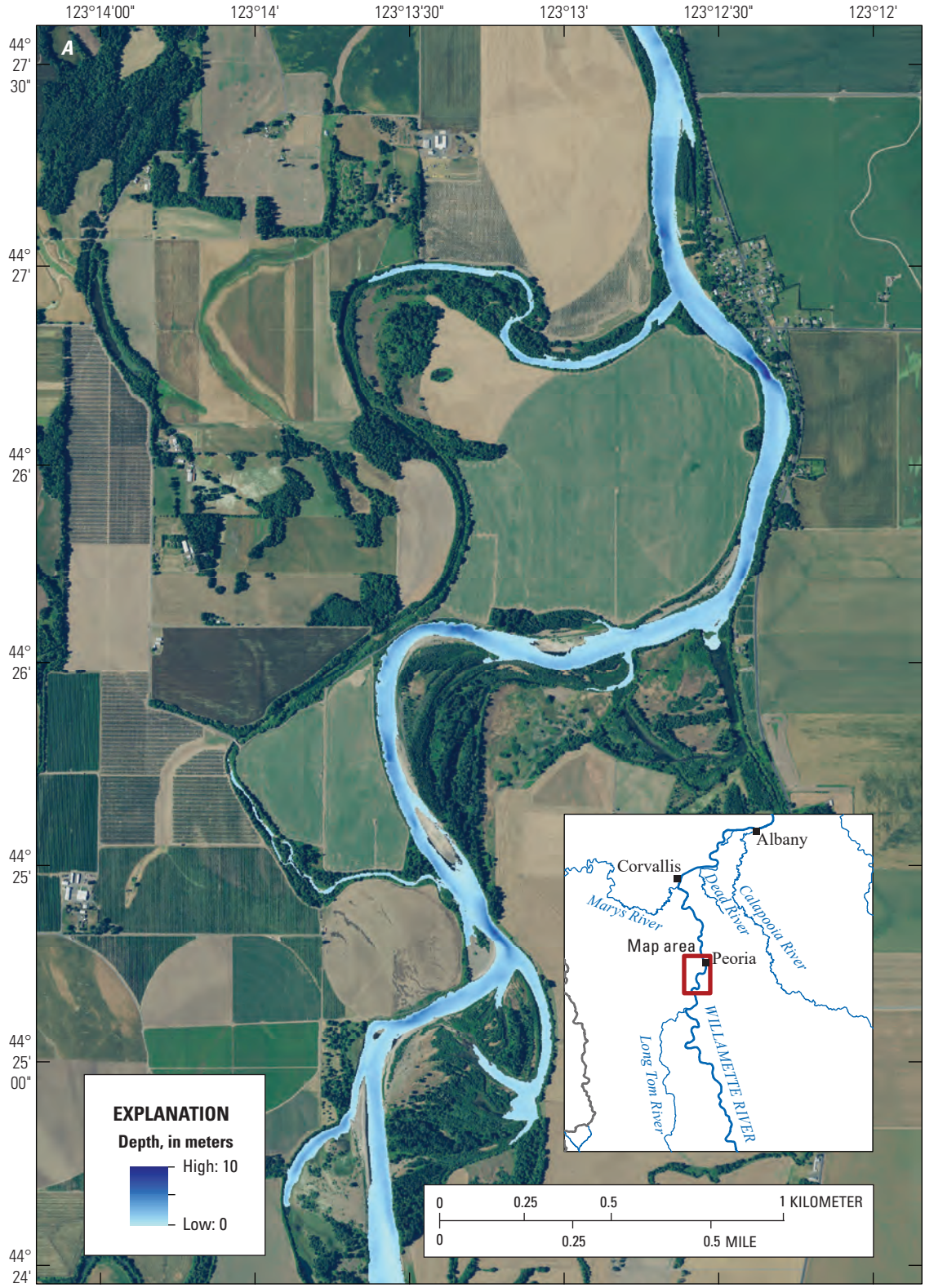

Base imagery from 2020 statewide National Agriculture Imagery Program, North American Vertical Datum of 1988

Figure 1.2. Example of water depth (*A*–*C*) and velocities (*D*–*F*) across three streamflow levels in the Peoria model reach of the Willamette River, Oregon, near River Kilometer 230.

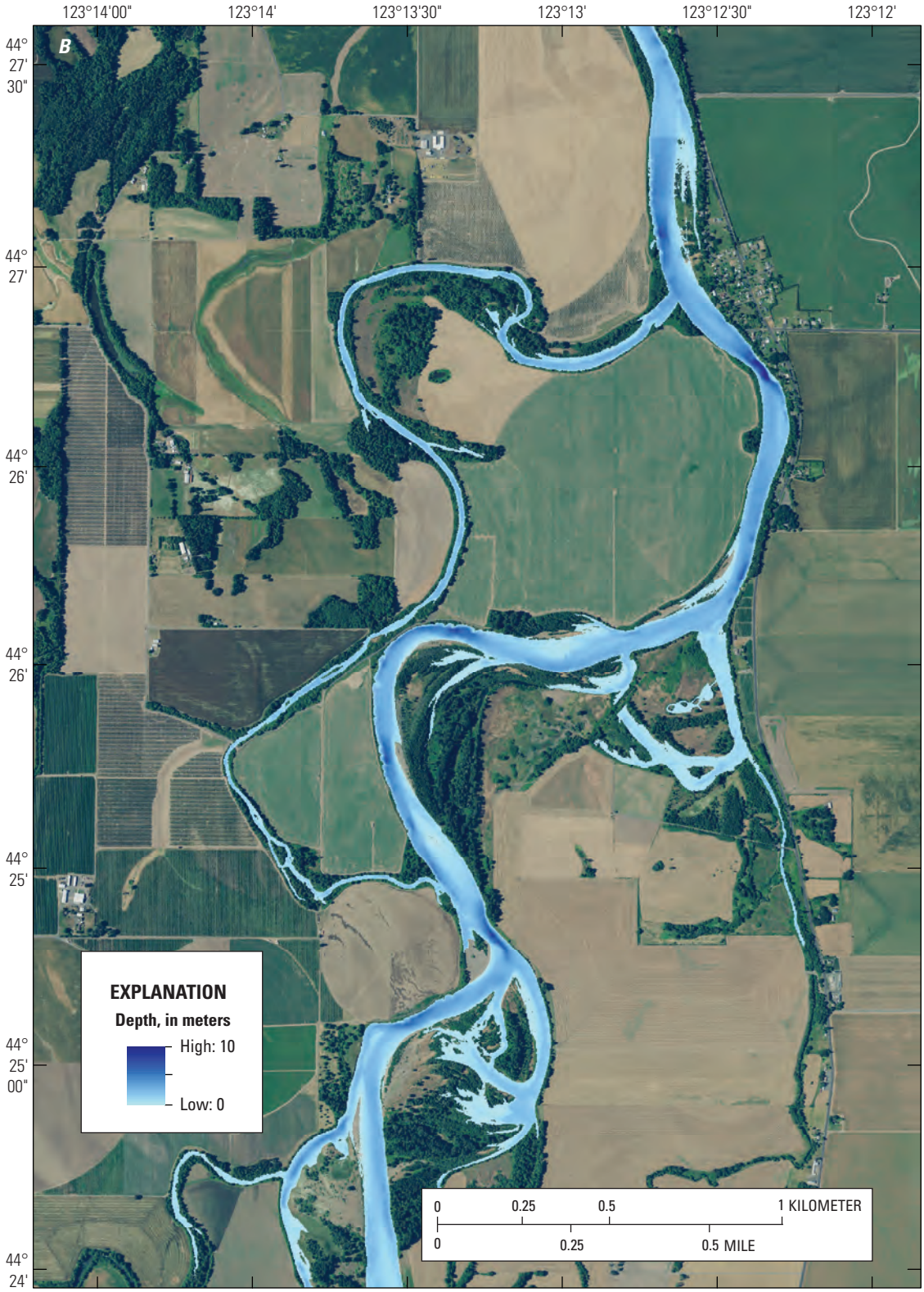

Base imagery from 2020 statewide National Agriculture Imagery Program, North American Vertical Datum of 1988

Figure 1.2.—Continued

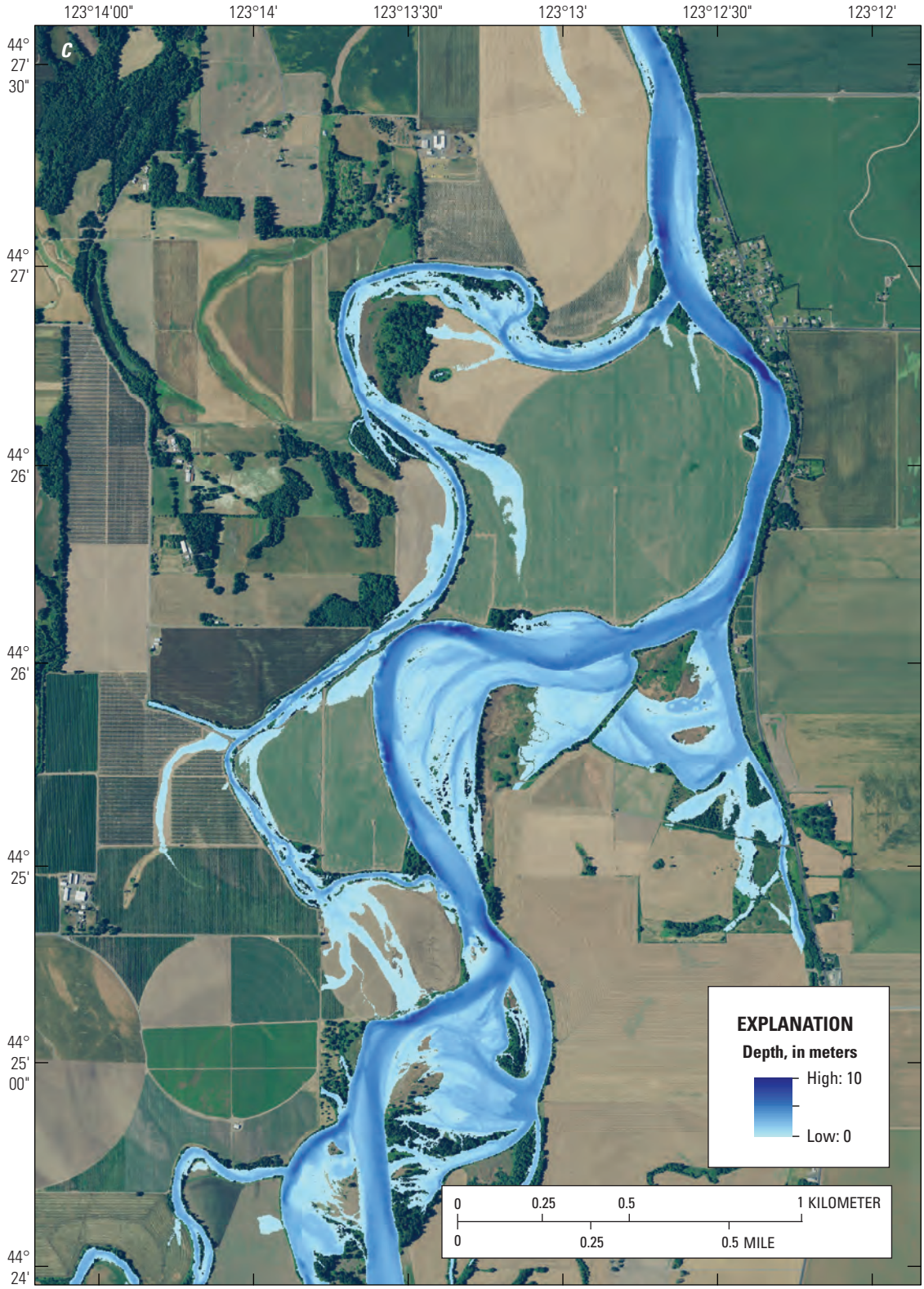

Base imagery from 2020 statewide National Agriculture Imagery Program, North American Vertical Datum of 1988

Figure 1.2.—Continued

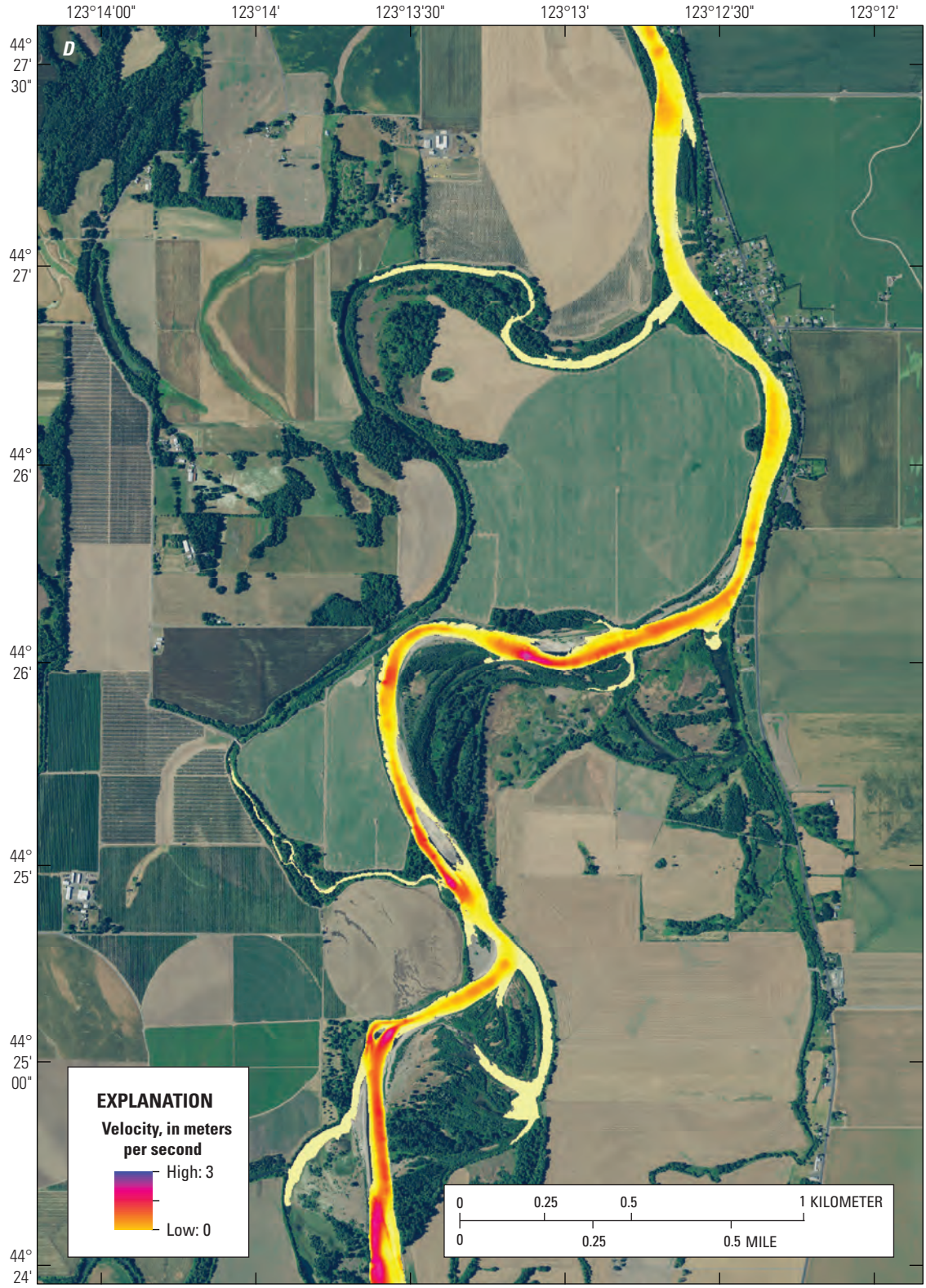

Base imagery from 2020 statewide National Agriculture Imagery Program, North American Vertical Datum of 1988

Figure 1.2.—Continued

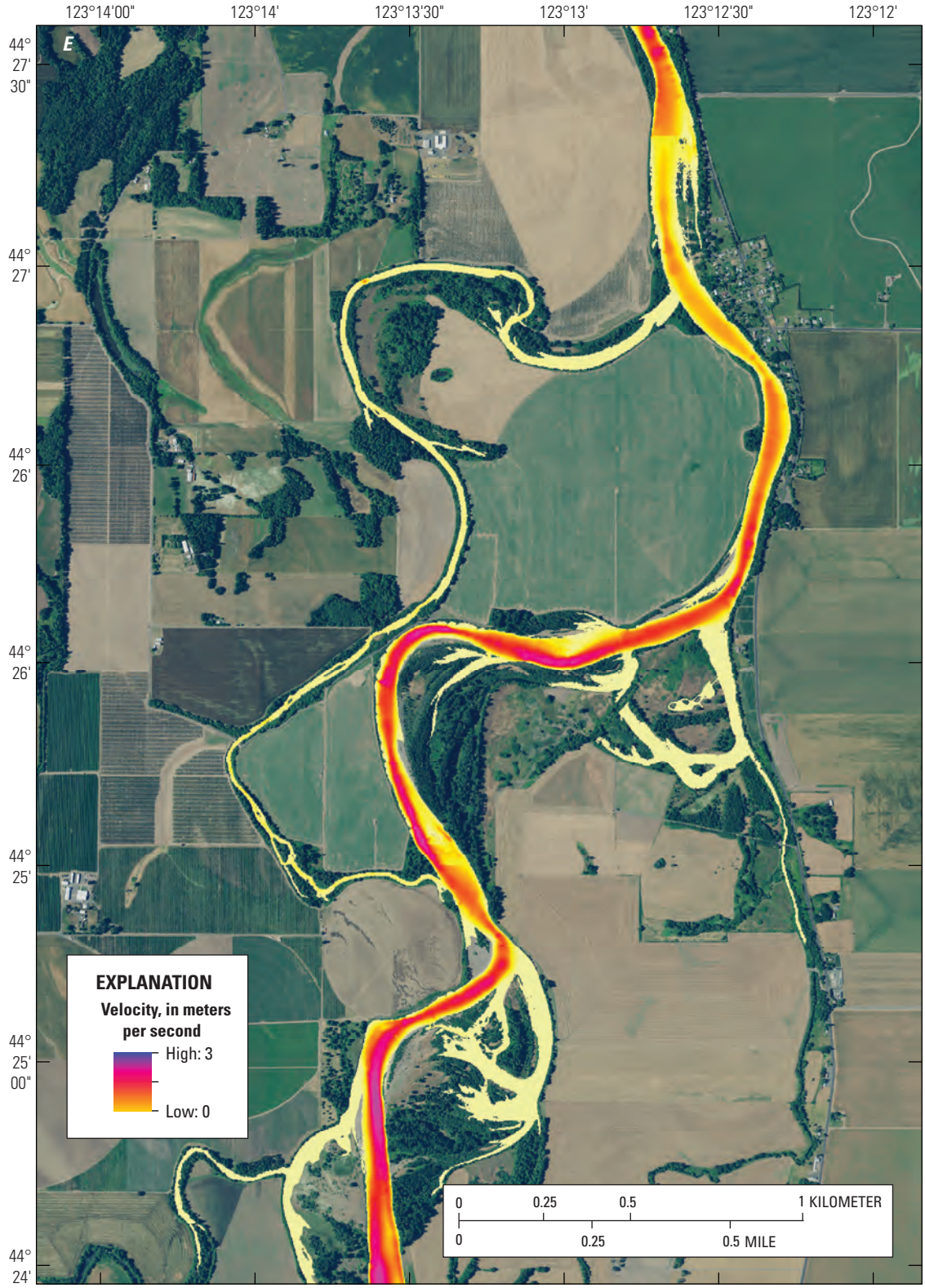

Base imagery from 2020 statewide National Agriculture Imagery Program, North American Vertical Datum of 1988

Figure 1.2.—Continued

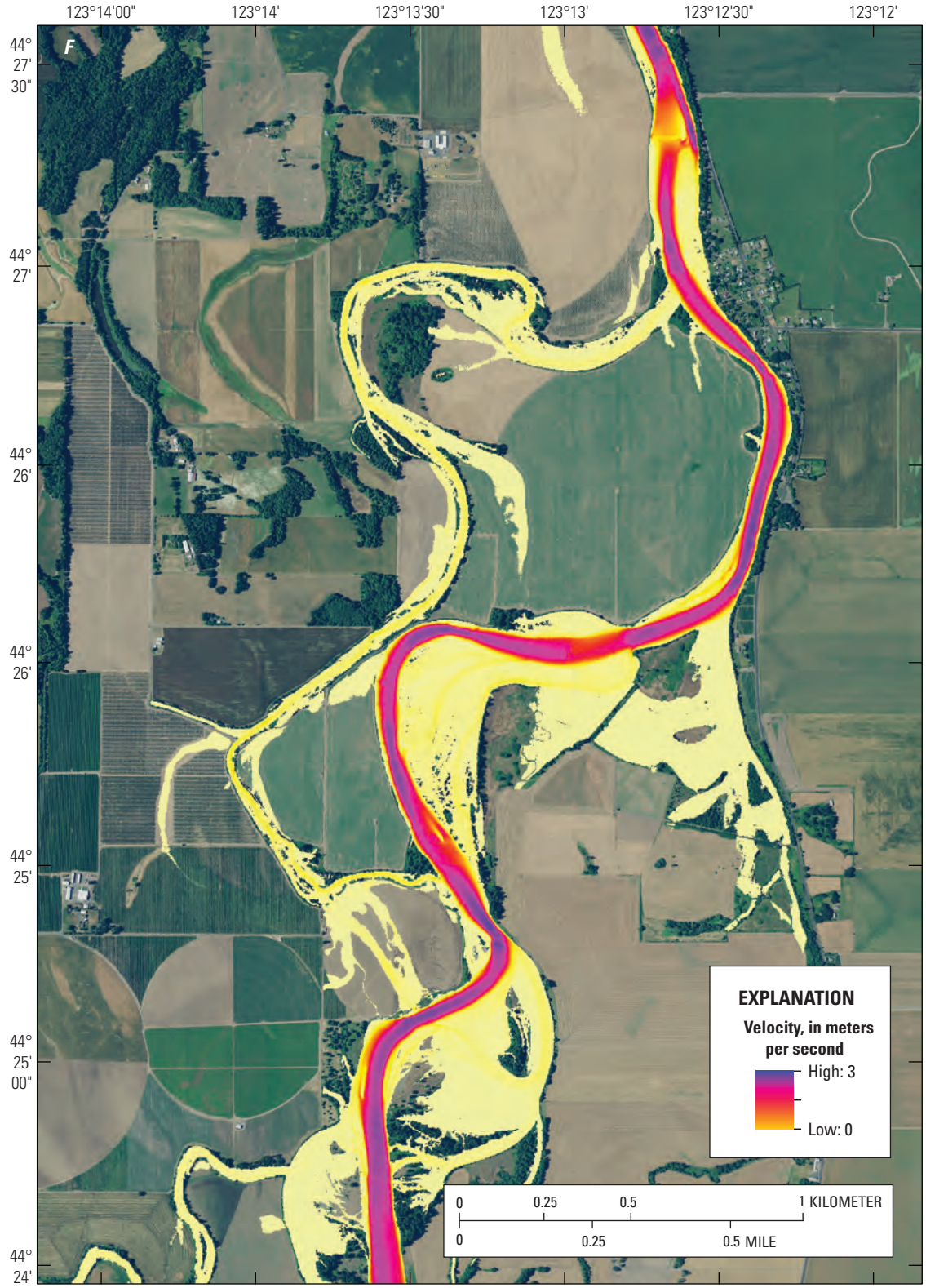

Base imagery from 2020 statewide National Agriculture Imagery Program, North American Vertical Datum of 1988

Figure 1.2.—Continued

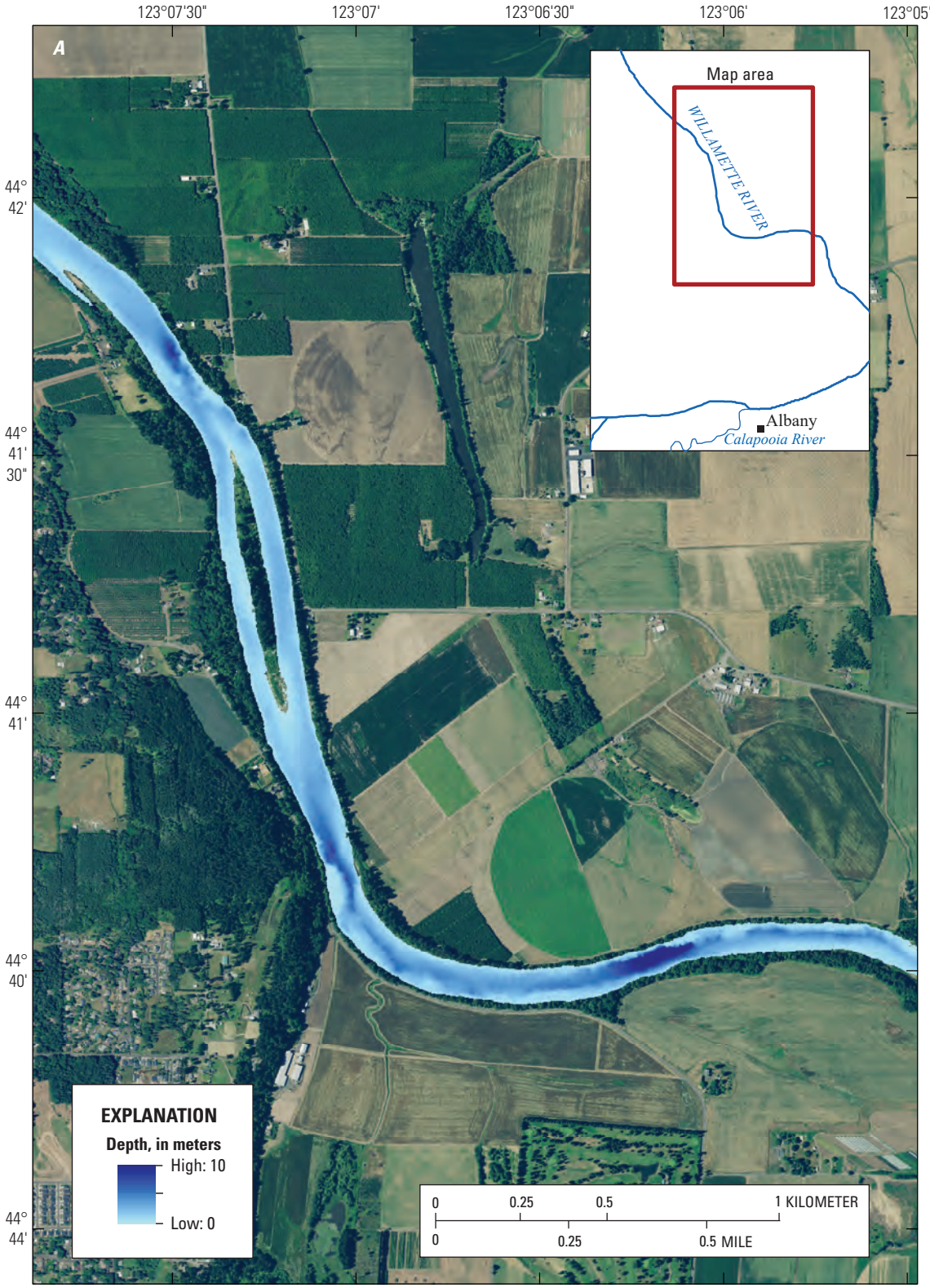

Base imagery from 2020 statewide National Agriculture Imagery Program, North American Vertical Datum of 1988

Figure 1.3. Example of water depth (*A*–*C*) and velocities (*D*–*F*) across three streamflow levels in the Albany model reach of the Willamette River, Oregon, near River Kilometer 184.

Base imagery from 2020 statewide National Agriculture Imagery Program, North American Vertical Datum of 1988

Figure 1.3.—Continued

Base imagery from 2020 statewide National Agriculture Imagery Program, North American Vertical Datum of 1988

Figure 1.3.—Continued

Base imagery from 2020 statewide National Agriculture Imagery Program, North American Vertical Datum of 1988

Figure 1.3.—Continued

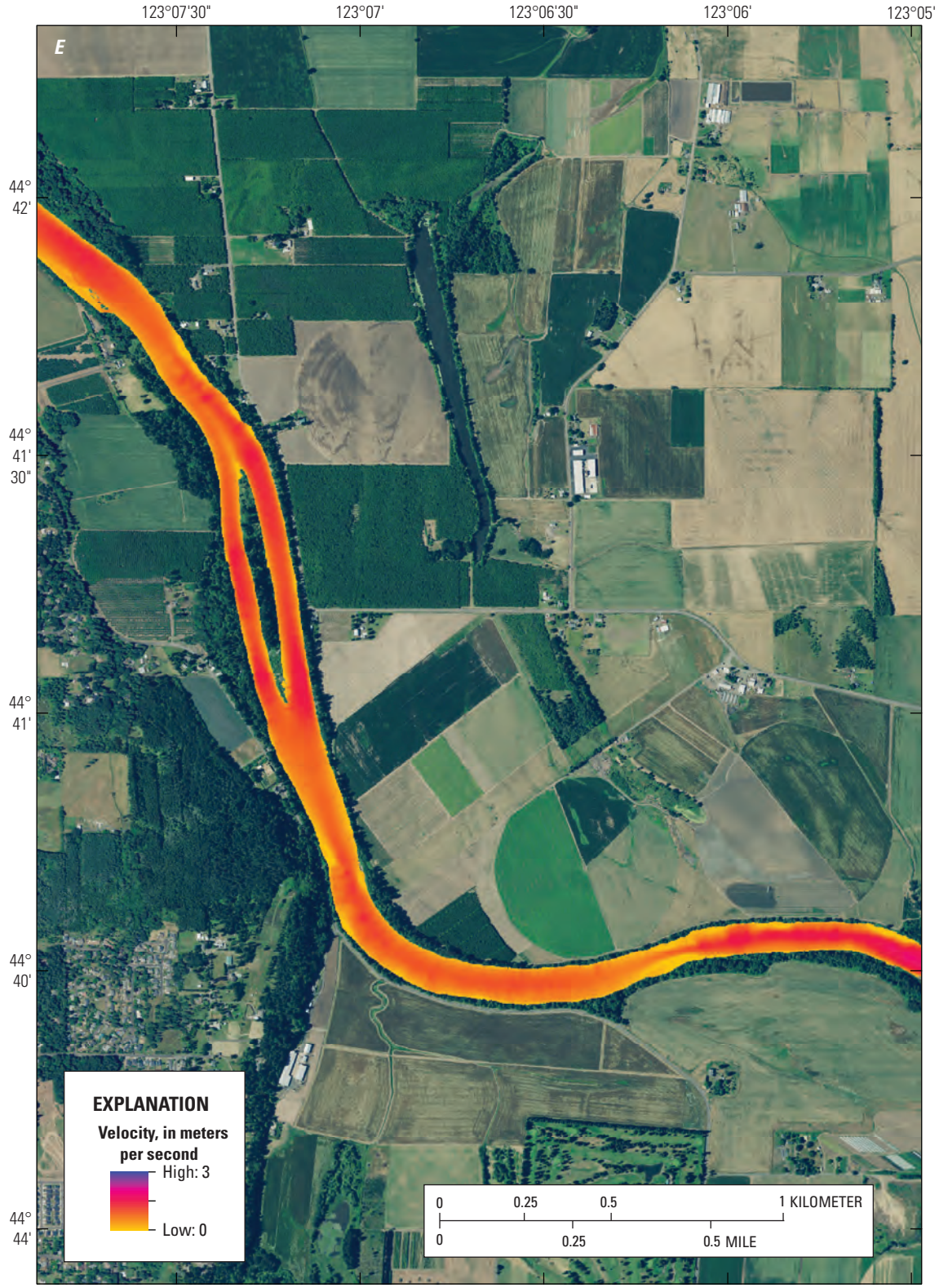

Base imagery from 2020 statewide National Agriculture Imagery Program, North American Vertical Datum of 1988

Figure 1.3.—Continued

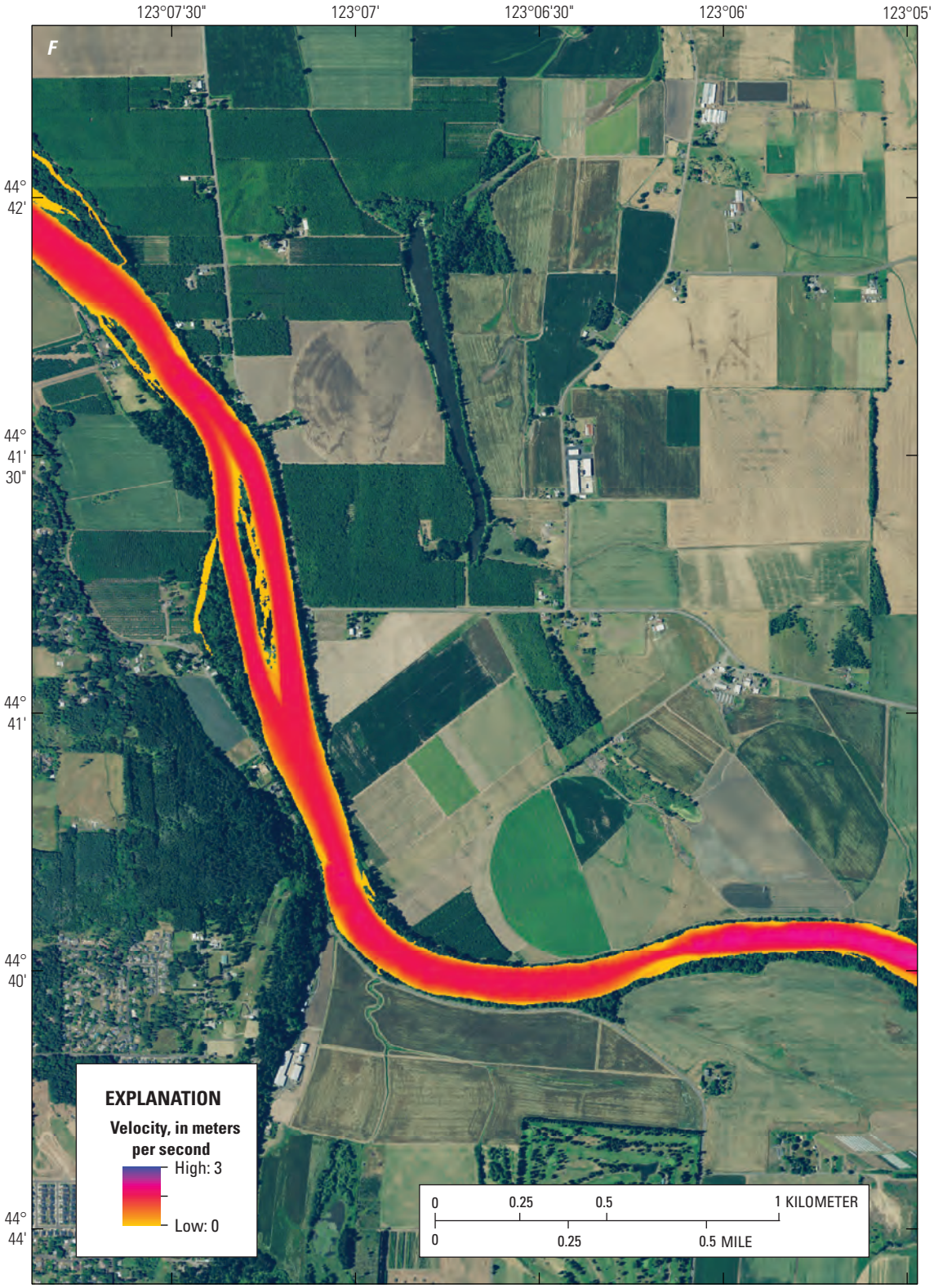

Base imagery from 2020 statewide National Agriculture Imagery Program, North American Vertical Datum of 1988

Figure 1.3.—Continued

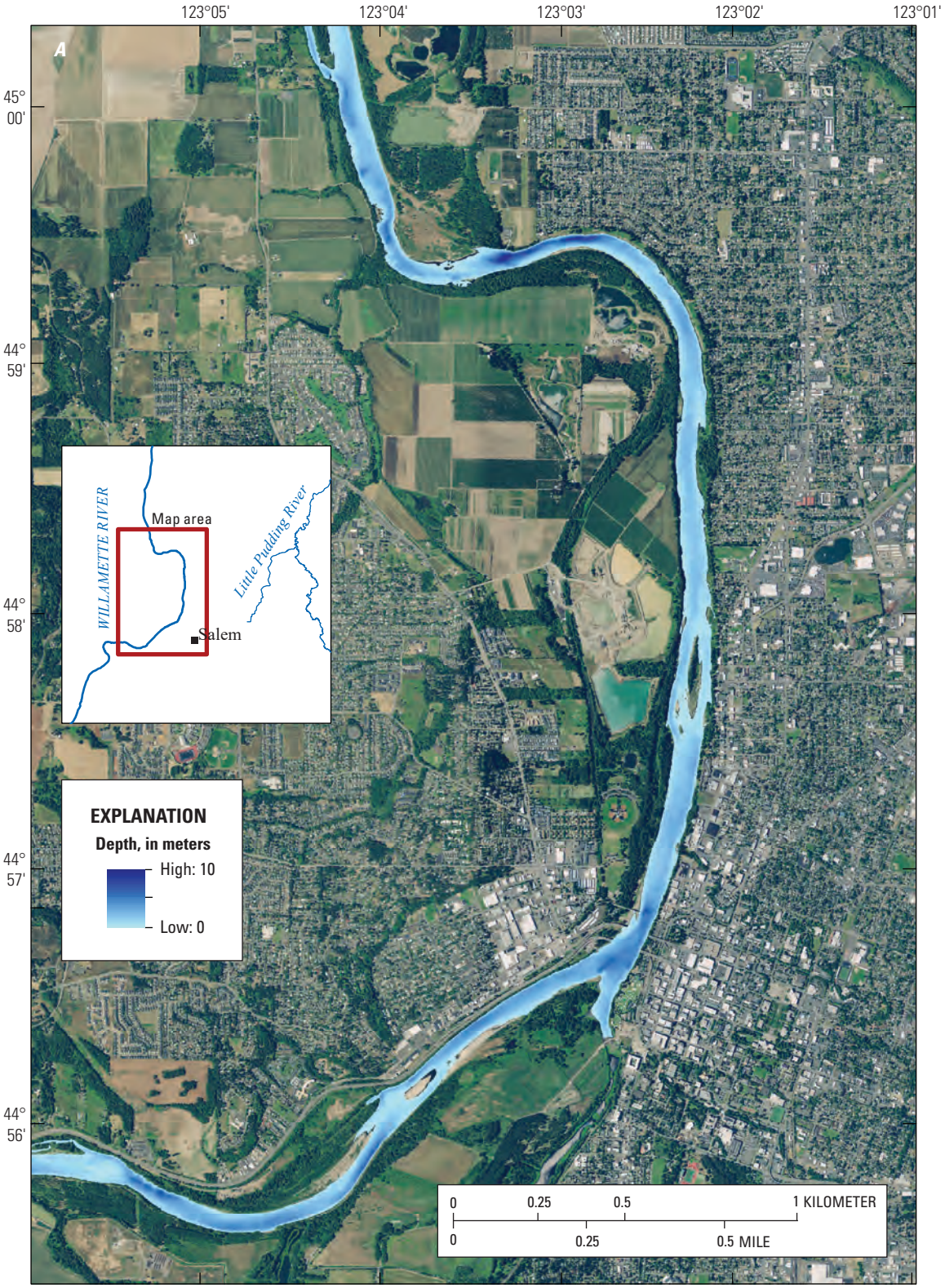

Base imagery from 2020 statewide National Agriculture Imagery Program, North American Vertical Datum of 1988

Figure 1.4. Example of water depth (*A*–*C*) and velocities (*D*–*F*) across three streamflow levels in the Salem model reach of the Willamette River, Oregon, near River Kilometer135.

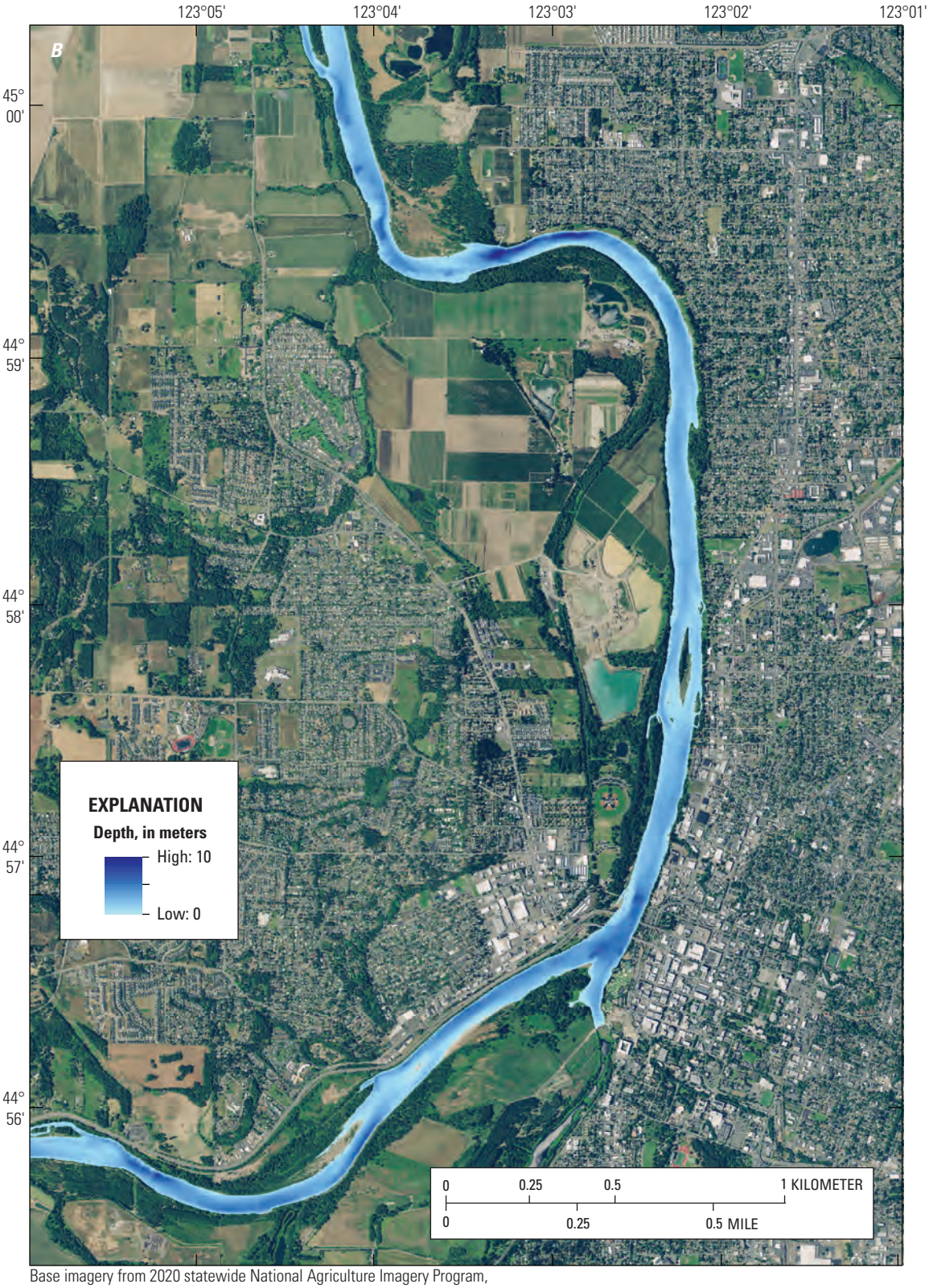

Base imagery from 2020 statewide National Agriculture Imagery Program, North American Vertical Datum of 1988

Figure 1.4.—Continued

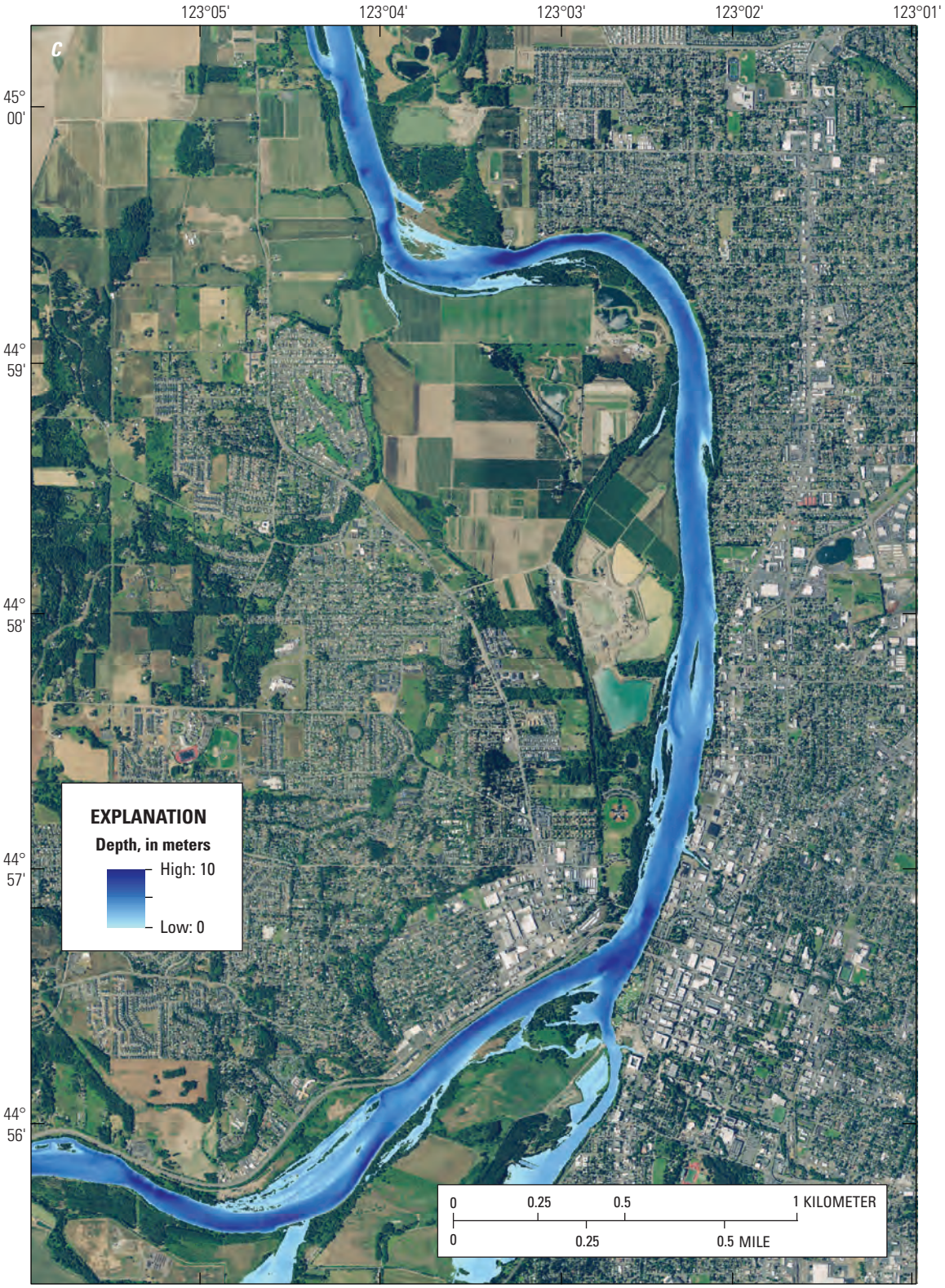

Base imagery from 2020 statewide National Agriculture Imagery Program, North American Vertical Datum of 1988

Figure 1.4.—Continued

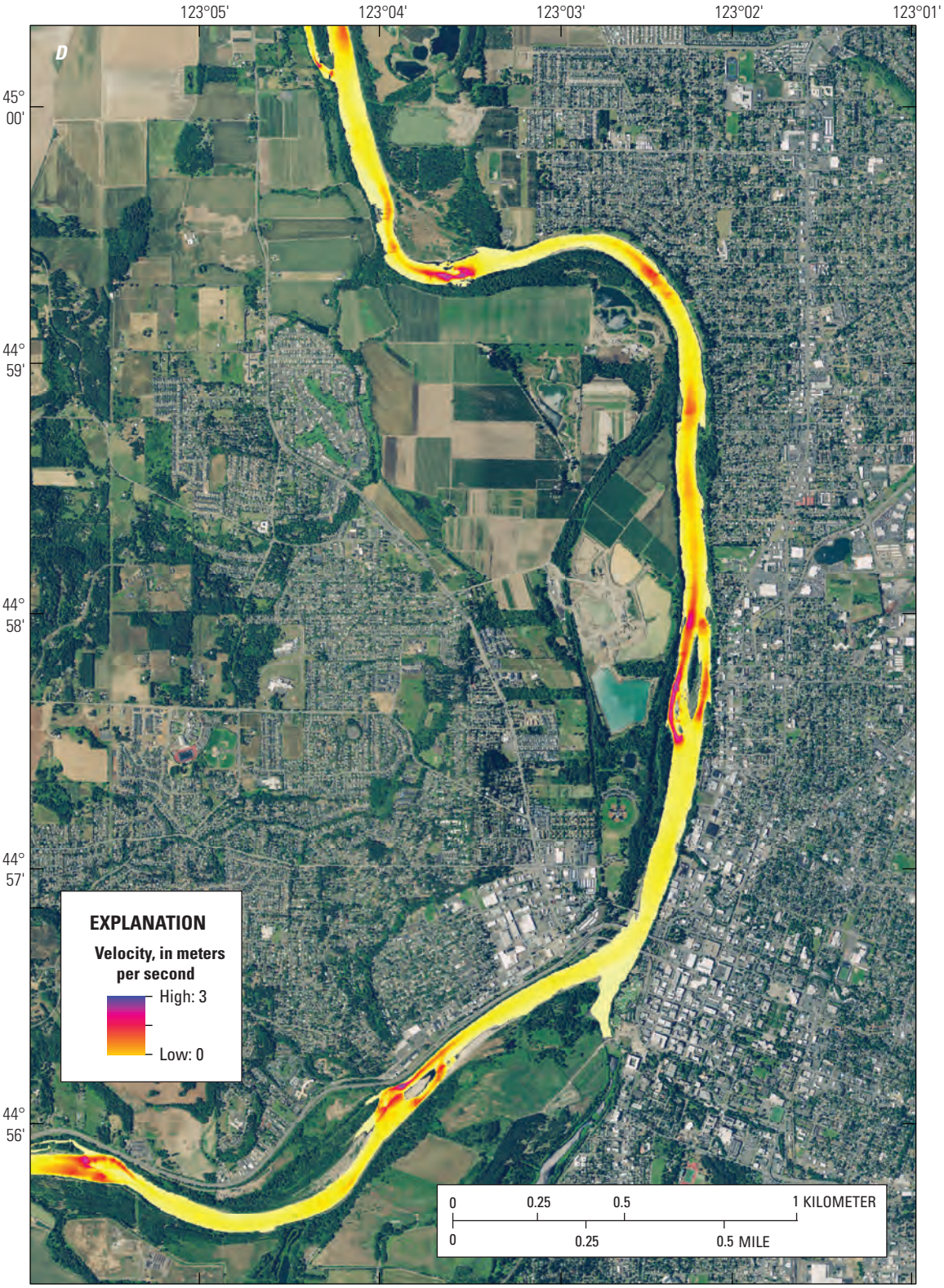

Base imagery from 2020 statewide National Agriculture Imagery Program, North American Vertical Datum of 1988

Figure 1.4.—Continued

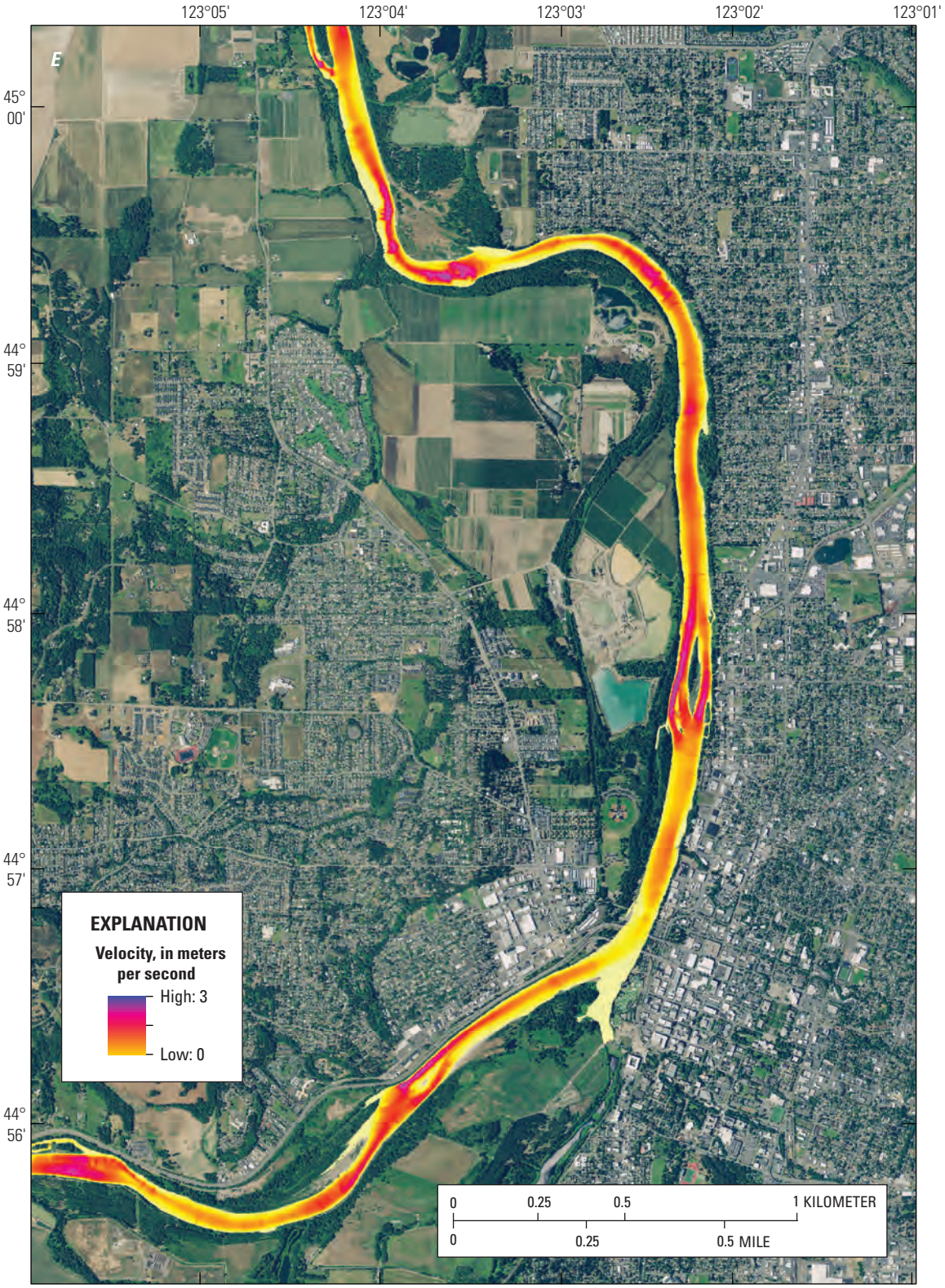

Base imagery from 2020 statewide National Agriculture Imagery Program, North American Vertical Datum of 1988

Figure 1.4.—Continued

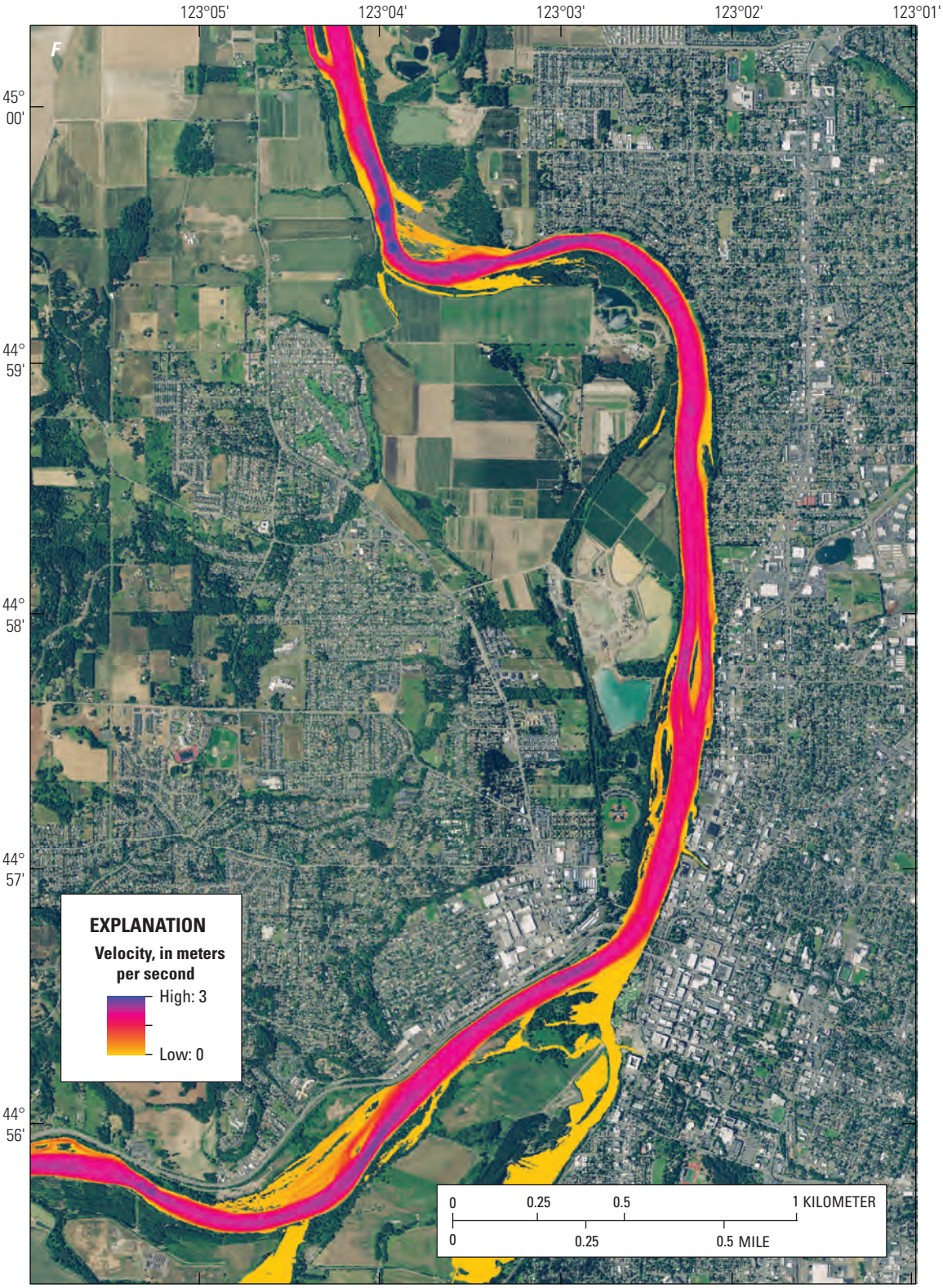

Base imagery from 2020 statewide National Agriculture Imagery Program, North American Vertical Datum of 1988

Figure 1.4.—Continued

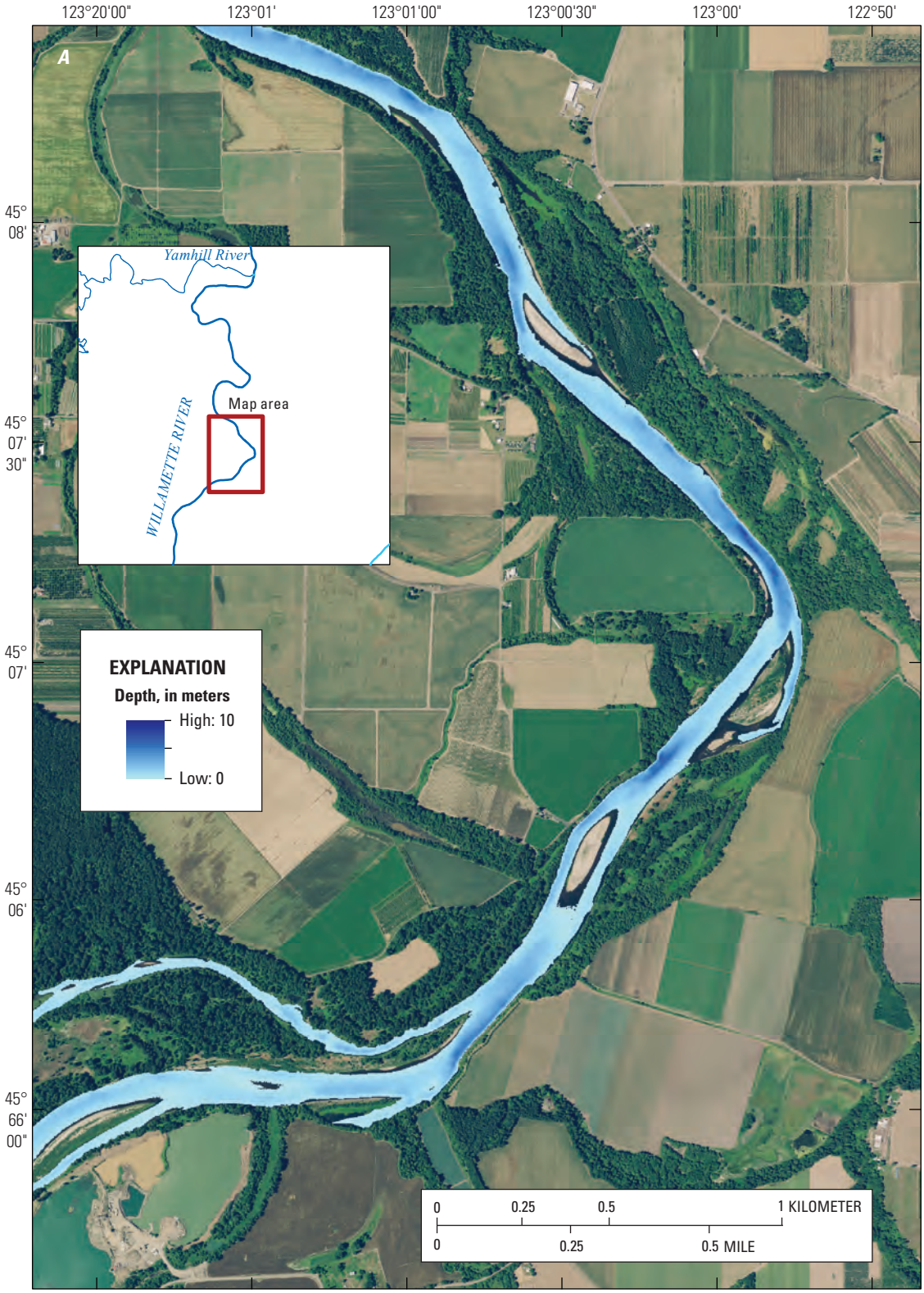

Base imagery from 2020 statewide National Agriculture Imagery Program, North American Vertical Datum of 1988

Figure 1.5. Example of water depth (*A*–*D*) and velocities (*E*–*G*) across three streamflow levels in the Newberg model reach of the Willamette River, Oregon, near River Kilometer 111.

Base imagery from 2020 statewide National Agriculture Imagery Program, North American Vertical Datum of 1988

Figure 1.5.—Continued

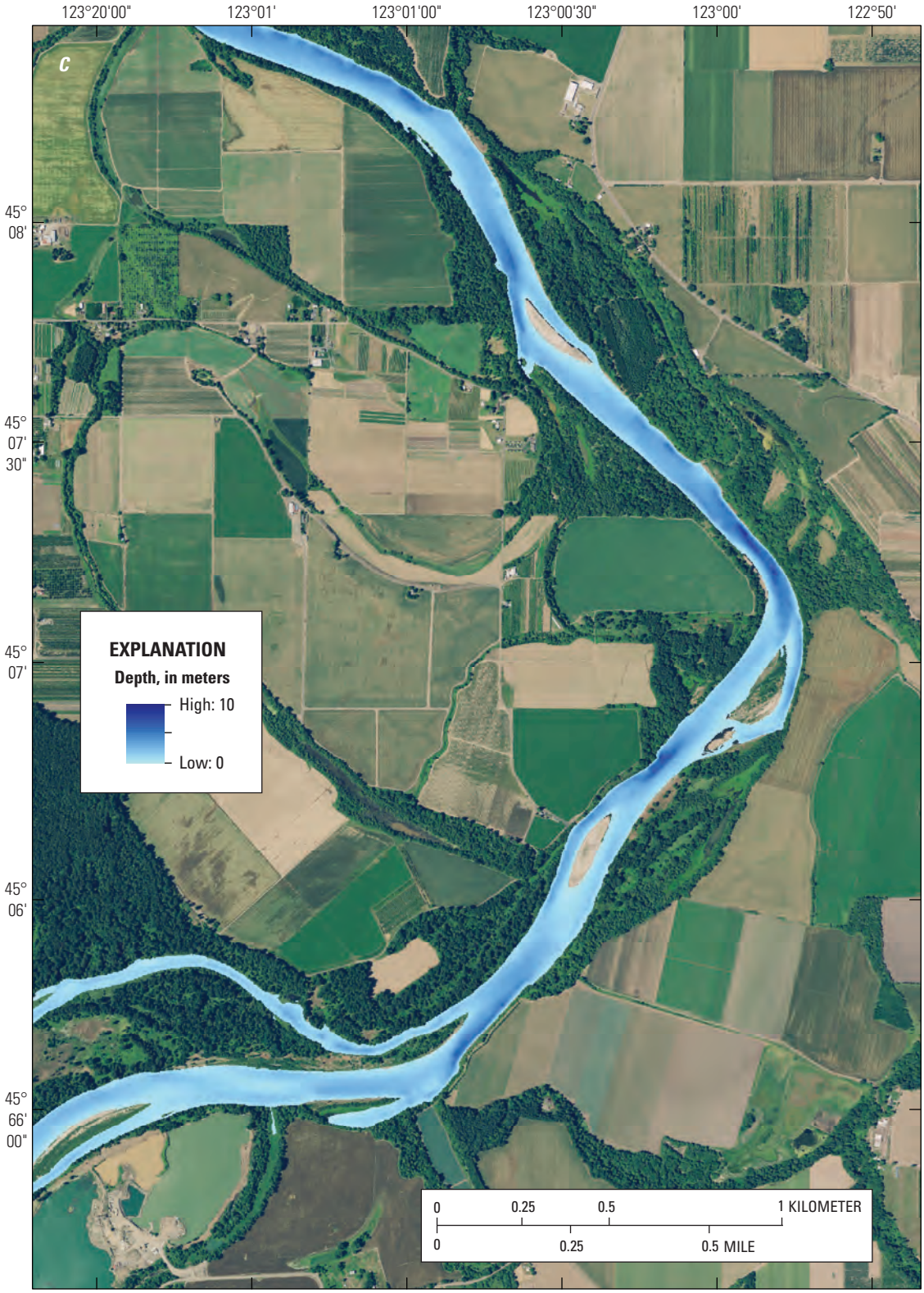

Base imagery from 2020 statewide National Agriculture Imagery Program, North American Vertical Datum of 1988

Figure 1.5.—Continued

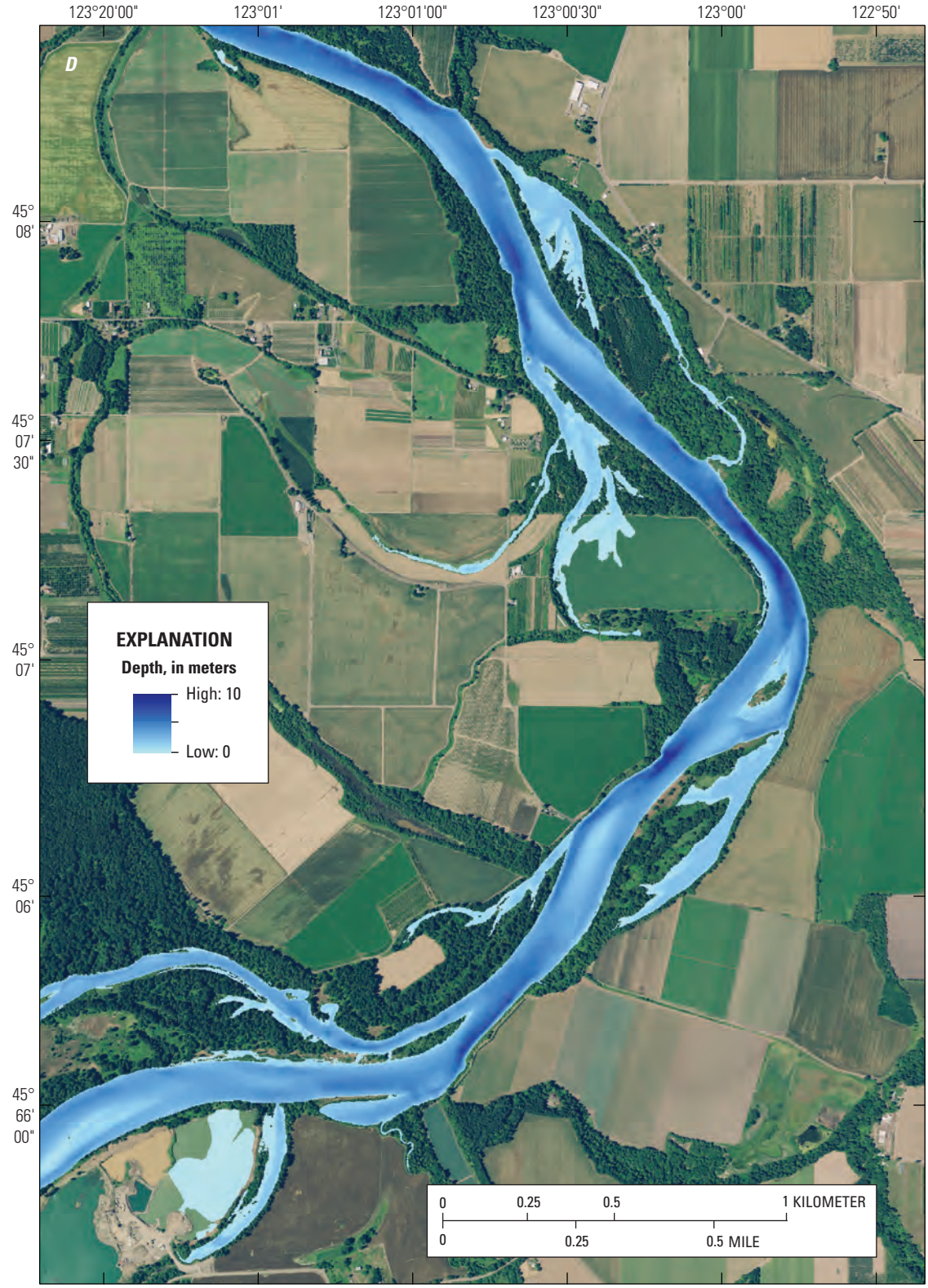

Base imagery from 2020 statewide National Agriculture Imagery Program, North American Vertical Datum of 1988

Figure 1.5.—Continued

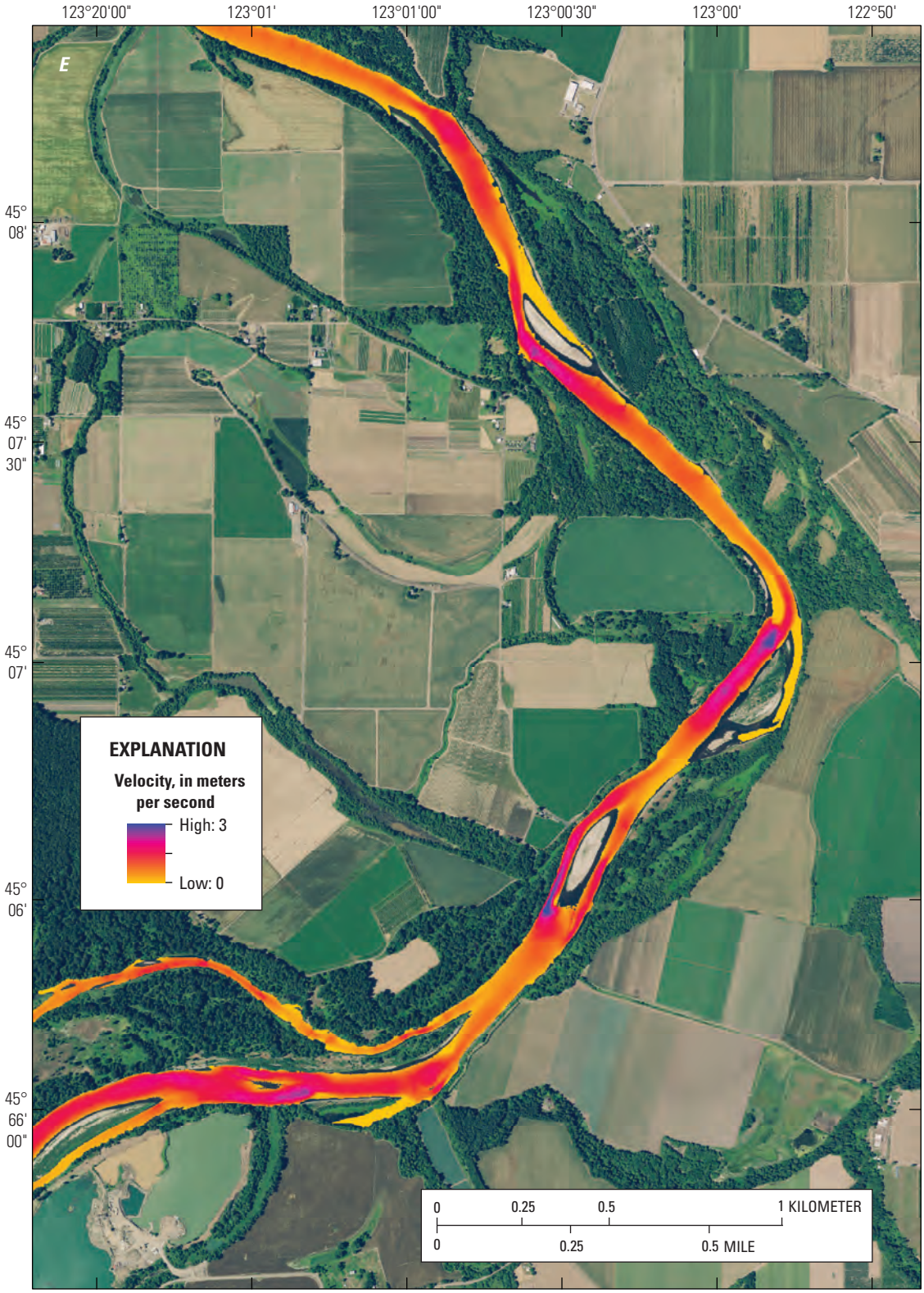

Base imagery from 2020 statewide National Agriculture Imagery Program, North American Vertical Datum of 1988

Figure 1.5.—Continued

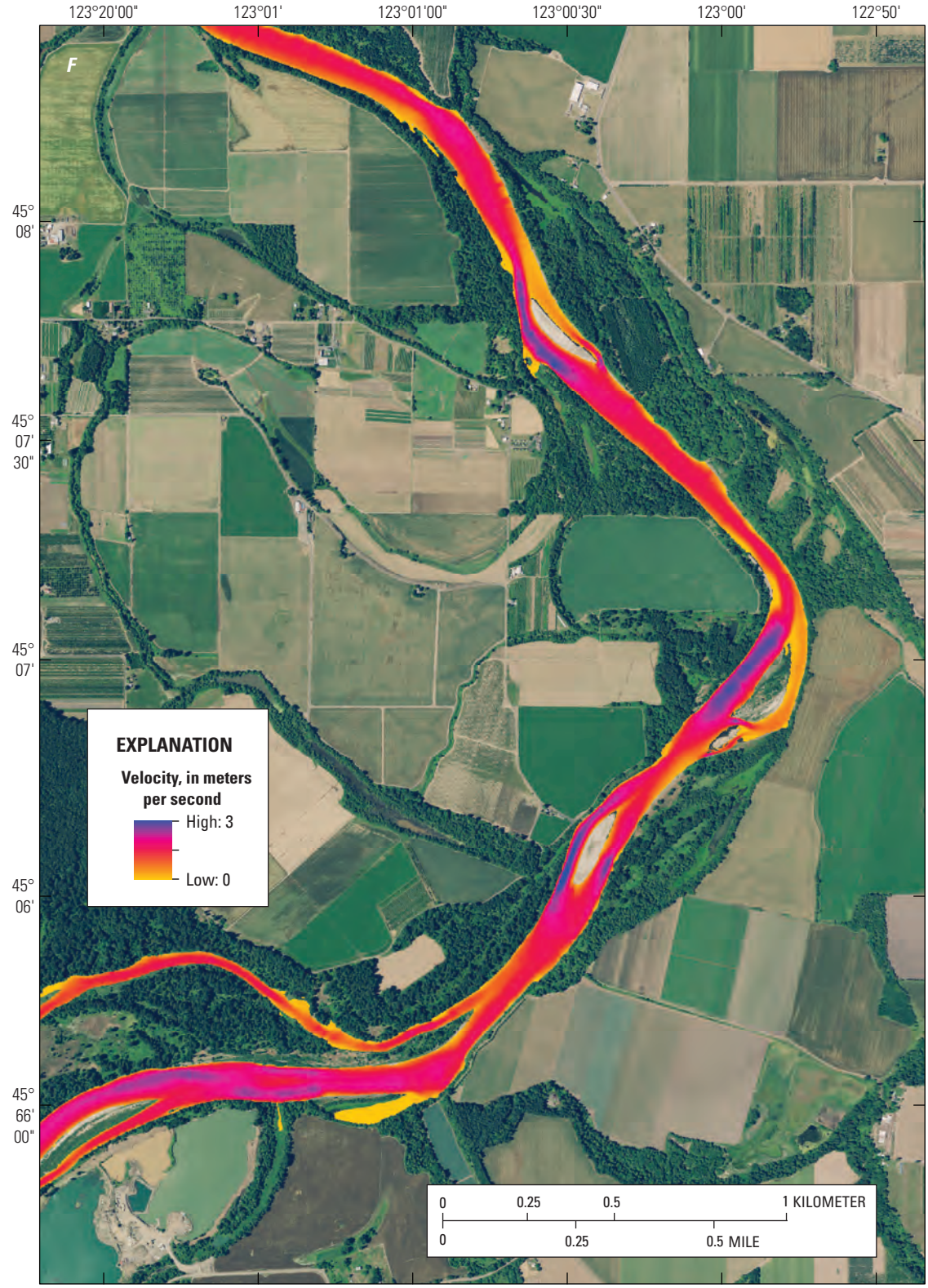

Base imagery from 2020 statewide National Agriculture Imagery Program, North American Vertical Datum of 1988

Figure 1.5.—Continued

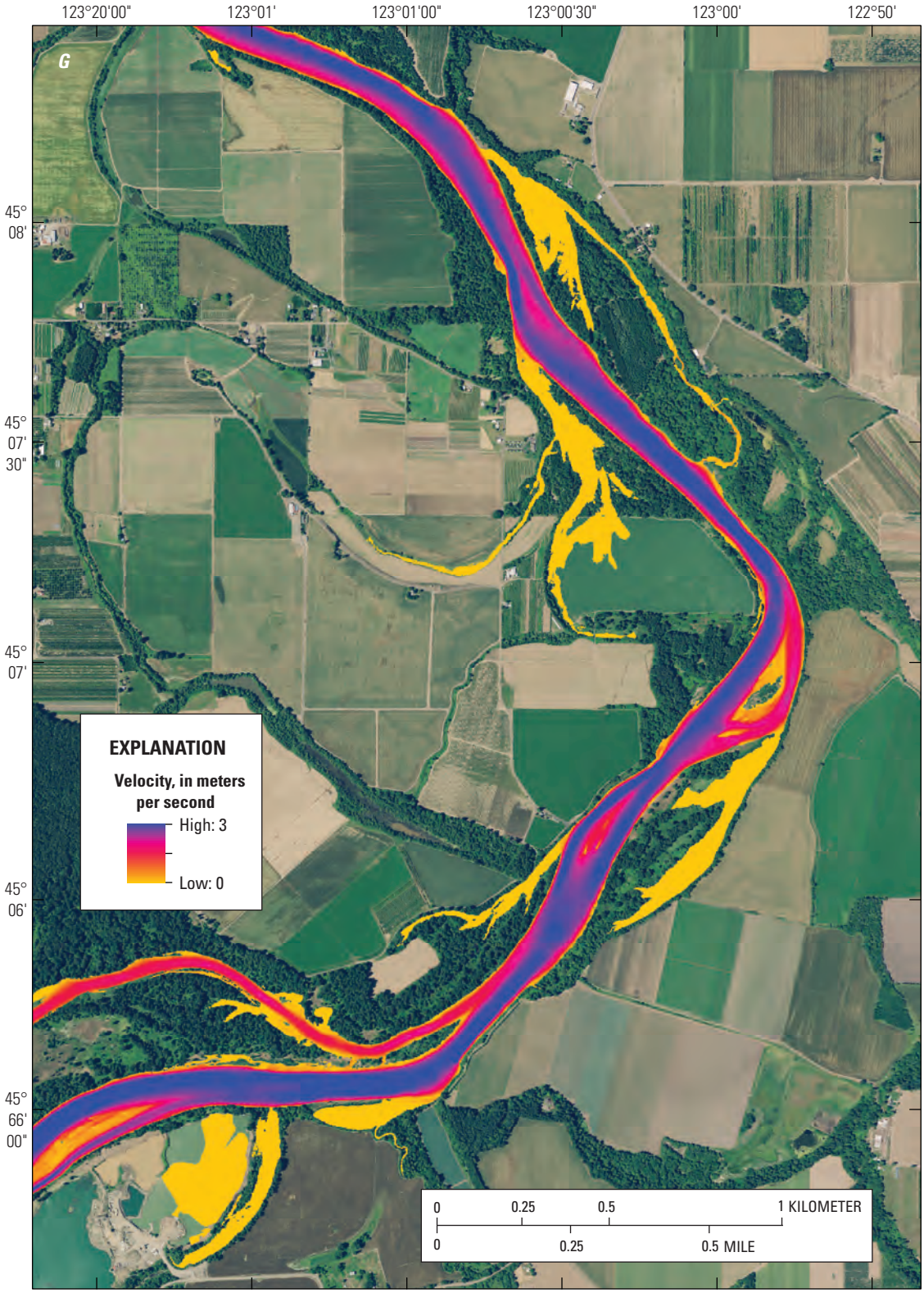

Base imagery from 2020 statewide National Agriculture Imagery Program, North American Vertical Datum of 1988

Figure 1.5.—Continued

Publishing support provided by the U.S. Geological Survey
Science Publishing Network, Tacoma Publishing Service Center

For more information concerning the research in this report, contact the
Director, Oregon Water Science Center
U.S. Geological Survey
2130 SW 5th Avenue
Portland, Oregon 97201
https://www.usgs.gov/centers/or-water

ISSN 2328-0328 (online)
https://doi.org/10.3133/sir20225025